Maximilian Mack, BSc

Investigation of micro RNAs deregulated in A549 lung adenocarcinoma cells in contrast to bronchial epithelial cells with a special focus on the Sonic Hedgehog pathway

MASTERARBEIT

zur Erlangung des akademischen Grades

Master of Science

Masterstudium Molekulare Mikrobiologie

Eingereicht an der

Technischen Universität Graz

Betreuer

Assoz. Prof. Priv.-Doz. Dr.rer.nat. Andelko Hrzenjak

Institut f. Innere Medizin, Klinische Abteilung f. Pulmonologie

Medizinische Universität Graz

Graz, Dezember 2019

EIDESSTATTLICHE ERKLÄRUNG

Ich erkläre an Eides statt, dass ich die vorliegende Arbeit selbstständig verfasst, andere als die angegebenen Quellen/Hilfsmittel nicht benutz, und die den benutzen Quellen wörtlich und inhaltlich entnommenen Stellen als solche kenntlich gemacht habe. Das in TUGRAZonline hochgeladene Textdokument ist mit der vorliegenden Masterarbeit identisch.

_____ _____

Datum Unterschrift

Danksagung

An dieser Stelle möchte ich mich bei allen bedanken, die mich auf dem Weg während meines Studiums und dieser Arbeit begleitet haben.

Ich möchte mich herzlich bei meiner Familie bedanken, die mich in allen meinen Lebenslagen und Vorhaben immer unterstützt. Danke, dass ihr mir immer mit guten Ratschlägen zur Seite gestanden seid. Besonderen Dank gilt auch meiner Freundin Lisa, die mich immer ermutigte, wenn arbeitsintensive Zeiten bevorstanden.

Ebenso möchte ich nicht auf Hr. Prof. Andelko Hrzenjak und dessen Team vergessen, deren Betreuung stets bemüht, produktiv und mit bester Stimmung gezeichnet war. Ich werde sicher noch lange an diese spannende Zeit zurückdenken.

Kurzfassung

Lungenkrebs ist verantwortlich für die meisten Todesfälle aller Krebsarten weltweit. Neue diagnostische Verfahren haben Hoffnung zur erfolgreichen Behandlung von Krebs wiedererwecken lassen. Die Analyse von sogenannten Biomarkern erlaubt eine genauere Charakterisierung des Tumors und somit die Möglichkeit des Einsatzes einer gezielteren, effektiveren Therapie zur Behandlung von Lungenkrebs. miRNAs sind ~22 Nukleotid lange Ribonukleinsäuren und Teil des Gen-regulierenden Netzwerkes in der Zelle. Es ist bekannt, dass abnormale Expressionen solcher miRNAs zur Formierung eines Tumors beitragen und miRNAs somit ein potenzielles Angriffsziel von gerichteten Krebstherapien sein können. In dieser Studie wurde untersucht, ob fehlregulierte miRNAs der Lungenkrebszelllinie A549 mit Genen des Sonic Hedgehog Signalwegs – ein in Krebs mit der Entwicklung von Krebsstammzellen in Verbindung gebrachter Signalweg – in Verbindung stehen. Zu diesem Zwecke wurden die Sequenzen der Gene des Signalweges mit Hilfe dreier unterschiedlicher „Target-Prediction“ – Werkzeuge auf mögliche Bindestellen der fehlregulierten miRNAs analysiert und vorhergesagt. Die vier vielversprechendsten vorhergesagten Interaktionen von runter- sowie hochregulierten miRNAs, die mit Genen des Sonic Hedgehog Signalweges interagieren könnten, wurden weiteren *in vitro* Untersuchungen unterzogen. Dabei wurde versucht den ursprünglichen Status einzelner miRNAs mit Hilfe von sogenannten miRNA-Mimics, für runterregulierte miRNAs, oder miRNA-Inhibitoren, für hochregulierte miRNAs, wiederherzustellen. Es konnte gezeigt werden, dass miR-503-5p die Expression des Sonic Hedgehog - Regulatorproteins βTRC in A549 Zellen posttranskriptionell beeinflusst. Weiters konnte gezeigt werden, dass jeweilige Inhibierung der hochregulierten miRNAs, miR-15b-3p und miR-196a-5p, das Wachstum von A549 Lungenkrebszellen stark einschränkt. Ob diese beiden hochregulierten miRNAs in Verbindung mit dem Sonic Hedgehog Signalweg stehen muss noch weiter untersucht werden.

Abstract

Lung cancer is the most common cause of cancer deaths for both sexes combined worldwide. New diagnostic approaches have raised hope in fighting lung cancer, as the analyses of biomarkers can further characterize the tumor. Depending on these biomarkers, targeted therapy methods can be applied to cure the patient's disease more efficiently. miRNAs are ~22 nucleotide long ribonucleic acids which are part of the gene regulatory network of the cell. Aberrant expression of these miRNAs is known to be related to tumor formation in many cancers, and might be targeted in directed treatments in the future. In this study, we wanted to investigate if any miRNA, deregulated in the lung cancer cell line A549, can be connected to the Sonic hedgehog pathway - a pathway known to be linked to cancer stem cell development. For this, a set of deregulated miRNAs in A549 cells were analyzed *in silico* with the help of three different miRNA-mRNA target prediction tools, on any connection to one of the Sonic hedgehog pathway genes. The four most promising up- as well as downregulated miRNAs were chosen for further *in vitro* characterization. The miRNAs' aberrant expression levels were either complemented by miRNA-mimics for investigating downregulated miRNAs, or inhibited by miRNA-inhibitors for investigating upregulated miRNAs. Analyzing the predicted interactions of downregulated miRNAs on different molecular levels revealed that miR-503-5p specifically affects βTRC, a regulatory protein of the Sonic hedgehog pathway, in a posttranscriptional manner in A549 lung cancer cells. Moreover, inhibiting the expression of upregulated miR-15b-3p and miR-196a-5p showed strong inhibiting effects on cell growth of A549 lung cancer cells. If miR-15b-3p and miR-196a-5p are regulating one of the Sonic hedgehog pathway genes has to be further investigated.

Index

Introduction

Epidemiology of Cancer

According to the latest press release of WHO`s IARC (International agency for research on cancer), the cancer burden is estimated to have risen to 18.1 million new cases and 9.6 million deaths in 2018. It is stated that one in five men and one in six women develop cancer during their lifetime. Seen from a global perspective, Asia accounts for the most, new cancer cases in 2018 worldwide. This can be explained by the fact, that Asia holds 60% of the world's population. In contrast, Europe reports 23.4% of the worldwide new cases and 20.3% cancer deaths in 2018, although holding only 9% of the world's population. If these approximations of new incidents of cancer cases are compared with the regions mentioned above, it can be misleadingly said, that cancer is much more prominent in Europe. But it must be considered that parts of the world, like Asia and Africa, have a much less effective cancer-screening system and, therefore, a higher frequency of certain cancer types with poorer prognosis compared to western parts of the world. This also reflects in a higher proportion of cancer deaths (57.3%) to cancer incidents (48.4%) in Asia (WHO Press Release N°263, 2018).

Lung cancer and female breast cancer are the most commonly diagnosed types for both sexes combined worldwide, with 11.6% of total cases - followed by colorectal cancer with 10.2% and prostate cancer with 7.1%. In terms of mortality, lung cancer is the leading cause of all cancer deaths (18.4%). Colorectal cancer (8.2%) follows on second place, while stomach and liver cancer (both 8.2%) are the third deadliest cancers worldwide (Bray et al., 2018).

Lung cancer classification

The general classification is based on histological characteristics and divides lung cancer in two main groups: small cell lung carcinoma (SCLC) and non-small cell lung cancer (NSCLC). While SCLC occurs in 20% of all cases, NSCLC accounts more frequently, for 80% (Zheng, 2016). NSCLC is further subdivided into adenocarcinoma, squamous cell carcinoma and large cell carcinoma. Improved immunohistochemical techniques and genetic testing approaches led to further classifications over the years.

In 2015, the WHO published their latest update of the histopathological classification of lung cancer, based on new targetable genetic alterations and newly identified molecular profiles. The first push for updating the classifications of lung cancer was given by the work of Travis et al. in 2011. In their paper, they reviewed the classifications of adenocarcinoma and suggested a new approach for organizing the different types of this subgroup of NSCLC in a new and revised order. This new strategy is based on clinical, molecular, radiologic, and surgical issues, but it is still primarily based on histology (Travis et al., 2011). The identification of new driver genes supported the groups work, which also led to the decision for updating lung cancer classifications (The Cancer Genome Atlas Research Network, 2014).

In the new WHO classification, Travis et al.' suggestions were adopted for adenocarcinoma. The NSCLC squamous cell carcinoma subgroup was also rearranged by abolishing the former "clear cell", "small cell" and "papillary" subtypes and replacing them with the "keratinizing" and "non-keratinizing" subtypes. The large cell carcinoma subtypes were removed all together, and only undifferentiated tumors comprises this category (Travis et al., 2015).

Molecular profile of lung cancer

Cancer arises from mutations in the genomic DNA of the cells, mostly triggered by mistakes of DNA-Polymerases during replication processes. The error-rate, and thereby the mutation rate, of these enzymes can be enhanced by exposing cells to cancerogenic or mutagenic substances, like tobacco-smoke. In contrast to other cancers, lung tumors carry three to six times more mutations. Genome-wide sequencing studies in lung cancer detected, about 200 nonsynonymous mutations per tumor, while in tumors derived from colon, breast or pancreas 33 to 66 genes display somatic mutations (Vogelstein et al., 2013). Lungs are much more exposed to mutagenic substances than other tissue of the body, leading to development of malignancies with higher probability.

These mutations do not occur all at once. Tumors evolve from benign to malignant over time. Also, only certain events, so called "Driver-mutations", open the door for an advantage of cancer cells over non-mutated cells.

In “Hallmarks of Cancer”, Hanahan and Weinberg broke down different aspects of challenges for cancer cells to become persistent. These hallmarks include sustaining proliferative signaling, evading growth suppressors, resisting cell death, enabling replicative immortality, inducing angiogenesis and activating invasion and metastasis (Hanahan and Weinberg, 2000). Later, they modified their proposal by two emerging hallmarks - programming of energy metabolism and evading immune destruction (Hanahan and Weinberg, 2011).

Cancer cells achieve these proposed hallmarks by activating oncogenes and deactivating tumor suppressors genes - by mutating their primary coding sequence or their expression-control systems. In lung cancer, especially the alterations of various tyrosine kinase pathways lead to an aberrant activation of proliferative signaling in the cells, therefore acting as oncogenic. In lung adenocarcinoma, 76% of all cases harbor mutations in these pathways (The Cancer Genome Atlas Research Network, 2014). In lung squamous cell carcinoma, key tumor suppressor genes are mutated more frequently. The genomic sequence of TP53 is altered in 90% and CDKNA2 is inactivated in 72% of all cases, respectively (The Cancer Genome Atlas Research Network, 2012). In the following, a selection of the most prominent lung cancer driver genes or pathways, which are discovered and exhaustively investigated in the last 30 years, will be presented in more detail.

Epidermal growth factor receptor (EGFR)

Together with HER2, HER3 and HER4, the receptor tyrosine kinase EGFR is part of the ERBB- family. These receptors are essential for cell to cell interaction mediation by EGF-ligand-depended activation, that is leading in organized embryogenesis (Chia et al., 1995) and also organogenesis in adulthood (Burden and Yarden, 1997). After binding of ligands, ERBB-family receptor tyrosine kinase (RTK) monomers interact with each other, resulting in an active homo- or heterodimerized form. This interplay autophosphorylates key cytoplasmic residues of the receptor and recruits different adaptor proteins (**Figure 1**). EGFR activates at least four major downstream signaling pathways including RAS-RAF-MEK (Buday et al., 1993), PI3K-AKT (Bjorge et al., 1990), PLCγ and some STAT modules (Silvennoinen et al., 1993).

Oncogenic mechanisms like gene mutation, protein overexpression and increased gene copy number lead to EGFRs deregulated tyrosine kinase activity. Numerous studies could show that certain mutations can aberrantly activate EGFR in lung cancer, with its most prominent deletion-mutated EGFRvIII variant (Palazzo et al., 1993). Others evince tumor formation after EGFR copy number alteration (Wulf et al., 2012).

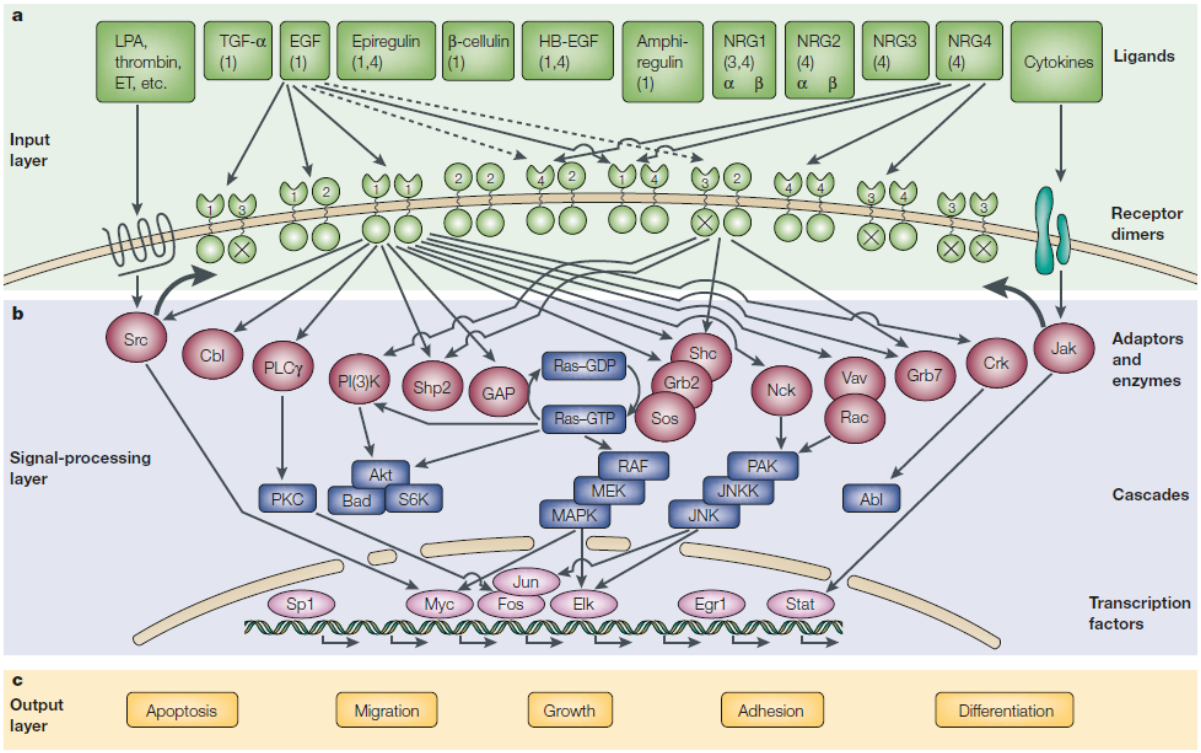

Figure 1: ERBB signalling network. **a)** Ligands and possible receptor formations are shown. Numbers indicate receptor tyrosine kinase 1 to 4 of the ERBB family. For reasons of simplicity, specificities of bindings are only shown for EGF and NRG4. Non-canonical activation of ERBBs, reached by G-protein coupled receptors, is indicated by wide arrows. The crossed out cytoplasmic domain of receptor 3 shows its enzymatic inability. **b)** Signaling cascade after receptor activation is shown only for EGF and NRG4 pathways. **c)** Signals are converted in different outputs, depicted in the output layer box. Figure adopted from Yarden and Sliwkowski (Yarden and Sliwkowski, 2001)

AKT – PI3K – mTOR

The AKT – PI3K – mTOR pathway is besides TP53 one of the most frequently targeted signaling cascade in a variety of human tumors, with a likelihood of mutations in one or more genes of this pathway, estimated with about 30% (Shaw and Cantley, 2006). It is triggered by activating PI3K via RTKs and RAS. PI3K phosphorylates the lipid second messenger PIP2 to PIP3 for further signaling. This molecule transduces the

extrinsic signals to AKT, which is then recruited to the cell membrane for its phosphorylation and hence its enzymatic function is turned on. Activated AKT promotes cell survival via various mechanisms such as negative regulation of NF-kappaB, leading to higher expression of antiapoptotic proteins (Duronio, 2008), as well as inhibition of BAD and BAX, both proapoptotic factors from the Bcl-2 protein family (Cantley, 2002; Engelman et al., 2006). AKT also regulates the nutrient sensor mTORC1 and thereby triggers initiation of ribosome biogenesis e.g. (Gentilella et al., 2015).

Alterations in the PI3K – AKT – mTOR pathway are described in NSCLC in detail. So different studies showed changes in the primary sequence (Rekhtman et al., 2012; Stjernström et al., 2014) as well as gene copy number amplifications of PI3K in NSCLC (Ji et al., 2011). Interestingly, only the PI3KCA subunit isoform is reported as mutated in various studies, while two other main variants PI3KCB and PI3KD, remain unchanged in lung tumors. Though AKT activation via mutation is rare, alteration due to overexpression is found more frequently (Rekhtman et al., 2012; Scrima et al., 2012). In addition, mutation or deletion of PTEN, leading to loss of function of this important regulatory protein, should be mentioned. The major cause of aberrant activation of the PI3K – AKT – mTOR pathway seems to be due to malfunction of PTEN in the signal cascade (Yanagawa et al., 2012).

RAS – RAF – MEK – ERK

RAS not only activates the AKT – PI3K – mTOR cascade described above, it also plays an essential role in a handful of signaling pathways. As a member of the small G-protein family, it is turned on by replacing the bound GDP with GTP by guanine nucleotide exchange factors after extrinsic signaling. In this state, it interacts with effector-proteins from the MEK/SEK/JNK pathway, the PI3K/AKT/NF-kappaB pathway, the p120-GAP/p190-B/RAC/NF-kappaB pathway, and the IKK/I-KappaB/NF-kappaB pathway, as well as the RAF-MEK- ERK pathway (Wellbrock et al., 2004). Binding of GTP induces conformational changes of RAS that lead to RAF activation, the first kinase in this signaling pathway. RAS recruits RAF to the cell membrane for dimerization. Activated RAF phosphorylates MEK, which in turn phosphorylates the effector kinase ERK. ERK phosphorylates several substrates. Among them are

transcription factors and other kinases, which accomplish cell cycle progression, differentiation and evasion from death (Samatar and Poulikakos, 2014).

In lung adenocarcinoma, 32% of all cases hold a mutation in K-RAS, one of three RAS isoforms, thus activating the pathway in an aberrant way. Within all mutations in lung adenocarcinoma, 76% appear to be driven by mutation in one of RAS' variants (McCormick, 2015). In cancer, RAS genes are frequently altered in a point-mutational manner. More specifically, mutations frequently occur in the GDP/GTP binding pocket in positions 12, 13 and 61 (Quinlan and Settleman, 2009). This sequence motive is shared by all three RAS isoforms. Mutations in this gene section effect a permanent activation of RAS by highly increasing the binding affinity of GDP/GTP.

Beside the dominant presence of mutated RAS in lung cancer, RAF distinguished itself as an important target for personalized medicine. Even though it is less likely to be mutated with a percentage of 4-5% (Sheikine et al., 2018), it has manifested itself as a driver gene in lung cancer. To be more precisely, the B-RAF isoform is the most common mutated one in lung cancer. Out of the 30 different B-RAF mutations identified to date, the constitutively active B-RAFV600E variant is mutated in about 90% of all B-RAF altered tumor cells (Wan et al., 2004).

Anaplastic lymphoma kinase (ALK)

ALK is as well as EGFR, part of the transmembrane tyrosine kinase family and is activated in a ligand-mediated manner. This protein plays an important role in neuron development and is expressed in the brain of adults (Iwahara et al., 1997).

Pleiotrophin (PTN) and Midkine (MDK), both secreted growth factors (Stoica et al., 2001, 2002), were originally believed to be ALKs interaction partners and lead to downstream activation of the MAPK- and PI3K-pathway (Bowden et al., 2002; Powers et al., 2002), due to receptor homodimerization. Follow-up studies showed no direct interaction of those two molecules, instead suggested heparin as a ligand (Murray et al., 2015).

In lung cancer, ALK signaling is aberrantly activated due to gene rearrangement. ALK most commonly fuses with EML4 in 6.7% of all NSCLC cases (Perner et al., 2008; Soda et al., 2007). In these cases, the echinoderm microtubule-associated protein like-

4 (EML4) replaces the original N-terminally located extracellular and transmembrane domain of ALK. The intracellular tyrosine kinase domain of ALK remains unchanged and activates downstream pathways in an uncontrolled way (Soda et al., 2007). ALK is also activated by other fusion rearrangements (Fang et al., 2014; Takeuchi et al., 2009; Togashi et al., 2012) and point mutation leading to gain of function (Wang et al., 2011). Interestingly the EML4-ALK fusion is unique in NSCLCs and is mutually exclusive with EGFR and KRAS mutations (Wong et al., 2009). This indicates EML4-ALK as an important biomarker in lung cancer for personalized and targeted treatment with ALK inhibitors.

The Hedgehog Pathway

The hedgehog signaling pathway was first discovered in 1980 by Nusslein-Volhard and Wieschaus during investigations on the fruit fly's (*Drosophila melanogaster*) body plan (Nüsslein-Volhard and Wieschaus, 1980). In their study, they could identify the HH gene, which was mandatory for accurate dorsal-ventral differentiation and polarity of different segments in *D. melanogaster*.

During the development of the species, the pathway has been conserved (Ingham et al., 2011) and can also be found in human in embryogenesis, limb formation and central nervous system development (McMahon et al., 2003). Additionally, hedgehog pathway maintains homeostatic mechanisms and organ repair in adults (Petrova and Joyner, 2014).

The pathway also participates in lung development and is responsible for bronchial budding. Epithelial cells induce hedgehog signaling in mesenchymal cells in a paracrine fashion. SHH, GLI2 and GLI3, three main components of the pathway, were knocked out in mice, leading to severe lung malformations and non-viable phenotypes (Grindley et al., 1997; Motoyama et al., 1998).

Abnormal activation of the hedgehog pathway conversely leads to tumor formation *in vivo*. For example, PTCH is constitutively mutated in Gorlin syndrome, leading to permanent SMO activation and excessive cell proliferation (Johnson et al., 1996). Together with the Wingless-type pathway and Notch signaling, the hedgehog pathway is frequently associated with the concept of cancer stem cells. These cells are believed to initiate tumor formation and proliferation in a potent manner. Cancer stem cells were

discovered in 1994 by Lapidot et al. in acute myeloid leukemia patients. In their study Lapidot and colleagues described a small population of cancer cells with a tremendous tumorigenic ability (Lapidot et al., 1994). Different studies showed that the hedgehog pathway is essential for cancer stem cells in hematopoietic cancers as well as in solid tumors (Milla et al., 2012). Additionally to its complexity, hedgehog-signaling is able to be activated canonically and non-canonically, which will be elucidated below.

Canonical Hedgehog Pathway activation

Hedgehog signaling pathway consists of four main parts – the ligands, the repressor, the activator and the transcription factors. In vertebrates, the pathway localizes near the primary cilium of the cell (Rohatgi et al., 2007). In the canonical mode of activation, one of hedgehogs three ligands (SHH, DHH, IHH) bind to the main repressor protein, Patched (PTCH). Ligand-receptor interaction triggers deactivation of PTCHs repressive manner on the activator Smoothened (SMO). SMO activates three transcription factors, the zinc-finger proteins GLI (GLI1, GLI2 and GLI3), by releasing Suppressor of Fused (SUFU) from the GLI-proteins.

This canonical activation of hedgehog signaling is fine regulated on different levels. For example, ligands need to be modified with cholesterol and palmitic acid after autoproteolytic cleavage in the endoplasmic reticulum (Chamoun, 2001; Porter et al., 1996). After externalization of these proteins, Hedgehog-interaction protein (HHIP) sequesters ligands in the extracellular matrix, leading to prevention of activating PTCH (Chuang, 2003). In addition, hedgehog co-receptors CDO, BOC, GAS1, and LRP promote ligand interaction by PTCH modulation and thereby pathway activation (Beachy et al., 2010).

Not only the hedgehog ligands are tightly regulated by post-translational modification, also the pathway effector proteins GLI undergo different steps of controlling. Phosphorylation of GLI1, GLI2 and GLI3 in an off-state, facilitates binding of E3 ubiquitin ligase β-transducing repeat-containing protein (βTRC) leading to proteolytic processing via the proteasome into their transcription repressor forms (Bhatia et al., 2006; Wang and Li, 2006). As mentioned above, SUFU intracellularly sequesters GLI-proteins and inhibit their migration to the cell nucleus, for regulation of transcription. Furthermore, phosphorylation of SMO is required for releasing SUFU from GLI. Also

leading a greater phosphorylation status of SMO to stronger signaling of the pathway (Jia et al., 2004).

Non-canonical hedgehog pathway activation

Modification and therefore activation of GLI proteins independently of ligand and SMO is referred to as non-canonical hedgehog signaling and often linked to the development of several types of cancer. This form of regulation modifies GLI1 and GLI2 resulting in enhanced transcriptional activity, protein stability, nuclear translocation, preventing SUFU association and GLI degradation in different cancers through different pathways (e.g. Ji et al., 2007; Kasper et al., 2006; Pan et al., 2006; Riobó et al., 2006; Stecca et al., 2007; Wang et al., 2012)

In NSCLC, GLI1 activation is often investigated despite epigenetically silenced SMO in cancer stem cells. In this case, GLI1 is phosphorylated by MAPK due to pathway activation by VEGFA, the ligand of Neuropilin 2 (Po et al., 2017). Also, PI3K-AKT-mTOR prevents GLI1 degradation via phosphorylation of GSK3β by S6 kinase and leads to elevated expression levels of GLI2 and concerned target genes (Kasiri et al., 2017; Mizuarai et al., 2009).

Non-canonical regulation not only results in activation of the hedgehog signaling, but also repressive interventions of not pathway-related proteins were investigated by different groups. In brain cancer, TP53 inhibits GLI1 transcriptional activity and nuclear translocation (Stecca and Ruiz i Altaba, 2009). NUMB, together with ITCH, induces GLI1 ubiquitination and proteasome degradation in medulloblastoma (Marcotullio et al., 2011). Proteins of the DYRK family regulates non-canonical hedgehog pathway in lung cancer, by F-actin-mediated GLI1 degradation (Schneider et al., 2015).

microRNAs

Generally speaking, microRNAs (miRNAs) are ~22 nucleotide long ribonucleic acids, which regulate gene expression in a post transcriptional manner. Beside siRNA and piRNA, miRNAs make up the largest group of small regulatory RNAs in the cell. *Caenorhabditis elegans*' lin-4 was the first discovered miRNA in 1980 and was originally believed to be an ordinary protein coding gene. 13 years later, scientist could

show that lin-4 is responsible for post transcriptional regulation due to antisense paring with the mRNA of lin-14 (Wightman et al., 1993). Because of its specialized role in body development limited to *C. elegans*, this discovery did not raise much attention outside the organisms' community, until the finding of another regulatory miRNA. let-7 could also be identified as a post transcriptional regulator but with the difference that its sequence is much more conserved upon species, conferring miRNAs as serious biological regulators. Since then, the research on miRNAs started to grow and different diseases could be assigned to misconduct of miRNAs, regarding their expressional levels. To date, the miRNA data base "miRBase" holds 1917 entries for human miRNAs (Kozomara et al., 2019).

Biogenesis

miRNAs are transcribed in the nucleus by RNA-polymerase II and are exported to their point of action, the cytosol. During this process miRNAs go through different maturation steps. Their genes can be coded independently on the genome or are located on intron regions of protein-coding genes. If miRNAs transcription is initiated independently by their own promotor, their unaltered form is called primary miRNA (pri-miRNA). The first maturation step of pri-miRNAs is to be truncated by the RNase III Drosha, before being exported into the cytosol. miRNAs, which genes are located on introns, are called primary mirtron (pri-mirtron). In the case of mRNA splicing, Drosha is replaced by the spliceosome for pri-mirtron maturation. Both types of precursor forms exhibit a secondary structured stem-loop. Cleavage of Drosha and the spliceosome occurs directly at the basal junction of this stem-loop.

After exportation by exportin 5, miRNAs are now termed pre-miRNAs. In the cytosol, pre-miRNAs are further processed by another RNase III, called Dicer. This enzyme performs a cut right in the apical region of the stem-loop, transforming the single stranded precursor into its activated double stranded mature miRNA form. In this form, one miRNA strand is loaded onto the so-called RNA-induced silencing complex (RISC). The other strand, which is not interacting with RISC, is degraded. The decision which strand is incorporated into the protein complex depends mostly on their thermodynamic stability (Khvorova et al., 2003), but also nucleotide sequence on position 1, where uracil is favored for loading (Ha and Kim, 2014), contribute to strand choice. These rules are not ultimate for every circumstance. Comparative studies of

miRNAs in different parts of the human body, showed different strand selection of the same pre-miRNA in various tissues (Chiang et al., 2010). For example, one strand of miR-142 is found to be dominant in the brain, while the other strand is preferably active in embryonic tissue (Wu et al., 2009). These “arm-switching” phenomena may due to alternative processing by Drosha, changing the thermodynamic stability of the later generated strands.

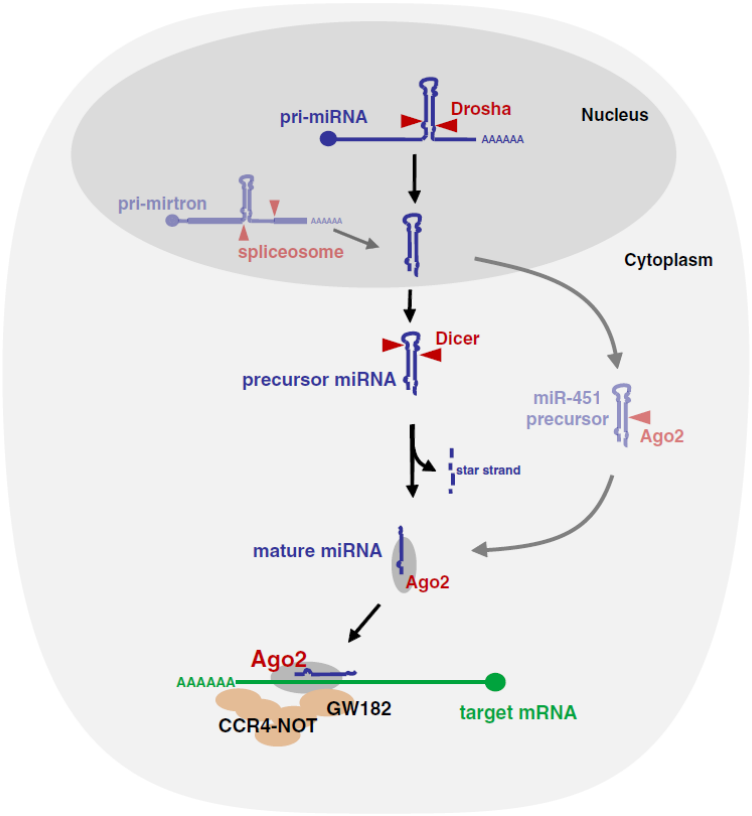

Figure 2: Pathway of miRNA biogenesis. Canonical pathway is shown in bold drawings, while non-canonical biogenesis is indicated in subtle shadings. After truncation by Drosha and Dicer, mature miRNA is integrated in RISC by interacting with Argonaut proteins (here Ago2). RISC mediated deadenylation of the target mRNA by CCR4-NOT via GW182 is shown. An example for non-canonical maturation is given by miR-451. In this case, Ago2 replaces Dicer in the final miRNA cleavage steps. Figure adopted from Hammond (Hammond 2015).

Selected strands are incorporated into RISC and directly associated with Argonaut proteins. After successful loading, the miRNA-protein complex interacts with the homologous mRNA in a sequence specific manner. The whole miRNA biogenesis pathway is indicated in **Figure 2**.

Mode of action

As mentioned above, miRNAs act as post transcriptional regulators of gene expression. They do so by leading the RNA-induced silencing complex to the point of action, which are complementary sequences of mRNAs. Most of the time, these areas can be found in the 3'UTR, but areas of miRNA pairing were also found in the open reading frame of mRNAs (Ott et al., 2011). Although they are present in all kind of eukaryotes, their mode of action differs between the subgroups. In plant cells for example, nearly all 22 nucleotides need to pair to the homologous mRNA, in order to inhibit the expression of target genes (Jones-Rhoades et al., 2006). In animals, only a subregion of the whole sequence, called the seed-region, was identified to interact with the miRNA's corresponding mRNA in animals (Lewis et al., 2003). This region consists of six nucleotides, from position 2 to 7, and is located at the 5' end of the miRNA strand.

Over time, the concept of seed-region paring was revised. Additional base paring at the 8th position, as well as the presence of adenine at the first position of the 5' end of miRNA, led to an increase in the efficiency of inhibiting gene expression (Grimson et al., 2007). Overall four canonical types of RNA interaction of miRNA depending gene regulation are formulated: 8mer, 7mer-m8, 7mer-A1 and 6mer. As technical options and methods for investigating miRNA-mRNA pairing improved, more types of interaction were observed, including variants with imperfect or non-Watson-Crick pairing. A majority of these non-canonical interactions reveled themselves as false-positive, due to the poor resolution of CLIP-seq (cross-linked immune precipitation combined with next generation sequencing), the method used for investigating miRNA pairing. CLIP-seq detects binding sequences via isolating Argonaut bound RNA (miRNA-mRNA). In this approach, also unspecific non-functional binding, with no repressive effect on the mRNA, was observed. CLIP-seq combined with large-scale microarray transcriptome studies could overcome these challenges by not only detecting which nucleotides are pairing, but also measuring the amount of targeted mRNA left after interaction, serving as a direct control for evaluating false-positive site-type identification (Kim et al., 2016).

miRNA research leaped forward as bioinformatics introduced miRNA-mRNA target-prediction tools. These online available tools make use of principles of site-type analyses described above. Among other things, their algorithms are also based on information of the site-type surroundings, in terms of secondary structure formation,

which can mask miRNA target-site recognition to certain extends. Conservational status of target-sites hints the biological relevance and is also incorporated into prediction, as well as thermodynamic stabilities of interactions. The most miRNA-mRNA target-prediction tools algorithms are based on the same parameters but differ in their choice of factor weighting, leading to different outcomes.

As mentioned above, the miRIS-complex can influence gene expression either by inhibiting translation, or in a more drastic way, by degrading paired mRNA. In *D. melanogaster* miRNA mediated mRNA decay is basically performed by two deadenylase complexes, CCR4-NOT and PAN2-PAN3. Both are incorporated into the miRISC by the major adaptor protein GW182. After cleaving off the poly(A)-tail, different factors of the miRISC gets exchanged for 5'-decapping of the mRNA. DCP1 and DCP2, together with various scaffold proteins, promote removal of 5'm^7G-Cap by endonuclease cleavage (Behm-Ansmant, 2006). 5' degradation is induced by recruited XRN1 endonuclease for complete mRNA degradation (Braun et al., 2012).

In comparison to mRNA decay, miRNAs second mode of action, translation inhibition, is less well described. Up to now, three different mechanism of inhibition of translation have been proposed – PABP displacement, recruitment of translational inhibitors, and dissociation of eIF4A by miRISC.

Although the Poly(A)-binding-protein (PABP) is associated with the poly(A)-tail and, therefore, localized at the other end of the mRNA, it activates translation via interaction with 5'Cap-proteins. GW182, one of the major mediators of miRNA induced silencing, harbors a conserved PABP binding domain, which triggers PABP dissociation from the poly(A)-tail (Zekri et al., 2013). PABP is not able to bind to 5'cap-proteins anymore and the ring-like structural integrity, which is needed for proper initiation of translation, is broken up.

GW182 is also able to directly inhibit initiation or elongation of translation by recruiting different factors, identified on mRNAs which lack a distinct poly(A)-tail (for example histone-mRNAs). In this process, DDX6 is recruited to CCR4-NOT and acts as a scaffold for 4E-T. Together DDX6 and 4E-T block translation, although on which level they intervene is still unclear (Chu and Rana, 2006).

Additionally, studies with labeled 5'cap-proteins and translation initiation factors could show that the RNA-helicase eIF4A is dissociated from the complex if miRNAs interact with mRNAs (Fukaya et al., 2014). How miRISC is able to do so is not known yet.

miRNAs in lung cancer

Over the last two decades, miRNAs manifested their significance in the development of cancer. Hundreds of deregulated miRNAs were identified to promote tumor formation. In contrast to protein coding driver-genes, the miRNAs' seed sequence is not mutated in the first place, but rather their expressional abundance in the cell is altered. miRNAs, which are downregulated in cancer are often referred as tumor-suppressor miRNAs, while miRNAs upregulated in cancer are often referred as oncomiRs.

Table 1: Examples of deregulated miRNAs in lung cancer.

miRNA	Regulation status in lung cancer	Target	Effect on host cell	Reference
miR-134-5p	down	EGFR	Sustaining proliferative signal	(Qin et al., 2016)
miR-449a	down	E2F3	Evading growth suppressors	(Ren et al., 2014)
miR-29a family	down	DNMT3A and -3B	Enabling replicative immortality	(Fabbri et al., 2007)
miR-200 family	down	ZEB1	Invasion and metastasis	(Chen et al., 2014)
miR-494-3p	up	PTEN	Inducing angiogenesis	(Mao et al., 2015)
miR-31-5p	up	FIH	Deregulating cellular energetics	(Zhu et al., 2019)
miR-197-3p	down	CKS1B	Avoiding immune destruction	(Fujita et al., 2015)
miR-130b-3p	up	PPARγ	Resisting cell death	(Tian et al., 2016)

Similar to oncogenes, deregulated miRNAs in cancer must facilitate to reach one of cancer's hallmarks, which have been described by Hanahan and Weinberg in 2011. In lung cancer, several dozen miRNAs have been described, whose deregulated expression status enables tumor formation. **Table 1** shows examples of deregulated miRNAs in lung cancer and their targets, as well as their expression status and their overall effect on the host cell.

Analyses of miRNAs adopt a specialized role in the treatment of cancer, as profiling the tumors miRNAs can indicate subtypes of the tumor (Iqbal et al., 2019), predict the patients' survival and the tumor resistance against chemo- or radiotherapy (Salim et al., 2012; Vescovo and Denti, 2015; Wei et al., 2018). Additionally, non-invasive methods to record the miRNA profile of individual patients in body fluids, like blood plasma, are in development (Zaporozhchenko et al., 2018).

The fact that miRNAs are able to alter the activity of certain pathways relevant in cancer, can be exploited by the use of certain pathway-specific drugs, to fight the disease more efficiently. Zhen et al. showed that miR-200a-3p directly targets EGFR and c-Met, two genes known to promote tumor progression in lung cancer. They also showed that increasing the amount of miR-200a-3p in Gefitinib-resistant lung cancer cell lines could reverse tumor resistance and make tumor cells more sensitive against the drug again (Zhen et al., 2015).

This synergy of miRNAome and chemotherapeutics emphasizes how miRNA research could rise the number of people cured from lung cancer in general, as already existing drugs can be used more efficiently.

Aims

The general aim of this study was to identify regulatory miRNAs of the Hedgehog signaling pathway in the lung cancer cell line A549. For accomplishing this objective, different sub goals were formulated:

- Analyzing deregulated miRNAs in lung carcinoma A549 cells in comparison to non-malignant bronchial epithelial cells regarding their regulatory targets within the Hedgehog pathway.

- Investigating the effects of *in vitro* manipulated expression-status of potential Hedgehog pathway modulating miRNAs on a phenotypical level.

- Investigating predicted miRNA – mRNA interactions on a molecular level.

Material and Methods

Overview

All experiments for this study were performed at the Center of Medical Research (ZMFI/II), Medical University of Graz, Austria. The tests mainly followed internally optimized manufacturer's protocols. **Figure 3** shows the workflow of investigating miRNAs in cancer in a simplified manner.

For this study, the detection of deregulated miRNAs in A549 was performed in previous work by Alexandra Bertsch. At this time, a predefined set of miRNAs were investigated in bronchial epithelial cells (BECs) of the lung and in two different cancer cell lines – A549 and H460. After detection of the miRNA expression level in each cell line, the datasets were compared and deregulation of certain miRNAs in cancer cell lines were identified.

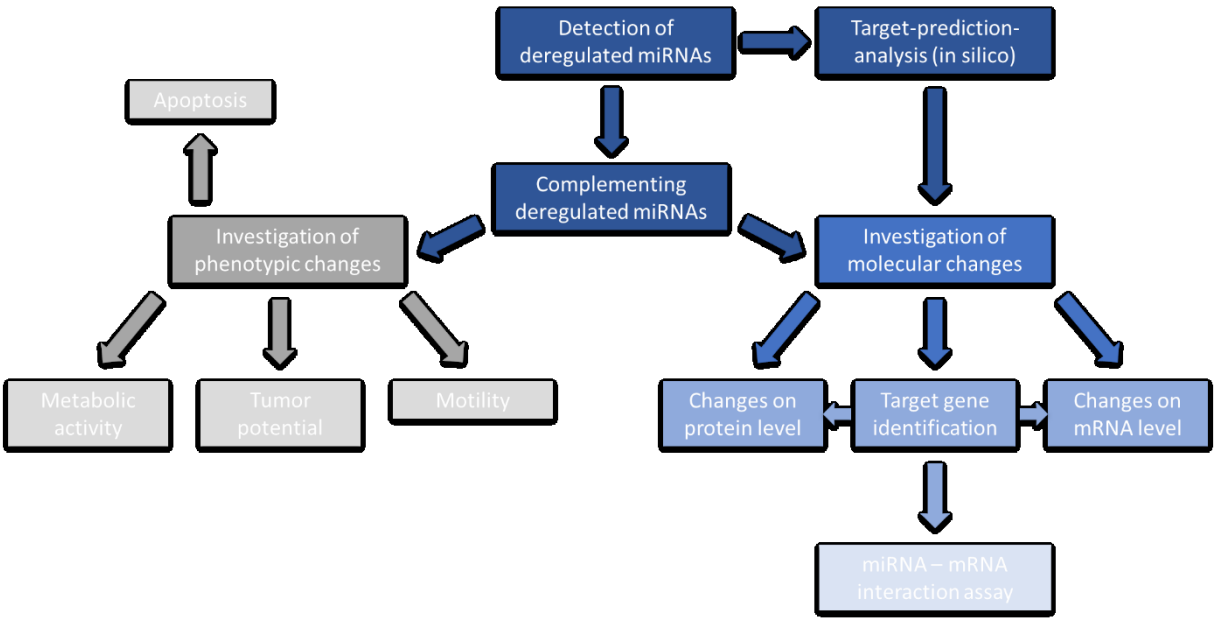

Figure 3: Workflow for investigating deregulated miRNAs used in this study. After the detection of deregulated miRNAs, the workflow splits up into an *in silico* part (Target-prediction-analysis) and an *in vitro* part. These two parts interact directly in terms of investigating different miRNAs on molecular level. Time course of the study is shown by the coloration of the background of the boxes. Darker background indicates earlier steps in the workflow, while weaker colors signifies later phases.

For further experiments, the highest deregulated miRNAs (with a cut-off of 2.8 times deregulated) were taken in consideration for investigation and therefore analyzed *in*

silico by different target-gene-prediction-software. In parallel, methods for complementing miRNAs in cancer cells back to BEC level were optimized. Detection of miRNAs was performed by RT-qPCR. Affecting miRNA-level were reached by transfecting tumor cells with certain amounts of miRNA-mimics for downregulated miRNAs, and miRNA-hairpin-inhibitors for upregulated miRNAs. All experiments were performed 24 h upon cell transfection with one of these two molecular miRNA operators. After optimization of transfection conditions, investigations on a phenotypic basis as well as on a molecular basis were performed. For metabolic activity and cell growth, AlamarBlue™ assay was performed. Wound healing assays was carried out for testing the cells motility and therefore metastatic potential. General tumorigenic potential was measured by colony assay. Lastly, apoptosis was quantified by flow cytometry measuring caspase 3 and caspase 7 activity staining.

As mentioned above, one of the first steps was to identify the target mRNAs of the deregulated miRNAs by *in silico* analysis. Based on these results, the target as well as its corresponding translated protein were investigated after transfection on molecular levels via RT-qPCR and Western Blot respectively. For showing the direct interaction between the miRNA and its predicted mRNA, luciferase reporter assays were performed.

General chemicals and kits

Table 2: General solutions and kits used in the laboratory.

Solution/Kit	Company
Acetic acid (glacial)	Merck, Darmstad, Germany
Acrylamid	Merck, Darmstad, Germany
Agarose	VWR, Darmstad, Germany
Alamar Blue®	Thermo Fisher Scientific, Fremont, USA
Ampicillin	Sigma Aldrich, Vienna, Austria
β-Mercaptoethanol	Sigma Aldrich, Vienna, Austria
Biozym Blue S´Green qPCR Kit	Biozym, Hessich Oldendorf, Germany
Bromophenol Blue	Sigma Aldrich, Vienna, Austria
BCA Protein Assay Kit	Merck, Darmstadt, Germany
CASYton	OMNI Life Science, Bremen, Germany

Collagen I, Rat-Tail, 100 mg	Szabo-Scandic HandelsgmbH & Co KG, Vienna, Austria
Color Prestained Protein Standard, Broad Range (11-245 kDa)	New England BioLabs, Ipswich, USA
Crystal Violet	Sigma Aldrich, Vienna, Austria
DMEM-F12	Gibco, Paisley, UK
DMSO	Sigma Aldrich, Vienna, Austria
DPBS	PAN Biotech, Aidenbach, Germany
PeqGOLD® DNase	Peqlab, Erlangen, Germany
Dual-Luciferase® Reporter Assay System	Promega, Mannheim, Germany
Endo – Free Plasmid DNA Maxi Kit E.Z.N.A.®	Omega Bio-tek, Inc., Norcorss, USA
Ethanol	Merck, Darmstadt, Germany
Fetal Calf Serum (FCS)	Biowest, Nuaillé, France
GeneRuler 100 bp Plus DNA Ladder	Thermo Fisher Scientific, Fremont, USA
Glycerol	Sigma Aldrich, Vienna, Austria
Glycin	Sigma Aldrich, Vienna, Austria
Isopropanol	Merck, Darmstadt, Germany
Jet Prime®	Polypus-transfection, Illkirch-Graffenstaden, France
LB-Medium	Roth, Karlsruhe, Germany
LB-Agar	Roth, Karlsruhe, Germany
L-Glutamine 200 nM (100x), liquid	Gibco, Paisley, UK
Methanol	Merck, Darmstadt, Germany
miRCURY LNA™ ExiLENT SYBR-Green Master MIx	Exiqon, Vedbaek, Denmark
miRCURY LNA™ Universal cDNA synthesis kit II	Exiqon, Vedbaek, Denmark
mirVana™ miRNA Isolation Kit	Invitrogen, Lithuania
Nitrocellulose Membran	BioRad Industries, Hercules, USA
N,N,N',N'-Tetramethylethylendiamin (TEMED)	Sigma Aldrich, Vienna, Austria

PeqGOLD® Plasmid Miniprep Kit II	Peqlab, Erlangen, Germany
PeqGOLD® Taq-DNA-Polymerase 'all inclusive'	Peqlab, Erlangen, Germany
PeqGOLD® Total RNA Kit	Peqlab, Erlangen, Germany
PeqGreen	VWR, Radnor, USA
Pierce protease inhibitor Minitablest	Thermo Fisher Scientific, Fermont, USA
Polyvinylidene Difluoride Membrane	GE Healthcare, Little Chalfont, UK
Ponceau-S	Merck, Darmstadt, Germany
qScript™ cDNA Synthesis Kit	Quanta Biosciences, Beverly, USA
Restore PLUS Western Blot Stripping buffer	Thermo Fisher Scientific, Fremont, USA
RIPA buffer	Sigma Aldrich, Vienna Austria
RLT Lysis buffer	Peqlab, Erlangen, Germany
RPMI 1640	Gibco, Paisley, UK
SOC Outgrowth Medium	New England BioLabs, Ipswitch,USA
Sodium Chloride	Roth, Karlsruhe, Germany
Skim Milk	Roth, Karlsruhe, Germany
Sodium Dodecyl Sulfate	Sigma Aldrich, Vienna, Austria
SuperSignal Western Pico Chemiluminescent Substrate	Thermo Fisher Scientific, Fremont, USA
TAE	LKH Graz Apotheke, Graz, Austria
TOPO® TA Cloning® Kit	Invitrogen, Carlsba, California, USA
Trizma Base	Sigma Aldrich, Vienna, Austria
Trizma HCl	Sigma Aldrich, Vienna, Austria
Trypan blue	Sigma Aldrich, Vienna, Austria
Trypsin	Gibco, Paisley, UK
Tween 20	Sigma Aldrich, Vienna, Austria
0.025% Trypsin-EDTA	Gibco, Paisley, UK
1000 U/ml Penicillin	Gibco, Paisley, UK
10 000 µg/ml Streptomycin	Gibco, Paisley, UK

Buffers and solutions

Table 3: Buffers and solutions for western blotting and DNA gel electrophoresis.

Buffer	Components
10x TBS	31.5 g Trizma HCl 80 g NaCl 1 L H_2O pH 7.5
TBS-T	1x TBS 0.1% Tween 20
10x Running buffer	30 g Trizma Base 144 g Glycine 100 ml SDS 1 L H_2O
10x Transfer buffer	56 g Trizma base 286 g Glycine 2 L H_2O
1x Transfer buffer	10x Transfer buffer 20% Methanol
5x Laemmli buffer	30 mM Tris HCl pH 6.8 2% SDS 10% Glycerol 5% β-Mercaptoethanol 0.01% Bromophenol blue
Ponceau-S-Red	0.5 g Ponceau-S 98.5 ml H_2O 1 ml Acetic acid (glacial) 10 ml RIPA buffer
Protein Lysis buffer	1 Pierce protease inhibitor Minitablet 10 ml RIPA buffer
TAE	40 nM Tris-Acetat 1 mM EDTA-Na_2 pH 8.5

Primer sequences

RT-qPCR Primer for miRNAs

Lyophilized miRCURY LNA™ miRNA PCR Assay Primer sets (Qiagen) were purchased from Qiagen and resuspended in 220 µl nuclease-free H_2O as recommended by manufacturer's protocol. After resuspending, primers were aliquoted and stored at -20°C.

Table 4: Primer for RT-qPCR detection of deregulated miRNAs in A549Par compared to bronchial epithelial cells.

Name	Target sequence (5'→ 3')	Cat. number	Seq.reference
hsa-miR-141-3p	UAACACUGUCUGGUAAAGAUGG	YP00204504	MIMAT0000432
hsa-miR-135a-5p	UAUGGCUUUUUAUUCCUAUGUGA	YP00204762	MIMAT0000428
hsa-miR-503-5p	UAGCAGCGGGAACAGUUCUGCAG	YP00204334	MIMAT0002874
hsa-miR-644a-3p	AGUGUGGCUUUCUUAGAGC	YP00204725	MIMAT0003314
hsa-miR-92a-3p	UAUUGCACUUGUCCCGGCCUGU	YP00204258	MIMAT0000092
hsa-miR-27b-5p	AGAGCUUAGCUGAUUGGUGAAC	YP00204219	MIMAT0004588
hsa-miR-15b-3p	CGAAUCAUUAUUUGCUGCUCUA	YP00205898	MIMAT0004586
hsa-miR-589-3p	UCAGAACAAAUGCCGGUUCCCAGA	YP00206048	MIMAT0003256
hsa-miR-196a-5p	UAGGUAGUUUCAUGUUGUUGGG	YP00204386	MIMAT0000226

RT-qPCR Primer for mRNA

Primer were purchased from Eurofins Genomics, Ebersberg, Germany. For appropriate usage, forward and reversed primer were diluted 1:10 with H_2O and an aliquot was mixed at equal parts. After preparation primer mix was stored at -20°C.

Table 5: Primer for RT-qPCR of potential target genes from the hedgehog pathway.

Name	Primer sequence (5'→ 3')	Tm [°C]	mRNA-reference
h_BTRC_f	GTCTACGGACCCTTGTGGAGCAT	64.2 °C	NM_033637.3
h_BTRC_r	GGGCAGCTGGATCATTTAGGAAGT	62.7 °C	
h_MTSS1_f	CTGCGGCCAGTGATTGAAGAA	59.8 °C	NM_001282971.1
h_MTSS1_r	GGGCAGTTTGTGAGGGTCCAT	61.8 °C	
h_PTCH1_f	CCCCTGTACGAAGTGGACACTCTC	66.1 °C	NM_001083602.2
h_PTCH1_r	AAGGAAGATCACCACTACCTTGGCT	63 °C	
h_FOXA2_f	TGGGAGCGGTGAAGATGGAA	59.3 °C	NM_021784.4
h_FOXA2_r	GAGGAGTAGCCCTCGGGCTCT	65.7 °C	

miRNA screening and *in silico* target-prediction analysis

Regulation status of miRNAs in A549 in contrast to BECs were determined by the work of A. Bertsch (A. Bertsch 2016, diploma thesis). Based on these findings, the top deregulated miRNAs should be investigated. miRNAs, with a deregulated status of +/- 2.8-fold compared to BEC cells, as detected by RT-qPCR, were taken into account for this investigation.

After this first discrimination, miRNAs were connected to a set of main Hedgehog-Pathway genes with the help of miRNA-mRNA-target prediction tools. Only hits present in three different tools were accounted as a strong indication for a possible interaction. As appropriate tools, Targetscan7.2 (http://www.targetscan.org/vert_72/), DIANAmicroT CDS (http://diana.imis.athena-innovation.gr/DianaTools/index.php?r=microT_CDS/index) and MirWalk v2 (http://zmf.umm.uni-heidelberg.de/apps/zmf/mirwalk2/) (Agarwal et al., 2015; Dweep and Gretz, 2015; Paraskevopoulou et al., 2013). For not missing any possible interactions, tools were chosen on differences in their algorithms for generating a wide spectrum of uncovering interactions based on calculations. For instance, MirWalk v2 also analyzes 5' untranslated regions, while DIANAmicroT and Targetscan v7.2 ignores this part as potential binding area for miRNAs.

Lastly, interaction scores of miRNA-mRNA pairs, predicted in all three tools, were analyzed for final selection. Because all scores have different units and different meanings in general, they could not be compared in a direct way. Therefore, every interaction was compared to each other within the same category (for example: inter-species conservation score of one target-prediction tool). The interactions with the top five highest scores were awarded with points from 5 to 1 (1 point for fifth place – 5 points for first place). All points from each category were summed up and the top five interactions with the most points were nominated for *in vitro* investigations.

Cultivation of cells

The human lung adenocarcinoma (LADC) cell line A549 was obtained as a kind gift from Dr. Martin Barr (Trinity College, Dublin, Ireland) (Barr et al., 2013). A549 cells were cultured in DMEM-F12 medium supplemented with 2 mM L-glutamine, 10% heat-inactivated FCS, 100 U/ml penicillin, and 100 µg/ml streptomycin. Human embryonic

kidney cells (HEK293) were purchased from American Type Culture Collection (ATCC®, Manassas, USA) and cultured in DMEM-F12 medium supplemented with 2mM L-glutamine, 10% heat-inactivated FCS, 100 U/ml penicillin, and 100 µg/ml streptomycin. This cell line was used for the luciferase assay experiment due to high transfection efficiency.

All cell lines were grown as monolayer cultures and maintained under 98% humidity and 5% CO_2 at 37°C. All cell lines were cultured in different flasks (**Table 6**), depending on the amount of cells needed for future experiments. Cells were grown adherently and passaged two times per week to prevent 100% confluency. For passaging, cells were washed with sterile DPBS and detached by adding Trypsin-EDTA, followed by 5 minutes incubation at 37°C. Subsequently, trypsin-treatment was stopped by adding medium containing 10% FCS. After a 5 minutes centrifugation step at 400 xg, the supernatant was removed, and cells were resuspended in fresh media. An aliquot of the suspension was used for further cultivation in cell culture flasks.

For generating back up of A549 cells, two million cells were diverted and suspended in media containing 10% DMSO as cryo-protectant. The cells were slowly frozen in cryo-tubes at -80°C over night. Then, the cell-suspension was transferred into liquid nitrogen to ensure long-term storage.

Table 6: Flasks/plates used in this study for cell growth maintenance/experiments.

Flask/Plate	Company
T25 flasks, PE vented cap	SARSTEDT AG & Co. KG, Nürnberg, Germany
CytoOne T-75 Tissue Cult Vented Green cap	STARLAB International GmbH, Hamburg, Germany
6-Well, TC-behandelt (BD)	VWR, Darmstadt, Germany
12-Well, TC-behandelt (BD)	VWR, Darmstadt, Germany
48-Well, TC-behandelt (BD)	VWR, Darmstadt, Germany
96-Well, TC-behandelt (BD)	VWR, Darmstadt, Germany
Nunc-Immuno™ MicroWell™ 96 well polystyrene plates BLACK	Sigma Aldrich, Vienna, Austria

Counting cells

For conducting precise and reproduceable experiments, each assay needed to be carried out with a defined number of cells. For this purpose, cells were counted by using an electric pulse area analysis method with CASY® cell counter (Innovatis, Reutlingen, Germany) after harvesting. A 1:200 cell dilution with Casyton (Innovatis, Reutlingen, Germany) was used for measuring. Aggregation factor smaller than "2" and viability of over 90% of the cells were considered as practicable for further procedure. For cell number evaluating, only the count of living cells was taken into calculations.

Transfection of A549 with miRNA-mimics or miRNA-inhibitors

A549 cells were cultured on cell culture plates with different sizes for different purposes. With changes in cell culture plate size, cell number and volume of medium varies, but transfection concentrations of miRNA-mimics and miRNA-inhibitors stay unchanged. Different plate sizes and related plating parameters and experimental approaches are indicated in **Table 7**. For transfection, JetPRIME®, a cationic polymer-based reagent, was used according to manufacturer's protocol. Transfection-ready reaction mix consists of JetPRIME® buffer and DNA, which are mixed primarily, as well as JetPRIME® reagent. After a 15 minutes incubation period, the transfection mix were dripped into the medium, onto the plated cells. During time of transfection, cells needed to reach a confluence of 60%, as recommended by company producing jetPRIME®. Media was changed directly before and 24 h after transfection.

Table 7: Cell culture parameters for different experiments conducted in this study.

Experiment	Cell line	Cell count	Plate size
RNA harvest	A549	60 000/Well	12-Well
Protein harvest	A549	150 000/Well	6-Well
Motility-Assay	A549	60 000/Well	12-Well
Alamar-Assay	A549	2 500/Well	96-Well
Colony-forming-Assay	A549	60 000/Well and 300 /Well	12-Well and 6-Well
Luciferase-Assay	HEK293	30 000/Well	48-Well

In general, all experiments were performed with a transfection concentration of 5 nM for miRNA-mimics and 30 nM for miRNA-Inhibitors, based on results of transfection optimization (see below). All miRNA-mimics as well as miRNA-inhibitors were purchased from Dharmacon, Lafayett, USA. All product details can be seen in **Table 8**.

Table 8: Product details of miRIDIAN mimics and miRIDIAN hairpin-inhibitors used in this study.

Micro RNA	Type	Accession nr.	Product nr.
hsa-miR-141-3p	Mimic	MIMAT0000432	C-300608-03-0020
hsa-miR-135a-5p	Mimic	MIMAT0000428	C-300603-05-0020
hsa-miR-503-5p	Mimic	MIMAT0002874	C-300841-05-0020
hsa-miR-589-3p	Hairpin-Inhibitor	MIMAT0003256	IH-300911-03-0005
hsa-miR-15b-3p	Hairpin-Inhibitor	MIMAT0004586	IH-301146-02-0005
hsa-miR-27b-5p	Hairpin-Inhibitor	MIMAT0004588	IH-301154-02-0005
hsa-miR-196a-5p	Hairpin-Inhibitor	MIMAT0000226	IH-300529-06-0005
microRNA MIMIC Negative Control #1	Mimic	-	CN-001000-01-20
Mimic Transfection Control with Dy547	Mimic	-	CP-004500-01-20
microRNA Hairpin Inhibitor Negative Control #1	Hairpin-Inhibitor	-	IN-001005-01-05

Co-Transfection of HEK293 with miRNA-mimics and Dual Luciferase reporter plasmid

For investigating the physical interaction between miRNAs and the predicted target sequence, a Dual Luciferase Assay was performed. For this purpose, 30000 HEK293 cells were plated and transfected with a concentration of 5/10/20 nM for miRNA-mimics and 0.5 µg/ml for pcDNA3.1(+) reporter plasmid. Before plating, all wells were treated with collagen for better attachment of HEK293 cells to the well. Changing the medium 24 h after transfection was dispensed for this experimental approach.

AlamarBlue™ assay

After transfection with miRNA-mimics/-inhibitors AlamarBlue™ assay was performed to determine proliferation rate by measuring the cells metabolic activity. The experiment was performed 24 h, 48 h and 72 h after transfection by measuring fluorescence at CLARIOstar Plus (BMG LABTECH GmbH, Ortenberg, Germany). The assay is based on the reducing ability of cells by converting the indigo-colored dye resazurin in resorufin. This molecule is highly fluorescent and can be excited at 530 nm. Emission can be detected at 590 nm.

Pre-mixed AlamarBlue™ reagent mix was added to cells in complete medium and incubated for two hours at 37°C before measuring fluorescence with CLARIOstar microplate reader (BMG LABTECH GmbH, Ortenberg, Germany).

Wound-healing assay (motility assay)

Wound-healing assay was performed to investigate cell migration after transfection with miRNA-mimics/-inhibitors. After transfection A549 cells with 5 nM miRNA-mimics or 30 nM miRNA-inhibitors for 24 h, media was changed. After reaching nearly 100% confluence, a scratch with a pipette tip (size 10-100 µl) was performed on the cell monolayer. Then cells were washed with DPBS one times for removing detached and dead cells. For investigating their ability to close this gap, pictures were taken at certain time points (0 h, 18 h, 24 h, 42 h) and evaluated with ImageJ (Schneider et al., 2012) and its “MRI-wound healing tool” – plugin (http://dev.mri.cnrs.fr/projects/imagej-macros/wiki/Wound_Healing_Tool) by measure the free area in between the cell monolayer.

Colony formation assay

Colony formation assay was performed to determine the tumorigenic ability of transfected A549 cells. Cells were seeded out in a 12-well plate and transfected with miRNA-mimics/-inhibitors 24 h later. 24 h after transfection, cells were harvested with trypsin and counted. 300 cells were then plated out in 6-well-plates and incubated at standard conditions. For A549 cells, colony formation took 9 day.

The experiment was stopped before colonies were merging. Cells were washed with DPBS and fixed with Methanol : glacial acetic acid (3:1 ratio) at room temperature for 10 minute. Fixation mixture was discarded, and plates were air-dried before cell colonies were stained with 0.4% crystal violet at RT for 10 minutes. Redundant staining solution was aspirated for reuse, cells were washed with H_2O three to five times and air-dried again. Colonies were counted manually. A cell accumulation was considered as a colony, if 50 or more cells were part of it. Additionally to colony number, average colony size was determined with ImageJ by using the “colony-area” plug-in (Guzmán et al., 2014).

Fluorescent-activated cell sorting (FACS)

Measuring apoptosis

For detecting activation of apoptosis after transfecting cells with an amount of 30 nM miRNA-inhibitor, fluorescent-activated cell sorting was performed. The CellEvent™ Caspase-3/7 Green Flow Cytometry Assay Kit (Invitrogen, Carlsbad CA, USA) was used for detecting activate form of caspase 3 and 7 indicating apoptosis. The detection reagent consists of a four amino acid peptide (DEVD) conjugated to dye. If caspase 3 and 7 are activated in the cells, the peptide is cleaved off and the dye binds to the cell’s nucleic acid for fluorescent detection.

For this analysis, 150000 cells/well were plated in a 6 – well plate and transfected with 30 nM of miRNA-inhibitors the next day. 24 h and 48 h after transfection, adherent and floating cells were harvested and washed with DPBS. For measuring apoptosis, CellEvent™ solution was diluted 1:125 in medium. Cells were incubated with 62.5 µl/sample of mixed substrate at 37°C for 45 minutes. After incubation, 140 µl of PBS was added and caspase activity/cell was measured by flow cytometry using CytoFLEX S (Beckman Coulter, Vienna, Austria). Data were analyzed using CytExpert software.

RNA isolation

As indicated in **Table 7**, 60 000 cells/well were plated out in 12-well plates. Cells were transfected with standard miRNA-mimics/-inhibitor concentrations the next day. Medium was changed 24 h after transfection. RNA was harvested at three different

time points after transfection (24h, 48h and 72h). Medium was aspirated, and cells were washed once with DPBS. 350 µl of RLT-Lysis buffer (VWR, Darmstadt, Germany) was added directly on to the cells for cell lysis.

RNA was purified by using PeqLab PeqGOLD Total RNA Kit (VWR, Darmstadt, Germany). For mRNA isolation, all steps were executed according to manufacturer's protocol. DNA digestion with DNase I was included for higher RNA quality. For additional miRNA isolation, the protocol was changed in step two. In this step 100% Isopropanol was applied instead of 70% ethanol for proper isolation of small miRNAs. RNAs were eluted in RNase free H_2O (Sigma Aldrich, Vienna, Austria) and stored at -20°C.

Measurement of RNA quantity/quality

To determine quantity and quality of isolated RNAs, all samples were measured on the NanoDrop™ 2000c UV-Vis Spectrophotometer (Thermo Fisher Scientific, Fremont, USA). For this purpose, RNase free H_2O (Sigma Aldrich, Vienna, Austria) was used as a blank. RNA was considered as pure, if samples could show 260/280 ratios of about 2.0 and 260/230 ratios of about 2.0 to 2.2.

cDNA-synthesis

mRNA

cDNA-synthesis with mRNA templates were performed using qSricpt cDNA Synthesis Kit (Quanta Biosciences). An amount of 1000 ng isolated and purified RNA was used as a template. Incubation steps were carried out in the MyCycler thermocycler (Bio-Rad Laboratories GesmbH, Vienna, Austria) according to the manufacturer's protocol. Exact composition of the reaction mix, as well as the temperature profile for cDNA-synthesis can be seen in **Table 9**.

Table 9: Temperature profile and reaction mix of mRNA cDNA-synthesis.

mRNA cDNA-synthesis		
Master mix	5x qScript reaction mix	4 µl
	Reverse Transcriptase	1 µl
	H_2O	x µl
	Template RNA [1000 ng]	x µl
	Total	20 µl
Temperature profile	22°C	5 minutes
	42°C	30 minutes
	85°C	5 minutes
	4°C	hold

miRNA

For reverse transcription of miRNA into complementary DNA (cDNA), miRCURY LNA™ Universal RT microRNA PCR kit (Exiqon, Vedbaek, Denmark) was used. Before setting up the reaction, template RNA was dilute to a concentration of 5 ng/µl. Incubation steps were conducted using the MyCycler thermocycler (Bio-Rad Laboratories GesmbH, Vienna, Austria). All parameters were adjusted according to the manufacturer's protocol. Exact composition of the reaction mix, as well as the temperature profile for cDNA-synthesis can be seen in **Table 10**.

Table 10: Temperature profile and reaction mix of miRNA cDNA-synthesis.

miRNA cDNA-synthesis		
Master mix	5x reaction buffer	2 µl
	Enzyme Mix	1 µl
	H_2O	5 µl
	Template RNA [5 ng/µl]	2 µl
	Total	10 µl
Temperature profil	42°C	60 minutes
	95°C	5 minutes
	4°C	hold

For long term storage, cDNA was frozen at -20°C.

Real-Time qPCR

For detecting changes in expression patterns of certain genes after cell transfection with miRNA-mimics/-inhibitors, RT - qPCRs were performed. All RT - qPCRs were SYBR-Green based and applied for semi-quantitative analysis. Sequential incubation steps were performed using Light Cycler 480 (Roche, Vienna, Austria).

mRNA

For detecting changes on mRNA-level, Blue S'Green qPCR mix (Biozym Scientific GmbH, Hessisch Oldendorf, Germany) was used. Primers used in this experiment are listed in **Table 5**. Before added to the reaction mix, primers were dilutes 1:10 with H_2O and forward and reverse primer were mixed to equal parts. All steps were performed according to manufacturer's protocol. Before use, cDNA was diluted 1:10 for efficient reaction. All reactions mRNA-qPCRs were performed using clear 384-well-plates. Temperature profiles and reaction mix composition are listed in **Table 11**.

Table 11: Temperature profile and reaction mix of mRNA RT – qPCR.

mRNA Real - Time qPCR			
Master mix	2x Blue S'Green qPCR mix		2.5 µl
	Primer mix [10 pmol/µl]		0.5 µl
	cDNA template [5 ng/µl]		2 µl
	Total		5 µl
Temperature profile		95°C	2 minutes
	40x	95°C	5 seconds
		60°C	30 seconds
Additional parameters	• Ramp-rate 4.8°C/s (for 95°C) and 2.5°C/s (for 60°C), optical read • Melting curve analysis activated • SYBR Green/HRMDye format		

miRNA

miRCURY LNA™ Universal RT microRNA PCR kit (Exiqon, Vedbaek, Denmark) was used to detect miRNA levels in A549 cells. Primers used in this experiment are listed in **Table 4**. In contrast to RT–qPCRs detecting mRNAs, primers for miRNA detection were not diluted in this approach. All steps were performed according to manufacturer's protocol. Before use, cDNA was diluted 1:80 for efficient reaction. All miRNA-qPCRs were performed using white 384-well-plates. Temperature profiles and reaction mix composition are listed in **Table 12**.

Table 12: Temperature profile and reaction mix of miRNA RT – qPCR.

miRNA Real – Time qPCR			
Master mix	PCR Master mix		5 µl
	PCR Primer mix		1 µl
	cDNA template [125 pg/µl]		4 µl
	Total		10 µl
Temperature profile		95°C	10 minutes
	45x	95°C	10 seconds
		60°C	1 minutes
Additional parameters	• Ramp-rate 4.8°C/s (for 95°C) and 2.5°C/s (for 60°C), optical read • Melting curve analysis activated • SYBR Green/HRMDye format		

RT–qPCR data processing and analysis

Ct–values and melting temperatures of two replicates per sample were analyzed with Light Cyclers calculation software (version 1.5.0.39) (Roche, Vienna, Austria). Ct–values were identified by using 2nd derivative method. This method measures the point, where the rate of change of a signal is itself changing. This is reflected in cycle numbers where the SYBR-green signal passes a certain threshold, determined by the detection

apparatus' sensitivity. The method is mainly used for absolute quantification. For investigating target gene expression, Ct–values greater than 37 for mRNA and 35 for miRNAs were considered as false positive signals according to manufacturer's recommendation.

C–values of the gene or miRNA of interest were subtracted from Ct – values of household genes or household miRNAs, resulting in generating ΔCt – values. This step is basically a normalization technique, comparable with loading controls in western blots. Only ΔCt–values of particular samples can be compared directly. Lastly ΔCt–values of two experimental groups can be compared. Mostly treated vs. untreated, were subtracted and ΔΔCt–values were generated. This calculation method gives relative quantifications of expression levels of certain genes or miRNAs.

ΔCt = Ct of housekeeping gene/miRNA – Ct of gene/miRNA of interest

(both Cts must be generated from the same sample)

ΔΔCt = ΔCt of treated sample – ΔCt of untreated sample

Light Cycler 480 software also provides melting curve analysis. Data were checked for double melting temperatures per sample, mostly indicating DNA-contamination or unspecific products. Melting temperatures were also compared to previous RT–qPCR runs for product specifity verification.

Protein isolation

For detecting changes on translational level after miRNA–mimics/-inhibitor transfection, cells were harvested, and total proteins were isolated for analysis. For this purpose, 150000 A549 cells per well were seeded out on 6-well plates. 48 h after transfection, cells were washed with DPBS and 100 µl of RIPA buffer, supplemented with a mix of protease inhibitors, were added to the adherent monolayer. Cells were detached via scrapping on ice. Final cell disruption and homogenization was achieved by sonification (Ultraschall-Desintegrator UP50H ROTH, Carl Roth GMbH+Co.KG

Karlsruhe, Germany). Each sample was sonicated two times for 5 seconds on ice (cycle 1 at amplitude 80). Homogenate was centrifuged at 13000 rpm for 10 minutes at 4°C to remove cell debris and insoluble material. Supernatant was used for further analysis. Protein samples were frozen at -20°C for long term storage.

BCA Assay

For measuring protein yield bicinchoninic acid assay was performed. The assay is based on the reduction of Cu^{2+} ions by peptide bonds and certain amino acids in side chains. Reduced Cu^{+} ions form a complex with bicinchoninic acid, which absorbs light at 562 nm and can therefore specifically detected.

Samples were diluted 1:5 with RIPA buffer and mixed with in copper sulfate, which was 1:50 diluted with BCA solution. For protein quantification, a standard curve was generated with BSA. A 2 mg/ml BSA stock solution was diluted in steps and mingled with copper sulfate/BCA mix (1:50). Before measuring absorption at 562 nm, samples were incubated at 37°C for 30 minutes. Absorption was measured using CLARIOstar Plus (BMG LABTECH GmbH, Ortenberg, Germany). Absorption values of samples were compared to absorption values of BSA samples with predefined amount of protein for determination of sample concentrations.

SDS-PAGE electrophoresis

For sample analysis by immunoblotting, proteins had to be separated according to their size by SDS-PAGE electrophoresis. 30 µg of total protein were loaded on each line of the gel. Before loading, samples were denatured with 5x Lämmli-buffer and incubated 10 minutes at 95°C on a thermoblock (Thermomixer comfort; Eppendorf, Hamburg, Germany). SDS poly-acrylamide gel density was varied, depending on the size of the protein of interest. Gel compositions of stacking gel is listed in **Table 13**, and composition of resolving gel is listed in **Table 14**.

Table 13: Composition of stacking gel for SDS – PAGE.

Stacking gel	4.5%
H_2O	2.05 ml
Acrylamid stock 30%	0.375 ml
Stacking gel buffer (0.5 M Tris, 0.4% SDS, pH 6.8)	0.5 ml
SDS 10%	30 µl
APS 10%	30 µl
TEMED	3 µl

Table 14: Composition of resolving gel (6% or 8%) for SDS – PAGE.

Resolving gel	6%	8%
H_2O	5.2 ml	4.6 ml
Acrylamid stock 30%	2 ml	2.6 ml
Resolving gel buffer (1.5 M Tris, 0.4% SDS, pH 8.8)	2.6 ml	2.6 ml
SDS 10%	100 µl	100 µl
APS 10%	100 µl	100 µl
TEMED	8 µl	8 µl

Electrophoresis itself was performed in running buffer (composition see **Table 2**) at 200 V.

Western blotting

After protein separation in SDS – PAGE electrophoresis, transfer from gel to the membrane was performed in transfer buffer (composition see **Table 2**) at 400 mA for 2 h. For making sure that transferring was efficient, membrane was stained with Ponceau-S solution. Before destaining with H_2O, membrane was tailored to protein bound area, for more effective antibody interaction. Next, membrane was incubated in 5% skimmed milk in TBS-T for a minimum for 1 h at room temperature for blocking

unoccupied interaction sites of the membrane. Then, membrane was washed three times with TBS-T for 5 minutes. Primary antibody was diluted 1:500 in 1% skimmed milk in TBS-T and incubated over night at 4°C for specific protein-antibody interaction. Secondary antibody was diluted 1:2000 for proteins of interest and 1:10000 for loading controls in TBS-T and incubated for 1 h at room temperature. Secondary antibodies were labeled with a horseradish peroxidase (HRP) for detection purposes. After three washing steps with TBS-T, blots were incubated with Amersham ECL Prime Western Blotting Detection Reagent (GE Healthcare Bio-Sciences, Pittsburgh, USA) for 5 minutes in dark surrounding. Specific interaction shown by enzymatic turnover of the HRP-labeled 2nd antibody was detected using ChemiDoc™ Touch Imaging System (BioRad Industries, Hercules, USA).

For detecting further proteins of interest, blots were stripped. For this purpose, membrane was washed two times with TBS-T for 5 min and incubated in restore PLUS Western Blot stripping buffer (Thermo Fisher Scientific, Fremont, USA). After stripping, membrane was washed twice in PBS and one time in TBS-T, before blocking with 5% skimmed milk in TBS-T for at least 1 h at room temperature. Then, blot was incubated with next antibody cascade for further detection.

Table 15: List of antibodies used in this study.

Antibody	Conc.	Host/Isotype	Cat. Nr.	Company
MTSS1 polyclonal	500 µg/ml	Rabbit / IgG	PA5-23200	Invitrogen
BTRC monoclonal	500 µg/ml	Mouse / IgG	1B1D2	Thermo Fisher
β-Actin monoclonal	200 µg/ml	Mouse / igG	SC-47778	Santa Cruz
Sec. anti-rabbit (HRP*-conjugated)	800 µg/ml	Goat / IgG	31460	Invitrogen
Sec. anti- mouse (HRP*-conjugated)	-	Horse / IgG	7076	Cell Signaling

* Horse Reddish Peroxidase

Interaction studies

For investigating interactions between miRNAs and their predicted target sequence on mRNAs, a Luciferase assay was the method of choice. This assay is based on luciferases as expression reporter, which catalyzes reactions with emitting light at certain wavelengths, depending on the enzyme itself, as a side product. This light can be detected and is proportional to the quantity of luciferases in the investigated sample.

This principle is mainly used for expression studies, like analysis on new identified promotors. In this study, regulation at post-transcriptional level was investigated. Therefore, the predicted wildtype target sequence of a certain miRNA, was copied from a certain mRNA and cloned in the 3' untranslated region of the mRNA of the luciferase-reporter gene *Renilla*. After its transcription, miRNA binds (or binds not) and inhibit translation via degrading mRNAs directly or hindering initiation of translation.

HEK293 cells were chosen as expression system, due to their high transfection efficiency. A reporter plasmid containing luciferase reporter gene with the predicted target sequence cloned in its 3' untranslated region and the miRNA expressed via plasmids or in the form of miRNA-mimics were transfected into HEK293 cells. As an internal control, the reporter gene plasmid also carries a second luciferase called Firefly. Detecting the amount of expressed Firefly, data must be normalized, due to different transfection efficiencies.

gBlock design

To generate plasmid constructs described above, miRNA target sequences of certain mRNAs were cloned in the plasmid psiCHECK™-2. Target sequence was cloned in the 3' UTR of the *Renilla* luciferase (*hRluc*). Most of hRluc 3'UTR was replaced by cloned predicted interaction position and their surrounding sequence. Only the last 32 3' nucleotides remained from the original 3'UTR. Gibson cloning was chosen for cloning desired sequences into the expression vector. This method is based on homologue recombination events with overlapped sequences. DNA fragments were designed with a 48-nucleotide overhang at 5' position and 32-nucleotide overhang at 3' position. Lengths of overhangs were determined empirically, based on previous Gibson clonings with psiCHECK™-2. miRNA target sequences with surrounding sequences from the original mRNA are located in between these overhangs. The

cloned original mRNA sequence is about 75 nucleotides long for each construct. These DNA fragments were synthetically manufactured as gBlocks (Integrated DNA Technologies, Coralville, IOWA, USA).

If one particular miRNA was able to repress the expression of the luciferase target genes, the cloned predicted interaction position was verified by mutating these regions. Mutating the predicted binding sequence should have led to a recovery of reporter gene expression. Therefore, similar gBlocks with mutations in the seed region of predicted binding sequence were designed. Constructs used in this study and their mutated counterparts are listed below. Overhangs are indicated in italic letters. Predicted interaction area is underlined and seed – region of interaction is indicated in bold letters.

Overhangs with 3'UTR mRNA of MTSS1 with predicted hsa-miR-135a-5p interaction position:

5' – *TGGAGCGCGTGCTGAAGAACGAGCAGTAATTCTAGGCGATCGCTCGAG*TTTCTTCTGGTAGCT
TCATGGTAAATGCATCCGAAT**AAGCCATA**CTGGATTGCAGTGTTTGTTTCTGTAGGGTGTTTA*GCGGC*
CGCTGGCCGCAATAAAATATCTTATT – 3'

Overhangs with 3'UTR mRNA of MTSS1 with predicted hsa-miR-135a-5p interaction position and mutated seed-binding region:

5' – *TGGAGCGCGTGCTGAAGAACGAGCAGTAATTCTAGGCGATCGCTCGAG*TTTCTTCTGGTAGCT
TCATGGTAAATGCATCCGAAT**GGTAAGCG**CTGGATTGCAGTGTTTGTTTCTGTAGGGTGTTTA*GCGGC*
CGCTGGCCGCAATAAAATATCTTATT – 3'

Overhangs with 3'UTR mRNA of BTRC with predicted hsa-miR-503-5p interaction position:

5' – *TGGAGCGCGTGCTGAAGAACGAGCAGTAATTCTAGGCGATCGCTCGAG*AGTCGGCCCAGGACGG
TCTACTCAGCACAACTGACTGCTTCAGT**GCTGCTA**TCAGAAGATGTCTTCTATCTTTTGTGAATGATT
GCGGCCGCTGGCCGCAATAAAATATCTTATT – 3'

Overhangs with 3'UTR mRNA of BTRC with predicted hsa-miR-503-5p interaction position and mutated seed-binding region:

5' – *TGGAGCGCGTGCTGAAGAACGAGCAGTAATTCTAGGCGATCGCTCGAG*AGTCGGCCCAGGACGG
TCTACTCAGCACAACTGACTGCTTCAGT**TACTACG**TCAGAAGATGTCTTCTATCTTTTGTGAATGATT
GCGGCCGCTGGCCGCAATAAAATATCTTATT – 3'

Overhangs with 3'UTR mRNA of PTCH1 with predicted hsa-miR-141-3p interaction position:

5' – *TGGAGCGCGTGCTGAAGAACGAGCAGTAATTCTAGGCGATCGCTCGAG*TGTAAATTACAGCAA
GGAAAGAAAATGTTTAA**CAGTGTTA**AGAGAGTCAGAGCAGAGTGGATAT*GCGGCCGCTGGCCGCAATA*
AAATATCTTATT – 3'

Gibson cloning

As mentioned above, reporter plasmids were cloned by Gibson assembly® using NEBuilder HiFi DNA assembly master mix (New England Biolabs, Ipswich, MA, USA). Cloning was performed according manufacturer's protocol with a vector to insert ratio of 1:2.

After cloning, plasmids were transformed in NEB® 5-aplha competent *E. coli* (New England Biolabs, Ipswich, MA, USA) for amplification. Transformed bacteria were plated out on LB-agar-plates containing ampicillin [1µg/ml] for selection and incubated over night at 37°C.

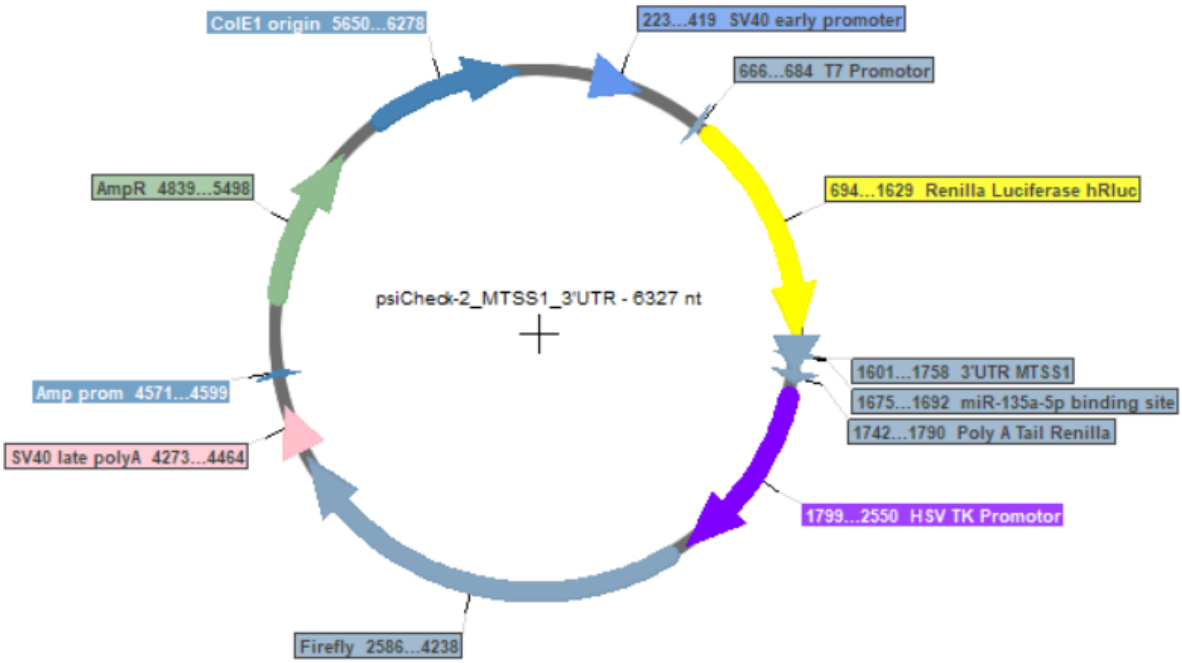

Figure 3: Example of PsiCheck-2 expression vector with integrated 3'UTR of MTSS1 for investigation of has-miR-135a-5p interaction. PsiCheck-2 vectors and mimics were transfected into HEK293 cells for 48h. miRNA interaction sequences of potential target genes were cloned in 3'UTR of *Renilla* luciferase for reporter repression under co-transfected conditions (reporter plasmid plus miRNA). Plasmid map was generated using Serial Cloner v.2.6.1 (http://serialbasics.free.fr/Home/Home.html)

Plasmid verification and preparation

For verifying plasmid construction, colonies were picked from LB-agar-plates containing ampicillin. 5 ml LB – medium containing ampicillin [1 µg/ml] were inoculated with single colonies and incubated over night at 37°C and 180 RPM (rounds per minute). Before plasmid isolation, an aliquot of 500 µl cell suspension was mixed with 500 µl of 50% glycerol and frozen at -80°C for long time storage.

Overnight culture was centrifuged at 3000 xg for 10 minutes, and plasmids were isolated using PeqGOLD® Plasmid Miniprep Kit II (VWR, Radnor, USA) according to manufacturer's protocol. Isolated DNA was analyzed by sequencing. 15 µl of recombinant plasmid-DNA with a concentration of 50 to 100 ng/µl were send to sequencing (Eurofins Genomics Germany GmbH, TubeSeq service, Ebersberg, Germany) with 15 µl Gli_2_mut_total_FWD primer 5' – TGGAGCGCGTGCTGAAGAAC – 3', 61°C melting temperature, [10 nmol/µl].

Luciferase assay

Luciferase assay was performed in HEK293, due to their high transfection rate. 0.5 µg/ml of psiCHECK™-2 with cloned target interaction sequences in the 3'UTR of the reporter gene were transfected together with 5 to 20 nM of mimics for 48h. In this experimental approach, medium was not changed 24h after transfection. Luciferase assay was performed using Dual-Luciferase® Reporter Assay System (DLR™ Assay System, Promega, Madison, Wisconsin, USA). All solutions were prepared according to manufacturer's protocol. All steps were performed according to manufacturer's protocol except for cell lysis. Volume of PBL lysis buffer was adapted to 25 µl/well and the cell lysate was frozen at -80°C for improved cell disruption. Lysate was then thawed on ice and transferred to white 96-well plates for detection

Luminescence of firefly luciferase was measured at 600 ± 30 nm for normalization purposes. Then signal was quenched and luminescence of *Renilla* luciferase was measured at 450 ± 15 nm for detecting miRNA interaction due to repression of expression. Luminescence was measured with CLARIOstar microplate reader (BMG LABTECH GmbH, Ortenberg, Germany) 36 times over a period of 25.96 seconds. The top five highest signals were averaged for final evaluation.

Statistical analysis

Data were checked for significances in differences with GraphPad Prism 7 using Dunnett's Multiple Comparison tests. For analysis, treated groups were compared to appropriate controls. Number of biological replicates are noted in caption of single figure. Number of asterisks indicate p-values smaller than 0.05, considered as significant. * $P < 0.05$, ** $P < 0.01$, *** $P < 0.001$, **** $P < 0.0001$.

Results

miR-503-5p, miR-135a-5p, miR-141-3p and miR-664a-3p showed the most promising actual interaction with a hedgehog–signaling gene after *in silico* target-prediction analysis

Based on the findings of previous work of our group on miRNA expression, 45 deregulated miRNAs of A549, with an minimum of 2.8 times fold-difference, were analyzed *in silico* with the help of three online prediction tools, regarding to possible interactions with 38 of the most relevant hedgehog pathway genes. For *in silico* analyses, TargetScan 7.2, DIANAmicroT CDS and MirWalk2.0 were chosen, based on different foci in their algorithms, predicting miRNA-mRNA interactions.

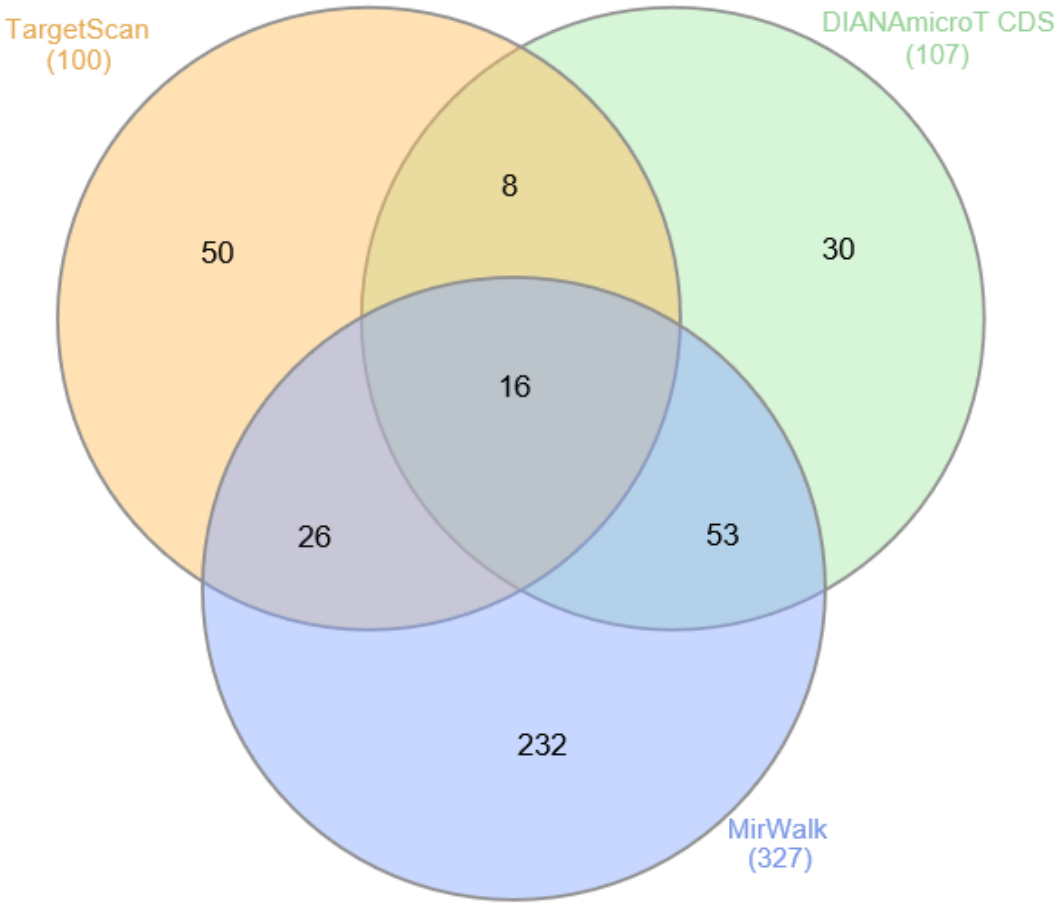

Figure 4: Quantitative presentation of predicted miRNA-mRNA interactions by TargetScan (orange), DIANAmicroT CDS (green) and MirWalk (blue). Numbers in different areas indicate positive hits in one, two or three target-prediction tools.

Thereby overlapping hits can be claimed as more representative, if a wider spectrum of target-prediction approaches is used.

Based on the quantity of hits, MirWalk (327) showed the least strict terms for possible interactions while TargetScan's (100) and DIANAmicroT CDS's (107) algorithms predicted almost the same number of interactions for the set. DIANAmicroT and MirWalk share the most positive hits (69) indicating greater similarities in their algorithms compared to overlapping hits with TargetScan. 16 miRNA-mRNA interactions were predicted in all three tools and, therefore, assumed as most likely possible (**Figure 4**).

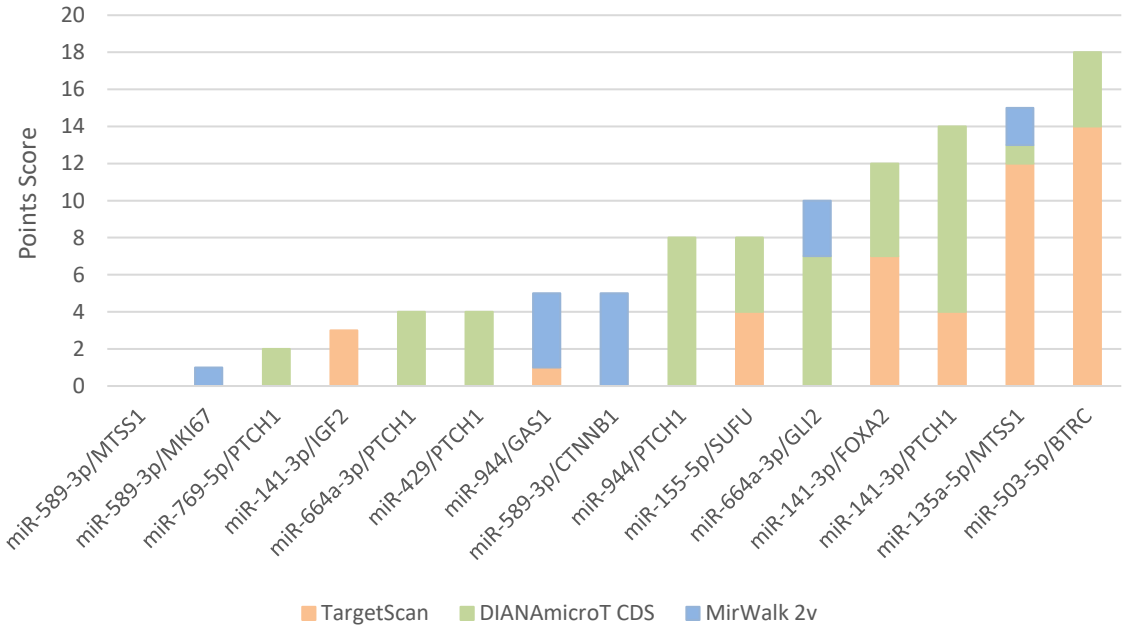

Figure 5: Final scores of miRNA-mRNA interactions after detailed analysis of the target-prediction tools parameter. 45 points were assigned by TargetScan and DIANAmicroT CDS respectively, while 15 points were assigned by MirWalk.

Detailed analysis of the tool's parameter scores for each interaction revealed five pairs with exact or more than "10" points (**Figure 5**) (see chapter "miRNA screening and *in silico* target-prediction analysis"). For TargetScan and DIANAmicroT CDS, three parameters were chosen to be considered for evaluation, while MirWalk contributed one score to overall ranking procedure (**Suppl. Figure 1**). miR-503-5p/-135a-5p/-141-3p/-664a-3p showed the most promising interactions with βTRC/MTSS1/PTCH1 as well as FOXA2/GLI2, respectively.

Among the top five ranked interactions, only miR-135a-5p/MTSS1 could show scorings in all three target-prediction tools, while points of the remaining four assembled from two tools. Based on those criteria, these top five predicted pairs qualified for further in vitro analyses.

For getting a deeper insight in the process of investigating deregulated miRNAs, and the fact that miR-503-5p, miR-135a-5p, miR-141-3p and miR-644a-3p are all down-regulated, four additional miRNAs with an upregulated status in A549 cells compared to bronchial epithelial cells were included for *in vitro* studies. These upregulated miRNAs were not chosen based on the exact selection procedure described above, but rather on studied literature in combination with sonic hedgehog target gene prediction results.

miR-589-3p and miR-27b-5p showed the most hits of potentially regulating sonic hedgehog genes, while miR-15b-3p was selected because of its upregulated status confirmed also *in vivo* in lung tissue by a different group (Wang et al., 2017). Additionally, miR-196a-5p were picked, due to its highest upregulated status in A549 compared to bronchial epithelial cells.

Except for miR-664a-3p, the deregulation status of all selected miRNAs can be verified in A549 lung cancer cell line

To clarify starting conditions for further experiments, deregulation status of selected miRNAs was verified by RT-qPCR. For miRNAs claimed as downregulated in previous panel-based screening, miR-141-3p/-135a-5p/-503-5p could be verified in a directed RT-qPCR approach, while miR-664a-3p did not show any differences in its expressional status in A549 compared to bronchial epithelial cells, and was therefore removed from further analyses (**Figure 6 (A)**).

Regulation status of additionally selected upregulated miRNAs were also tested in a directed RT-qPCR approach. miR-589-3p/-15b-3p/-27b-5p/-196a-5p expression status was upregulated in A549 cells compared to bronchial epithelial cells (**Figure 6 (B)**).

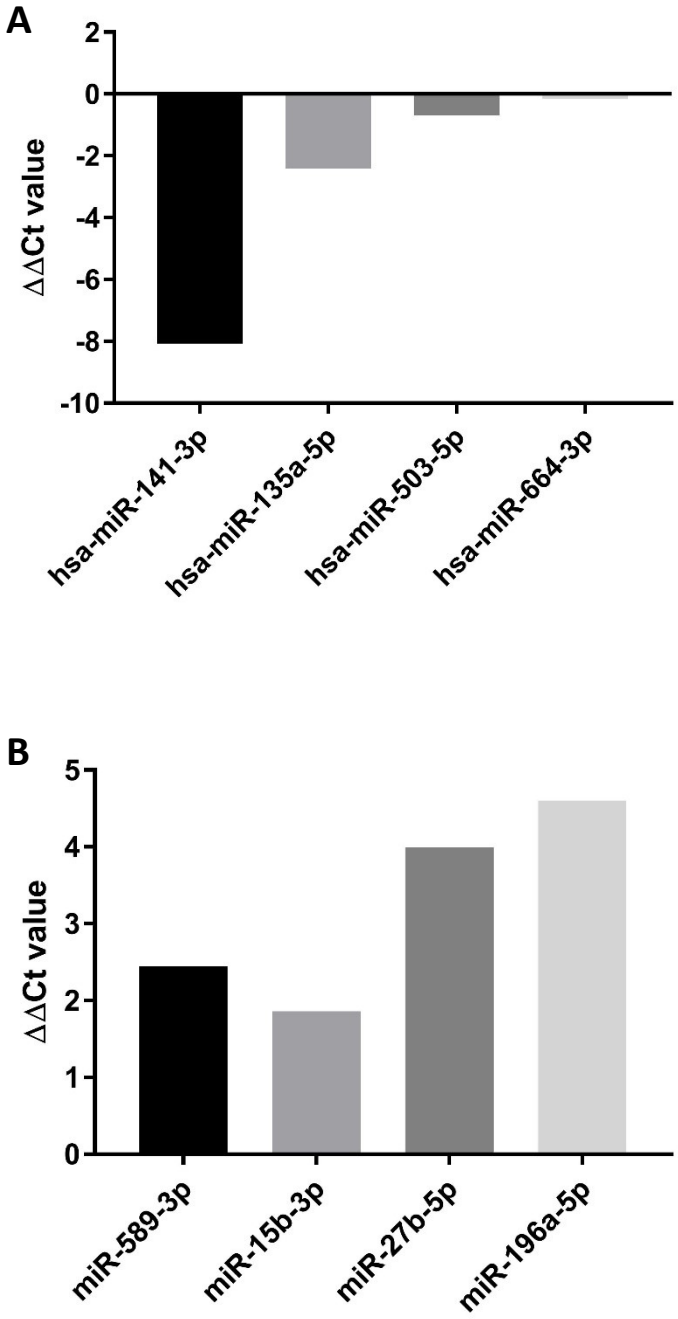

Figure 6: Expression levels of selected miRNAs in A549 compared to bronchial epithelial cells. Deregulation status is presented as ΔΔCt value, which was calculated by a two-step normalizing process. First, detection cycles of miRNAs were normalized to miR-92a-3p, a household-miRNA, by subtraction. Next, normalized cycle numbers for desired miRNAs of A549 were subtracted from the cycle number of the same miRNAs in bronchial epithelial cells, resulting in ΔΔCt values. **(A)** Regulation status of selected downregulated miRNAs, miR-141-3p/-135a-5p/-503-5p/-664-3p. **(B)** Regulation status of the additionally selected upregulated miRNAs, hsa-miR-589-3p/-15b-3p/-27b-5p/-196a-5p.

Expression of downregulated miR-141-3p, miR-135a-5p and miR-503-5p can be complemented by transfecting A549 cells with mimics

For investigating the phenotypic effect of underrepresented miRNAs in A549 cells, synthetical miRNAs, called miRNA-mimics, were used to complement their expressional level *in vitro*. miRNA expression levels should not be overrepresented, nor too low after transfection with miRNA-mimics. For ideal experimental conditions, the amount of transfected mimics should compensate missing miRNAs back to levels in bronchial epihelial cells.

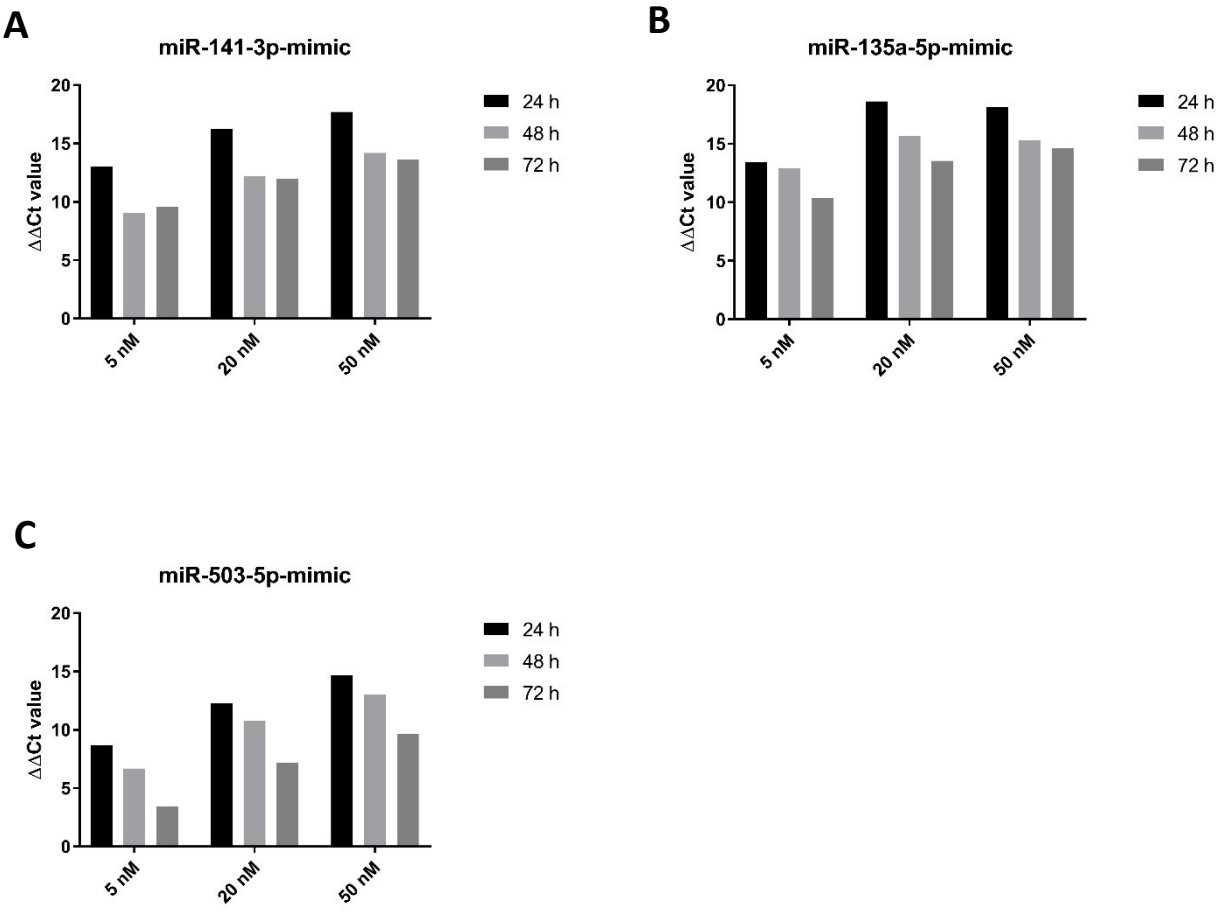

Figure 7: miRNA expression levels of mimic transfected A549 cells compared to appropriate controls. Three different mimic concentrations as well as three different time points were investigated after transfection. Expression status is shown in ΔΔCt values. **(A)** hsa-miR-141-3p levels after mimic transfection. **(B)** hsa-miR-135a-5p levels after mimic transfection. **(C)** hsa-miR-503-5p levels after mimic transfection.

For evaluating the amount of miRNA-mimics needed for appropriate compensation, mimic transfection was quantified by RT-qPCR. Also, transfection efficiency was checked by detecting DY544 labeld control-mimic via fluorescence microscopy.

All tested concentrations of transfected miRNA-mimics led to elevated levels of investigating miRNAs to all three time points (**Figure 7**). As expected, the amount of miRNA shrinks over time, due to their degradation during biological activity in the cells. Also, cell division leads to thinning out of miRNA-mimics over time. The same phenomena could have been observed with the help of fluorescence dye (DY544) labeled control-mimic based on fluorescence microscopy (**Figure 8**).

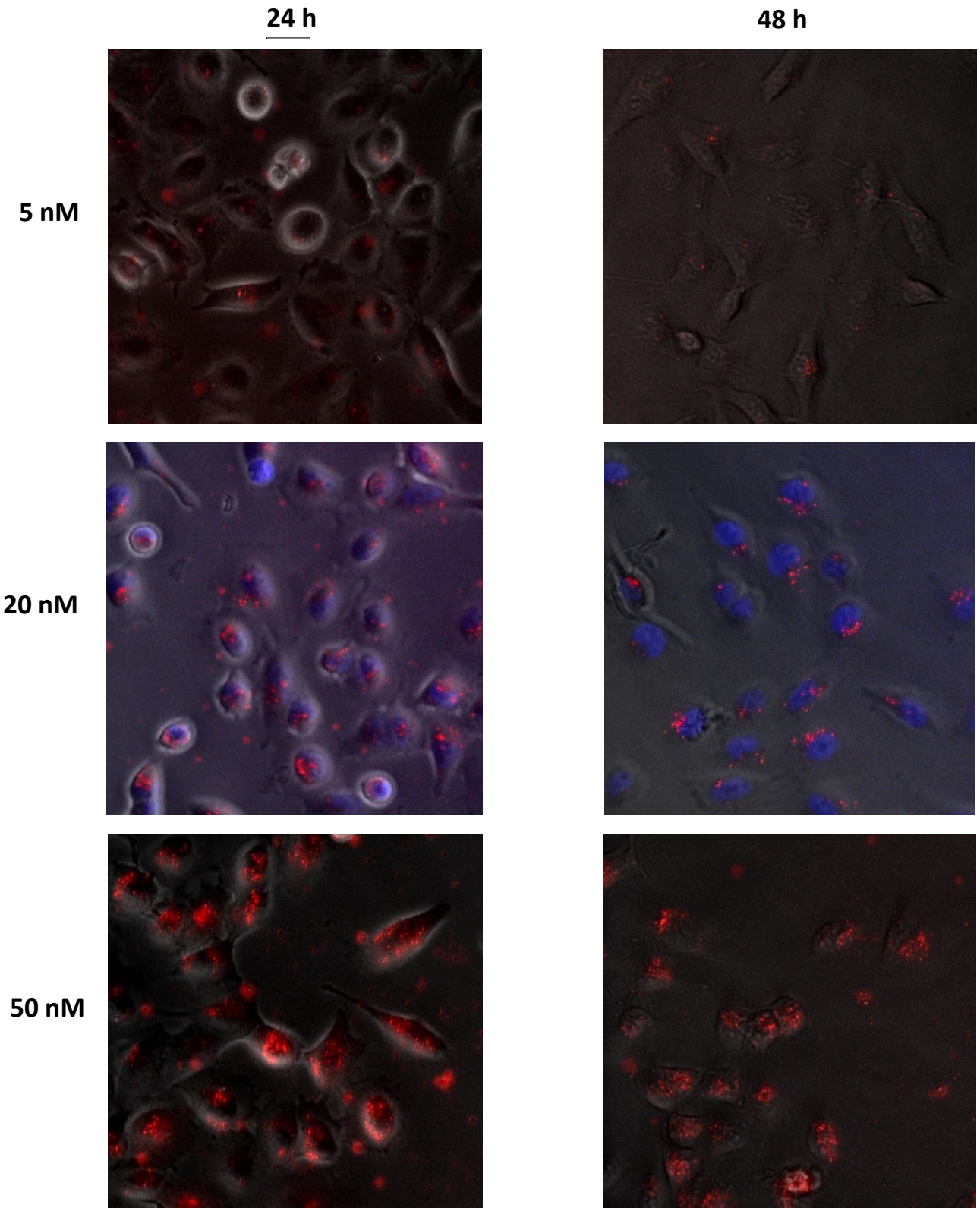

Figure 8: Testing transfection efficiency by detection of control-mimics tagged with DY544 in A549 cells via fluorescence microscopy. A549 cells were transfected with three different concentrations of control-mimic and observed 24 h and 48 h after transfection. Nulcei of cells transfected with 20 nM of control-mimic were additionally stained with Hoechst 33342.

After 24 h, transfecting cells with 5 nM of miRNA-mimics induced an increase in miRNAs expression of ~416 ($2^{\Delta\Delta Ct}$ of miR-503-5p) to ~8335 ($2^{\Delta\Delta Ct}$ of miR-141-3p) times compared to control-mimic transfected cells. With an expression difference of -308 times in A549 compared to bronchial epithelial cells, miR-141-3p is the most downregulated miRNA of all selected ones and could already be complemented by a mimic transfection concentration of 5 nM. Due to this fact, we decided to use 5 nM of mimics for all variants. **Figure 9** shows concentration of elected miRNAs after transfecting A549 cells with 5 nM of mimics as a function of time.

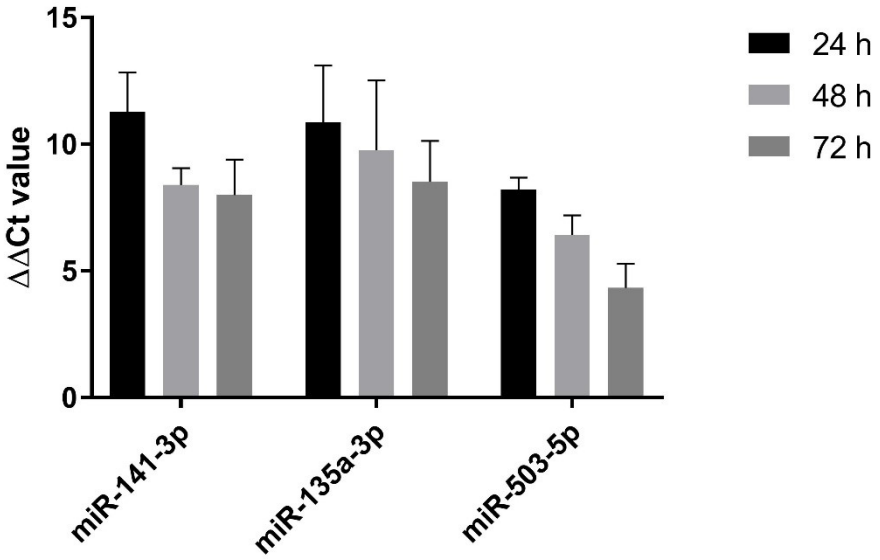

Figure 9: Validation of miRNA expression after complementation with miRNA-mimics. A549 cells were transfected with 5 nM of miRNA mimics and miRNA levels were measured by RT-qPCR after 24 h, 48 h and 72 h after transfection. Expression status is shown in ΔΔCt values. n = 3 for all samples.

As mentioned above, the amount of mimics in transfected cells decreases over time. Although different mimics share the same starting concentration for transfection, their depletion course differ from each other. miR-141-3p mimics show decreasing activity at 48 h, but from that point on their concentration remains unaltered until the 72 h time point. miR-135a-5p and miR-503-5p mimics share almost the same pattern of depletion over time but show differences in overall amounts of detectable mimics among all time points (**Figure 9**).

Expression level compensation of downregulated miRNAs does not influence the A549 cell growth

Alamar Assay based analysis of proliferation of A549 cells after transfected with 5 nM mimics for 24 h, showed no significant differences compared to the control group for all investigated miRNAs (**Figure 10**).

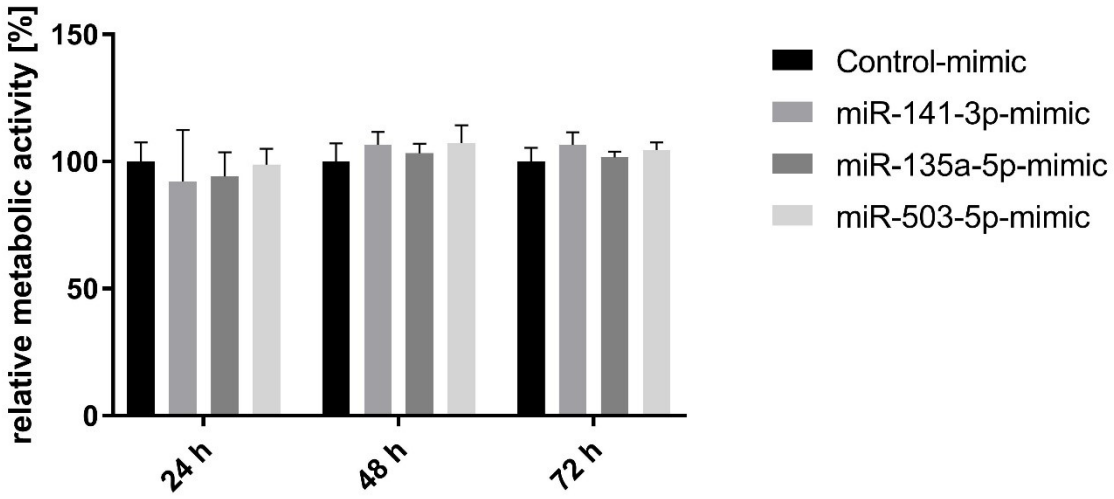

Figure 10: Proliferation/metabolic activity of mimic-transfected A549 cells measured by Alamar assay at three different time points. For measuring the cells proliferation rate/metabolic activity, pre-mixed Alamar reagent mix were added to cells in complete media and incubated for two hours at 37°C. Effects of 5 nM mimics were measured 24 h, 48 h and 72 h after transfection. All data were normalized to the control group at every time point. n = 3 for all samples.

Similar results were observed by analyzing the tumorigenic ability of A549 cells after transfection with 5 nM miRNA-mimics for 24 h (**Figure 11**) and 48 h (**Figure 12**). Neither in the count of cells, which were able to form colonies on their own, nor their colony size were affected by complementing downregulated miRNAs, compared to the control group.

After re-plating 300 cells 48 h upon transfection with miR-141-3p, slight differences in colony formation can be observed. These cells tended to form bigger colonies, but data were not confirmed as significant due to large standard deviation.

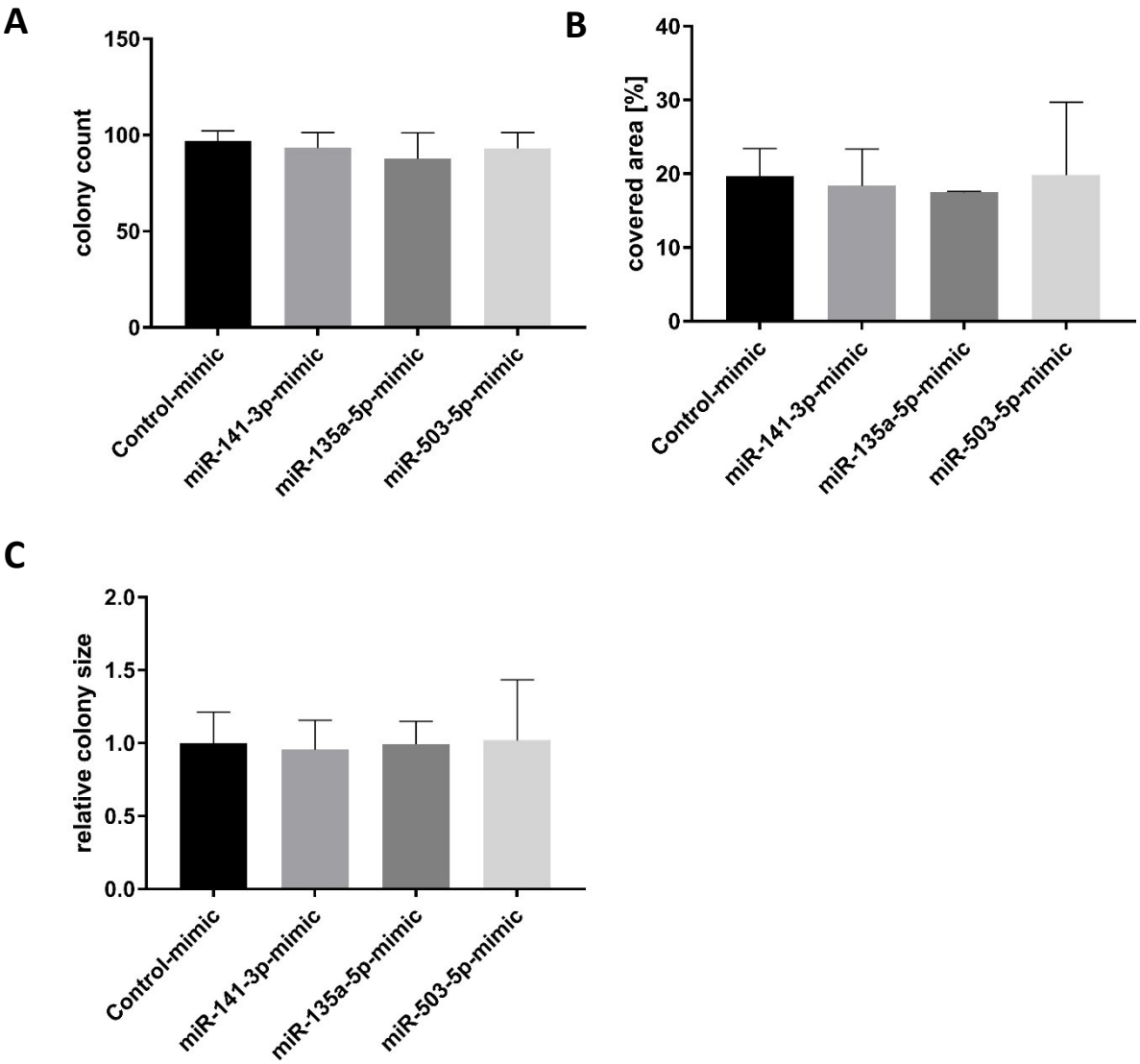

Figure 11: Investigation of A549 tumorigenic ability after transfection with 5 nM of miRNA-mimics for 24 h. 300 transfected cells were transferred on a fresh plate and incubated under standard conditions for 8 days. Cells were fixed, stained with crystal violet, and colonies were counted. **(A)** absolute colony count, **(B)** colony covered area of a 6-well plate, **(C)** shows colony-size (covered area – colony count) relative to the control group. n = 3 for all samples.

While investigating the cells proliferation rate and the ability to form colonies did not show any differences, testing the metastatic ability of miRNA-mimic-transfected cells showed significant differences for miR-141-3p at one time point. 24 h after performing a scratch on the cell monolayer, cells transfected with miR-141-3p-mimics showed significantly faster closure of the gap, compared to control cells. The same tendency can be recognized after 18 h of scratching but were not considered as significant (**Figure 13**).

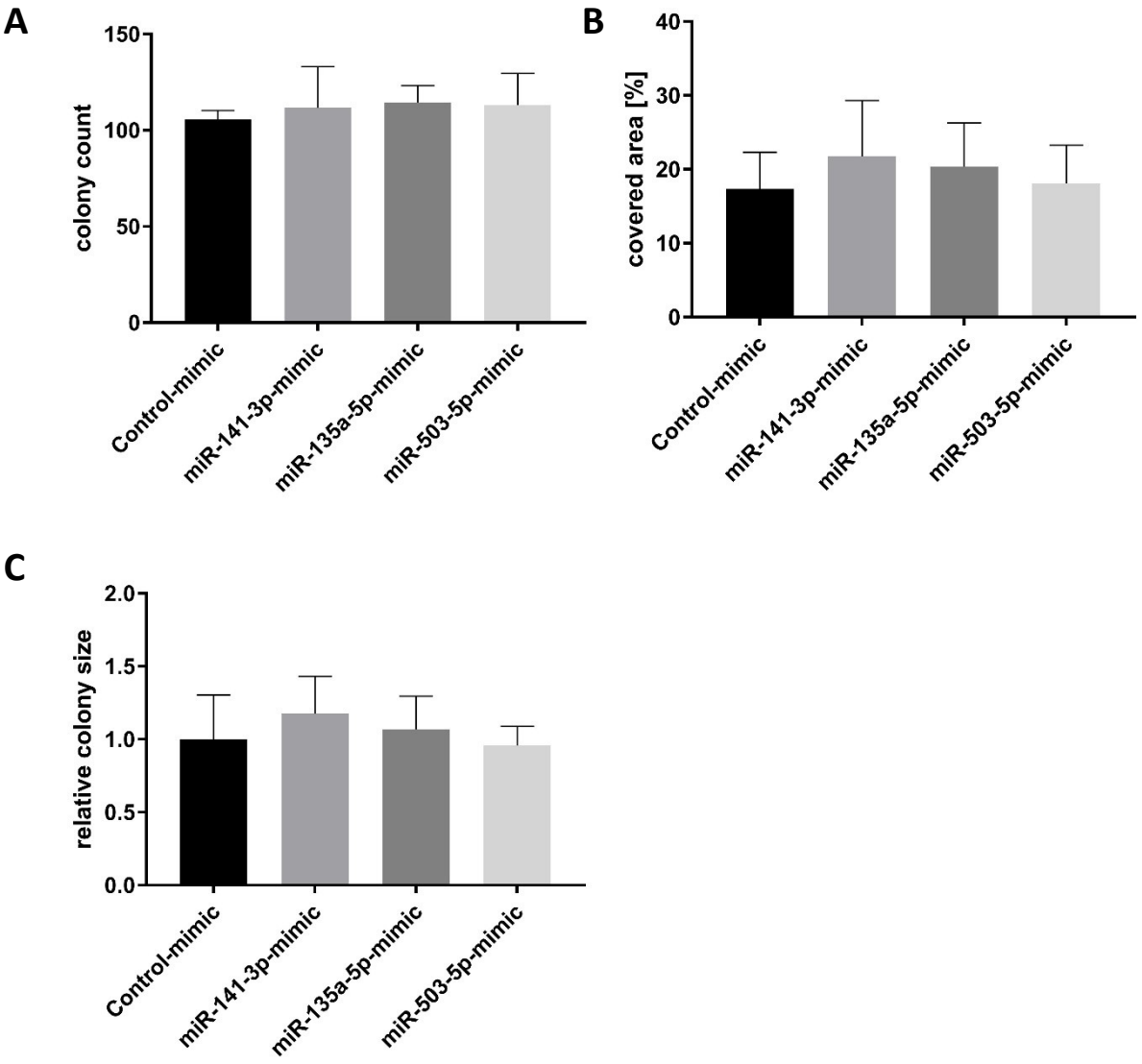

Figure 12: Investigation of A549 tumorigenic ability after transfection with 5 nM miRNA-mimics for 48 h. 300 transfected cells were transferred on a fresh plate and incubated under standard conditions for 8 days. Cells were fixed, stained with crystal violet, and colonies were counted. **(A)** absolute colony count, **(B)** colony covered area of a 6-well plate, **(C)** colony-size (covered area – colony count) relative to the control group. n = 3 for all samples.

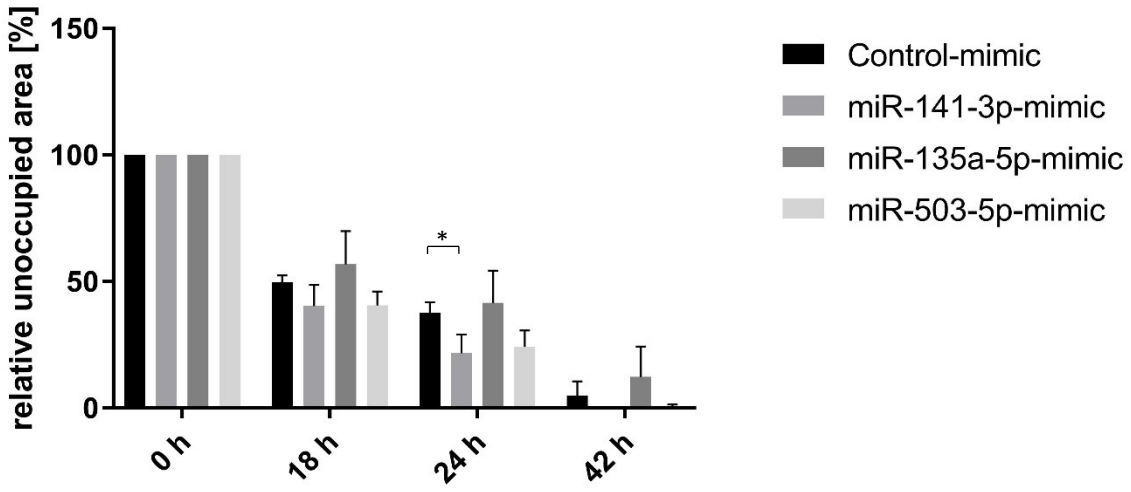

Figure 13: Metastatic ability of A549 cells transfected with 5 nM mimics for 24 h. Cells were cultured and transfected with 5 nM of mimics in 12-well plates. Once the cells reached a confluency of 85-95%, an artificial gap were generated by performing a straight scratch on the cell monolayer. At different time points, the cells ability of migration as well as their growth rate was observed by measuring the width of the gap. All data were normalized to the 0 h time point measurements of each construct. n = 3 for all samples.

miR-503-5p-mimic transfection leads to lower βTRC expression in A549 cells

Due to the fact that miRNAs regulate gene expression in a post-transcriptional manner, the mRNA of potential target genes were measured after transfection. Cells were transfected with 5 nM of miRNA-mimics for 24 h and RNA was harvested 24 h, 48 h and 72 h after transfection. FOXA2 and MTSS1 did not show any significant differences in changes of their mRNA at any of the three time points (**Figure 14 (A) – (C)**). PTCH1 mRNA levels after miR-141-3p-mimic treatment showed differences after 48 h but were considered as significant due to too small sample number.

Transfection with 5 nM of miR-503-5p-mimics showed a deregulating effect on βTRC mRNA, 24 h and 48 h after treatment. The level of mRNA was reduced to 50% at both time points. The signal recovers after 72 h of treatment nearly back to the amount of βTRC mRNA level in the control group. (**Figure 14 (D)**).

A

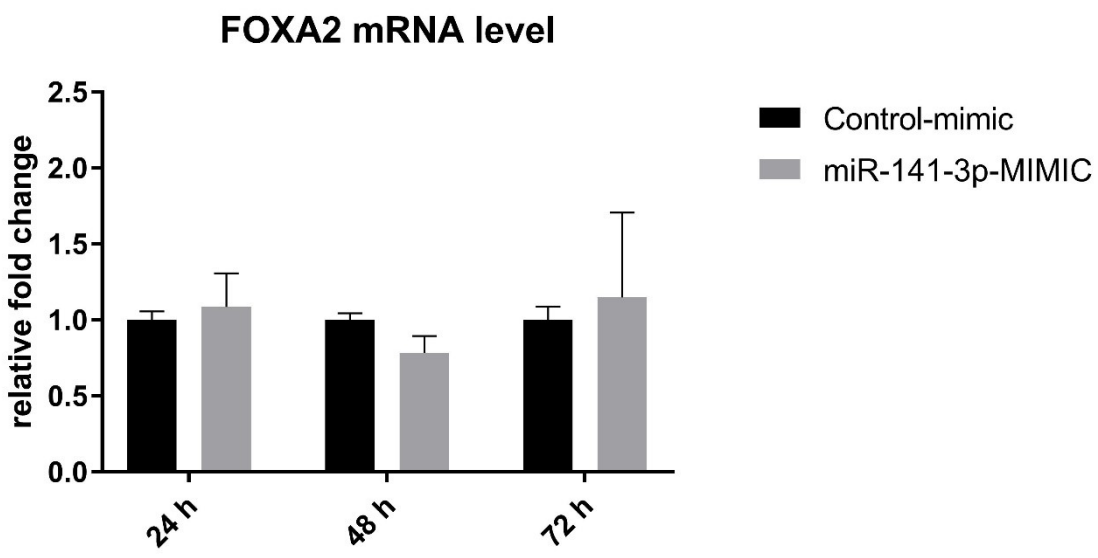
FOXA2 mRNA level
relative fold change
2.5
2.0
1.5
1.0
0.5
0.0
24 h
48 h
72 h
Control-mimic
miR-141-3p-MIMIC

B

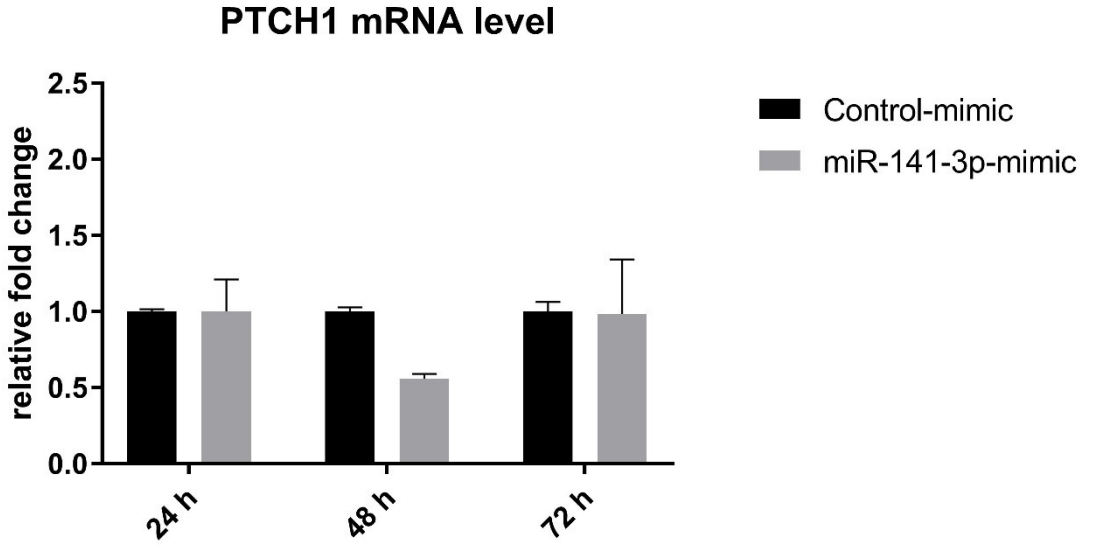
PTCH1 mRNA level
relative fold change
2.5
2.0
1.5
1.0
0.5
0.0
24 h
48 h
72 h
Control-mimic
miR-141-3p-mimic

C

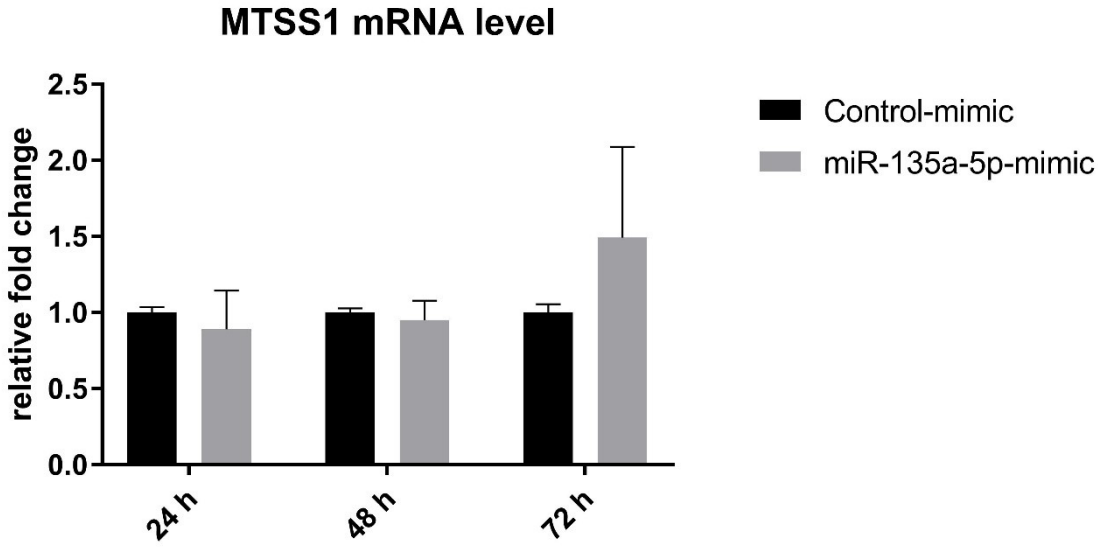
MTSS1 mRNA level
relative fold change
2.5
2.0
1.5
1.0
0.5
0.0
24 h
48 h
72 h
Control-mimic
miR-135a-5p-mimic

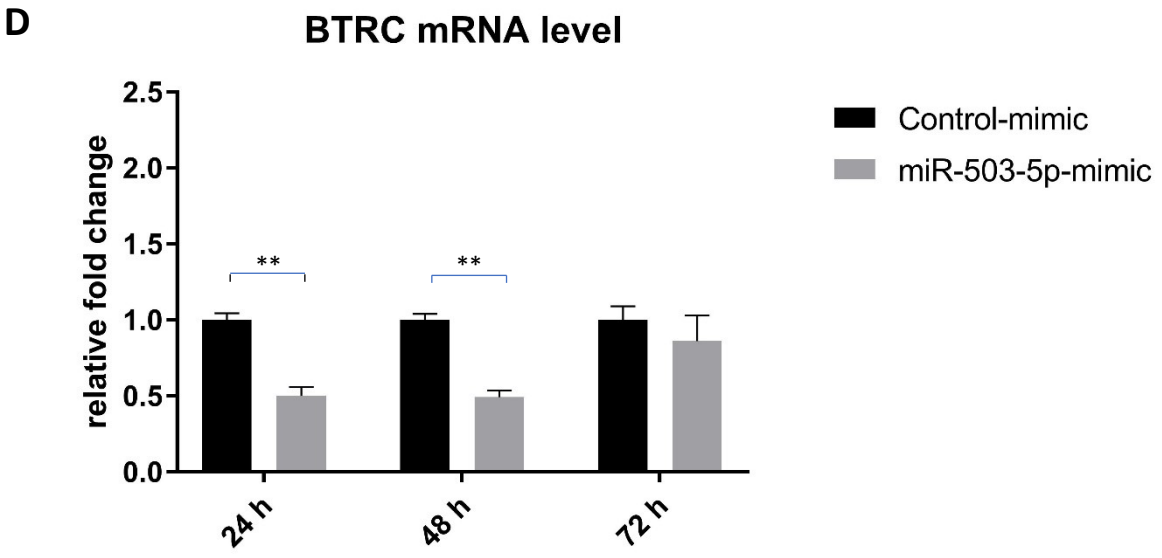

Figure 14: mRNA expression level of target genes after transfection of A549 cells with miRNA-mimics. RNA of miRNA-mimic-transfected cells was harvested at three different time points (24 h, 48 h and 72h). Transcriptional status of miRNA related target genes was evaluated by RT-qPCR. (**A**) and (**B**) mRNA level of FOXA2 and PTCH1 respectively, after transfection with 5 nM of miR-141-3p-mimic. (**C**) MTSS1 transcriptional level after transfection with 5 nM of miR-135a-5p-mimic. (**D**) βTRC transcriptional level after transfection with 5 nM of miR-503-5p-mimic. n =3 for all samples.

All results from measuring mRNA levels of target genes can be directly connected with results from verifying miRNA complementation via 5 nM miRNA-mimic transfection (**Figure G**), since mRNA/miRNA levels were detected from the same samples.

Furthermore, the effect of cell transfection with miR-135a-5p and miR-503-5p mimics on target genes on protein level were analyzed by western blotting.

MTSS1 was not downregulated on protein level after any time period of transfection with 20 nM miRNA-mimics (**Figure 15 (A)**). Protein expression levels of miR-503-5p-mimic transfected cells showed the same patterns as recognized on mRNA-level before. It seems that for 24 h and 48 h, βTRC is downregulated due to transfection with miRNA-mimics. After 72 h, no differences compared to the control-mimic transfected cells can be detected anymore. It appears that miR-503-5p-mimic has the most impact on protein level of βTRC after 48 h of transfection. This also can be misleading due to slightly unequal amount of protein loaded on the gel, if β-Actin references are compared.

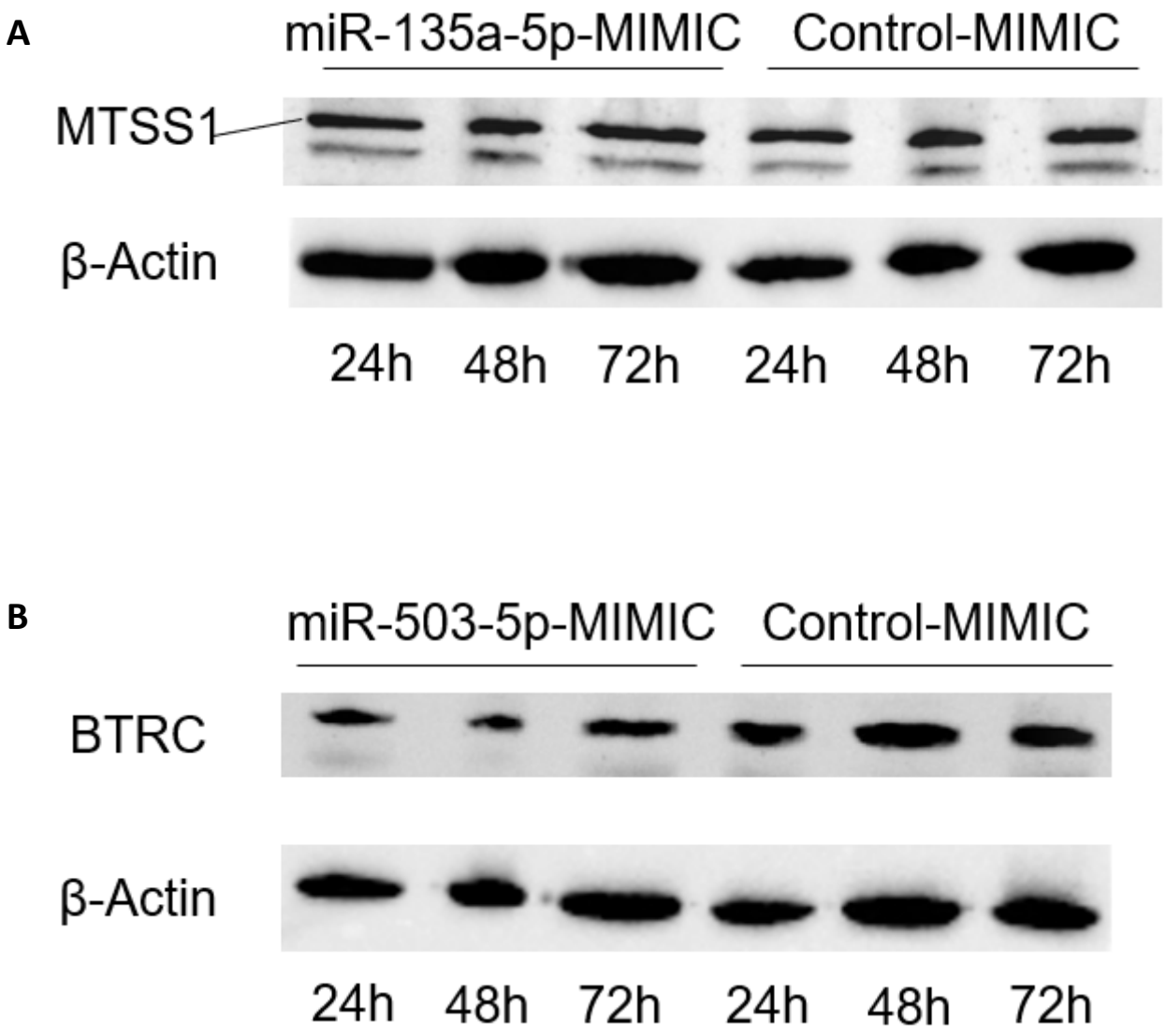

Figure 15: Protein expression analysis of target genes by western blotting after A549 transfection with miRNA-mimics. (A) A549 cells were transfected with 20 nM of miR-135a-5p-mimics for three different time points. β-Actin served as loading control for all samples. **(B)** Cells were transfected with 20 nM of miR-503-5p-mimic for three different time points. β-Actin served as loading control for all samples.

miR-135a-5p inhibits gene expression through binding on predicted target side

To examine direct interaction between miRNAs and their predicted target genes, luciferase assays were performed. For this purpose, the predicted seed sequence of miRNA – mRNA interaction was cloned in the 3'UTR of the *Renilla* reporter gene. If there is a real interaction with this cloned sequence, expression of *Renilla* will be post-transcriptionally repressed in the presence of the associated miRNA.

miR-135a-5p-mimic transfection could repress *Renilla* gene expression by 40% compared to the control group. This hints to a true interaction between miR-135a-5p and the cloned 3'UTR seed -region of MTSS1. Moreover, "MTSS1 MUT + miR-135a-5p" confirms the interaction at this particular site by recovering the signal almost back to the level of the control group (**Figure 16**). On the other hand, miR-503-5p-mimics could not reduce expression levels of *Renilla* in a significant way. Although a repression of 25% can be detected, the number of experiments was too little too low for significance differences. Again, mutating predicted interaction position recovers the signal back to the control groups activity (**Figure 17**).

Experiments were also performed with different amounts of miRNA-mimics, but the same amount of plasmid. 5 nM and 10 nM of MIMICs transfected into HEK293 showed less repression of the reporter gene for "MTSS1 WT + miR-135a-5p" and "βTRC WT + miR-503-5p" constructs (data not shown). All other combinations acted with no differences when used less mimics. This mimic - concentration depended behavior of reporter gene expression indicates further assumptions that the effect originates from transfected miRNA-mimics.

A

```
MTSS1   3'UTR   5'  -  ...TAAATGCATCCGAATAAGCCATACTGG... - 3'
(WT)                                      ||||||||
   miR-135a-5p     3'  -  AGUGUAUCCUUAUUUUCGGUAU  - 5'
MTSS1   3'UTR   5'  -  ...TAAATGCATCCGAATGGTAAGCGCTGG... - 3'
(MUT)
```

B

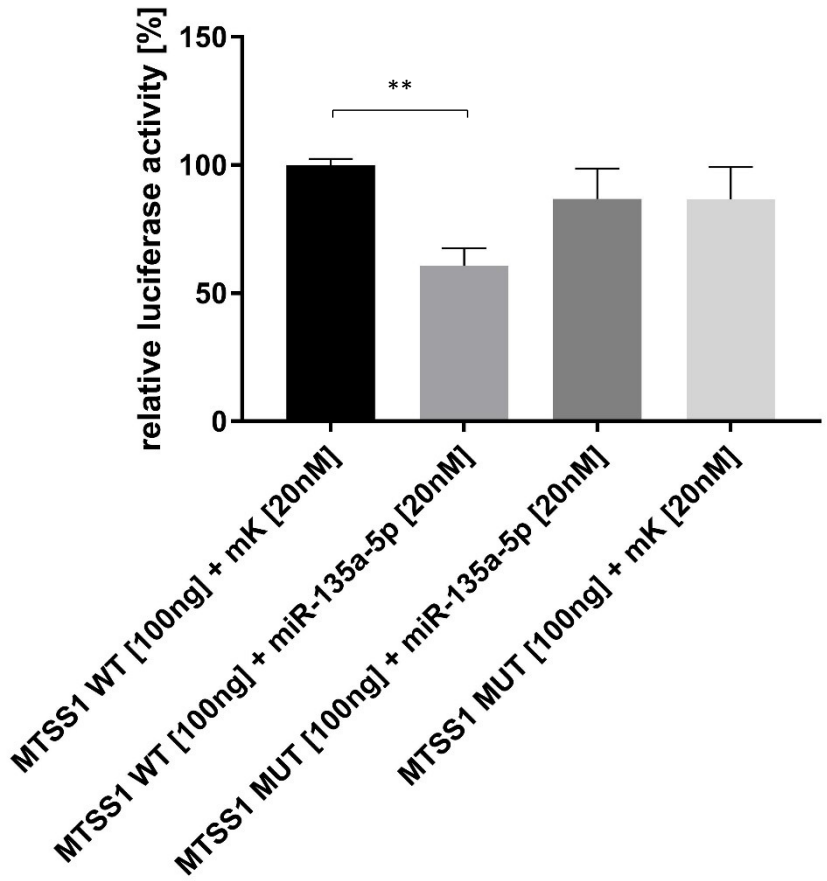

Figure 16: Dual luciferase interaction assay of miR-135a-5p and 3'UTR of MTSS1. (A) DNA sequences with wild-type and mutated predicted interaction position (indicated in bold letters) used in luciferase assay. Exact mRNA/miRNA interaction is indicated with dashes. **(B)** Relative luciferase activity was measured 48 h after transfection in HEK293. Cells were transfected with 0.5 µg/ml of dual luciferase reporter plasmid and 20 nM of miR-135a-5p-mimic. Luciferase activity was normalized two times for comparison. Firstly, treatment altered expression of the reporter-gene *Renilla* is normalized to firefly, an independent expression/transfection control on the same plasmid. Thus, "WT" and "MUT" are not quite the same plasmids and therefore their expressional ability cannot compared directly, all data were normalized to the base expression of the target gene to its corresponding plasmid as a second normalization step. "WT" indicates wild-type seed region of miRNA/mRNA interaction, "MUT" indicates mutated seed region and "mK" stands for control-mimic. n = 3 for all samples.

A

```
BTRC    3'UTR   5'  - ...CACAACTGACTGCTTCAGTGCTGCTAT... - 3'
(WT)                                       |||||||
      miR-503-5p      3' - GACGUCUUGACAAGGGCGACGAU- 5'
BTRC    3'UTR   5'  - ...CACAACTGACTGCTTCAGTTACTACGT... - 3'
(MUT)
```

B

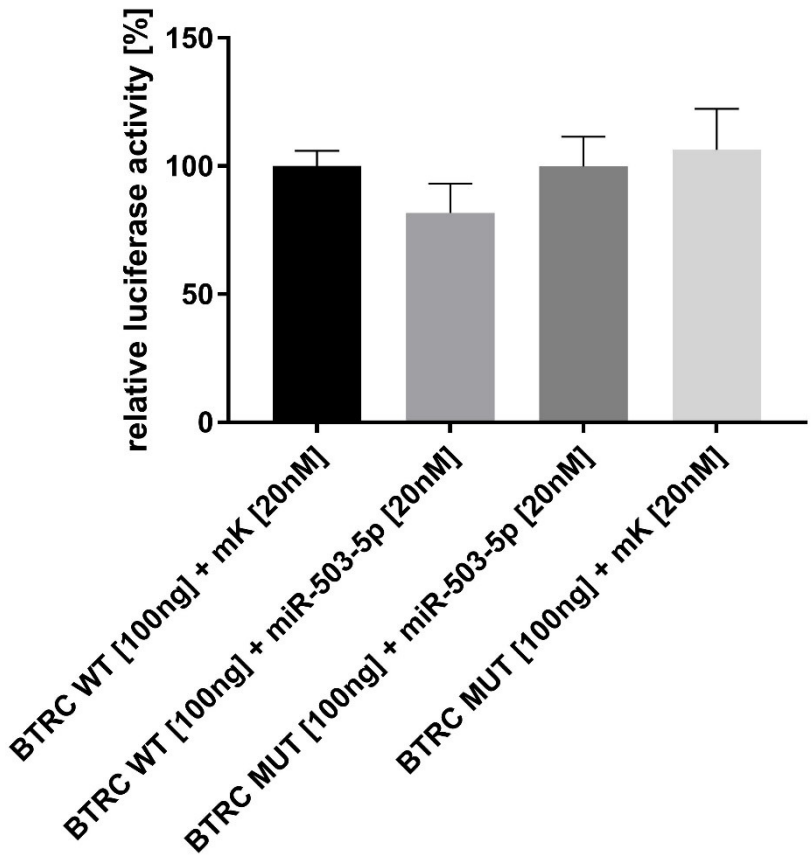

Figure 17: Dual luciferase interaction assay of miR-503-5p and 3'UTR of βTRC. (A) DNA sequences with wild-type and mutated predicted interaction position (indicated in bold letters) used in luciferase assay. Exact mRNA/miRNA interaction is indicated with dashes. **(B)** Relative luciferase activity was measured 48 h after transfection in HEK293. Cells were transfected with 0.5 µg/ml of dual luciferase reporter plasmid and 20 nM of miR-503-5p-mimic. Luciferase activity was normalized two times for comparison. Firstly, treatment altered expression of the reporter-gene *Renilla* is normalized to firefly, an independent expression/transfection control on the same plasmid. Thus, "WT" and "MUT" are not quite the same plasmids and therefore their expressional ability cannot compared directly, all data were normalized to the base expression of the target gene to its corresponding plasmid as a second normalization step. "WT" indicates wild-type seed region of miRNA/mRNA interaction, "MUT" indicates mutated seed region and "mK" stands for control-mimic. n = 3 for all samples.

Inhibitors for miR-27b-5p, miR-15b-3p and miR-196a-5p could repress overexpression of corresponding miRNAs in A549 cells

To investigate if the overexpression of certain miRNAs in A549 contribute to their cancerous ability, cells were transfected with specific miRNA-hairpin-inhibitors. To determine what amount of inhibitor is necessary for efficient miRNA inhibition, A549 cells were transfected with 10 nM and 30 nM for three different time points.

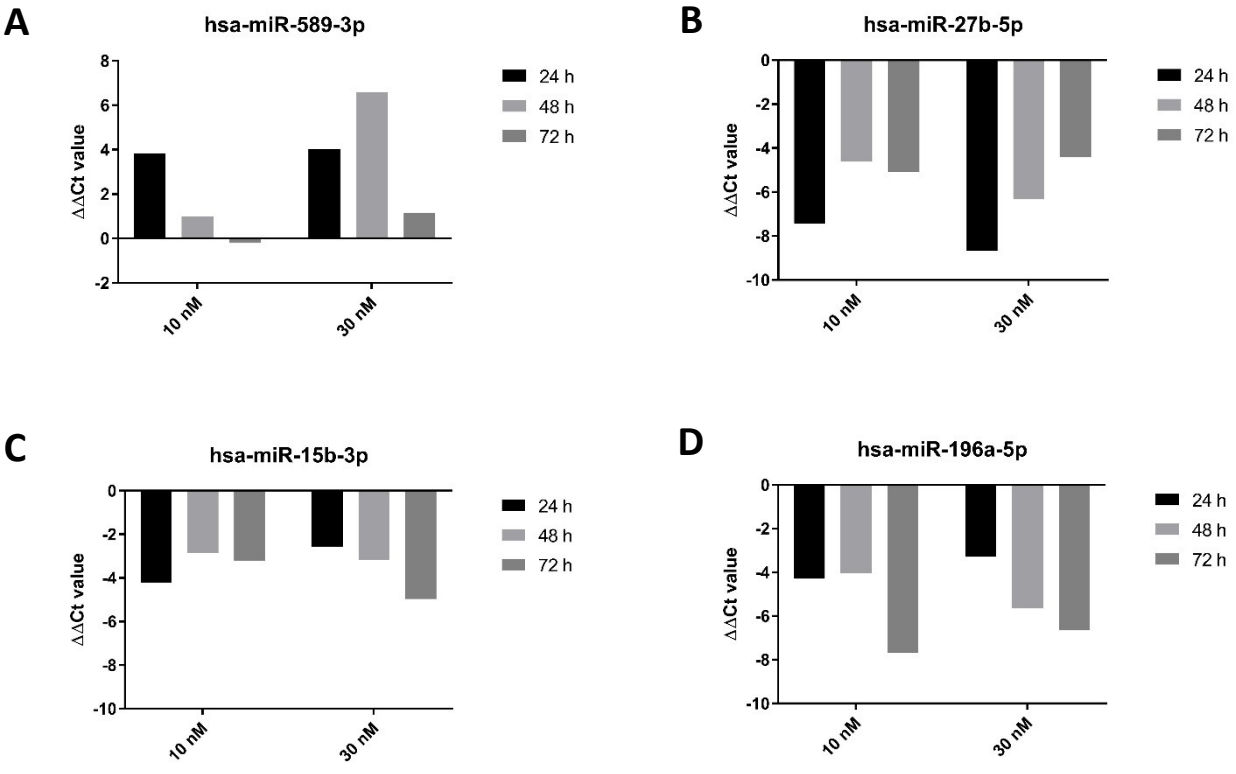

Figure 18: Validation of inhibition of upregulated miRNAs in A549 cells after transfecting with certain miRNA-hairpin-inhibitor. Two different inhibitor concentrations as well as three different time points were analyzed after transfection. Expression status is shown in ΔΔCt values. **(A)** miR-589-3p levels after mimic transfection. **(B)** miR-27b-5p levels after mimic transfection. **(C)** miR-15b-3p levels after mimic transfection. **(D)** miR-196a-5p levels after inhibitor transfection.

Different outcomes of inhibitor transfection can be observed for different miRNAs. miR-589-3p could not be repressed at any time point, but rather were more expressed after transfection. Inhibitors of miR-27b-5p could counteract overexpression in an expected way. Transfection with 30 nM of inhibitors led to a greater depletion than with 10 nM. Repressive ability of inhibitors subsides from time to time, which could also be observed upon cell transfecting with mimics. Inhibitors of miR-15b-3p and miR-196a-5p were also able to lower the expression of these miRNAs in A549 at all analyzed time point but showed rather unexpected ways of repression. Especially transfection of miR-196a-5p-inhibitor increased its effects on the corresponding miRNA over time, when compared to miR-27-5p expression course after inhibition (**Figure 18**).

Since miR-589-3p could not be repressed after cell transfection with miRNA-inhibitor, it was not considered for further investigation. Thus, miR-27b-5p, miR-15b-3p and miR-196a-5p were considered for further analyzing. We also decided that all follow-up experiments should be performed with 30 nM of miRNA-inhibitors.

Inhibition of miR-15b-3p and miR--196a-5p leads to overall suppression of A549 tumorigenic abilities

After optimization of the experimental conditions, cells were investigated regarding their proliferation, metastatic and tumorigenic abilities. Overall, inhibiting miR-15b-3p and miR-196a-5p in A549 cells implied poorer performance in all tests compared to the control group. Inhibition of miR-27b-5p on the other hand, showed boosting the cells cancerogenic abilities.

Especially proliferation was enhanced after treatment with 30 nM of miR-27b-5p inhibitors by up to 100%. Inhibition of miR-15b-3p led to a significantly lower proliferation rate after 72 h. In general, changes in cell proliferation as a consequence of transfection with miRNA-inhibitors can only be seen after 48 h. Theses alterations gets more drastic over time as it can be seen for 72 h (**Figure 19**).

Similar effects can be observed when performing motility assays. After 24 hours after scratching the transfected cell monolayer, differences in extents of occupying the free space can be observed in the same manner as seen in the proliferation assays. Inhibition of miR-27b-5p leads to faster closing of the gap, while cells with inhibited miR-15b-3p and miR-196a-5p need more time for sealing (**Figure 20**).

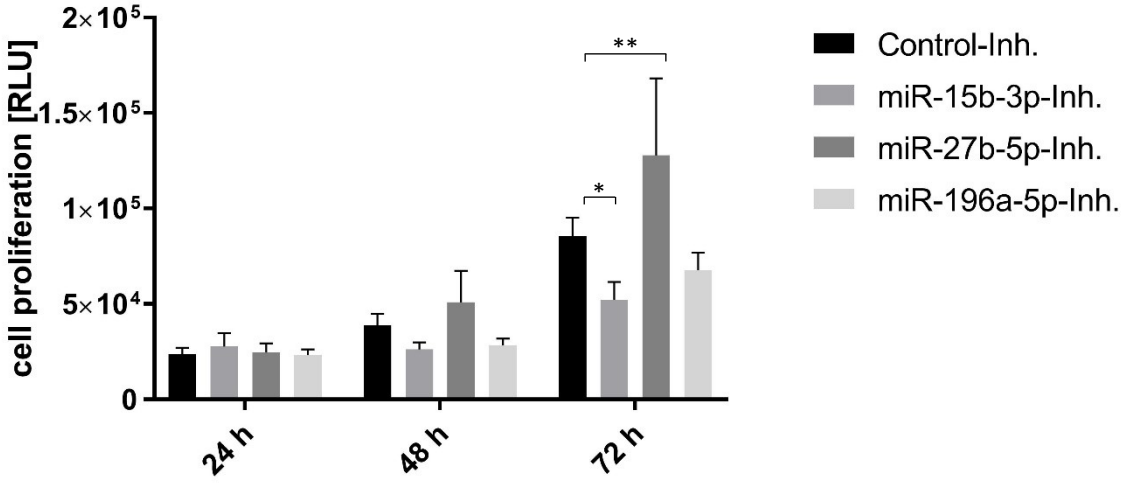

Figure 19: Proliferation/metabolic activity of A549 cells transfected with miRNA-inhibitors as measured by Alamar assay. For measuring the cells proliferation rate/metabolic activity, pre-mixed alamarBlue™ reagent mix were added to cells in complete media and incubated for two hours at 37°C. Then, by the cells converted substrate can be measured at a certain wavelength. Effects of 30 nM miRNA-hairpin-inhibitors were measured 24h, 48h and 72h after transfection. Values are shown in relative light units (RLU). n = 3 for all samples.

and hsa-miR-196a-5p in A549 cells implied poorer performance in all tests compared to the control group. Inhibition of miR-27b-5p on the other hand, showed boosting the cells cancerogenic abilities.

Especially proliferation was enhanced after treatment with 30 nM of miR-27b-5p inhibitors by up to 100%. Inhibition of miR-15b-3p led to a significant lower proliferation rate after 72 h. In general, changes as a consequence of transfection can only be seen after 48 h. Theses alterations gets more drastic over time as it can be seen for 72 h (**Figure 19**). The same effect can be observed when performing motility assays. After 24 h of scratching the transfected cells monolayer, differences in extents of occupying the free space can be observed in the same manner as seen before. Inhibiting miR-27b-5p leads to faster closing of the gap, while cells with inhibited miR-15b-3p and miR-196a-5p need more time for sealing (**Figure 20**).

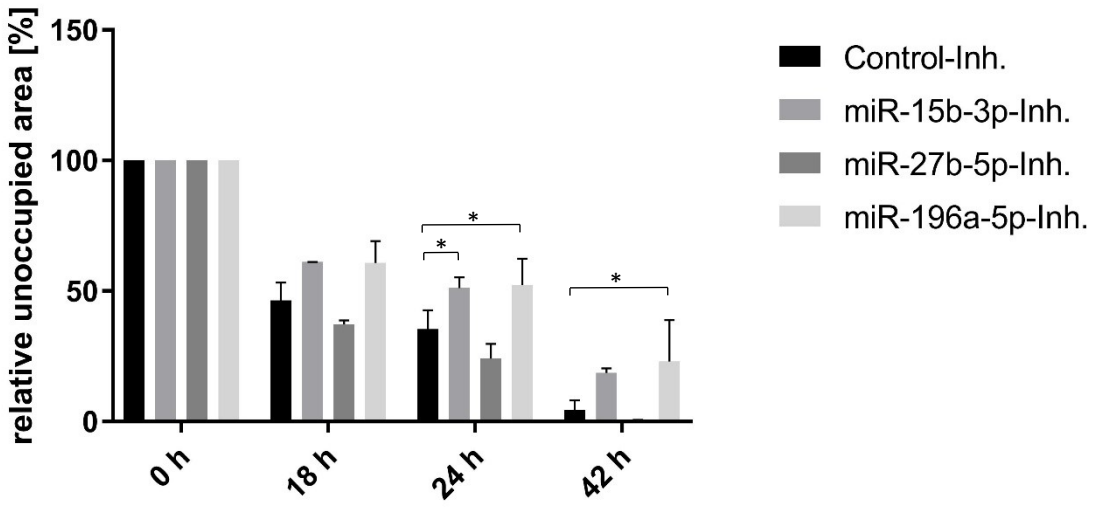

Figure 20: Metastatic ability of A549 cells after transfection with 30 nM miRNA-inhibitors. Cells were cultured and transfected with 30 nM of miRNA-inhibitors in 12-well plates for 24 h. Once the cells reached a confluence of 85-95%, an artificial gap were generated by performing a straight scratch on the cell monolayer. At indicated time points, the cells ability of migration as well as their growth rate was analyzed by measuring the width of the gap. Data for each construct were normalized to measurements at 0 h time point. n = 3 for all samples.

A549 cells show stronger activation of apoptosis after inhibiting miR-15b-3p and hsa-miR-196a-5p

Due to observations of dead cells upon transfection with miR-15b-3p and miR-196a-5p inhibitors, we decided to analyze their apoptotic status. For the sake of completeness, cells transfected with miR-27b-5p inhibitors were also analyzed. Cells transfected with miR-15b-3p as well as hsa-miR-196a-5p inhibitors did show higher signals for caspase 3 and 7 activities. Inhibiting miR-27b-5p led to lower activities of caspases, indicating a decrease of activation of apoptosis.

Although differences in apoptosis can be detected for all samples, they are relatively low – speaking of differences of about 1% in general, compared to the control (**Figure 21**).

Apoptosis could not have been measured for the 72 h time point due to experimental difficulties regarding cell density used in this approach. Due to lack of time, only one experiment was performed, which was not enough to fully represent the apoptotic status of A549 cells after transfection with miRNA-inhibitors in any significant way.

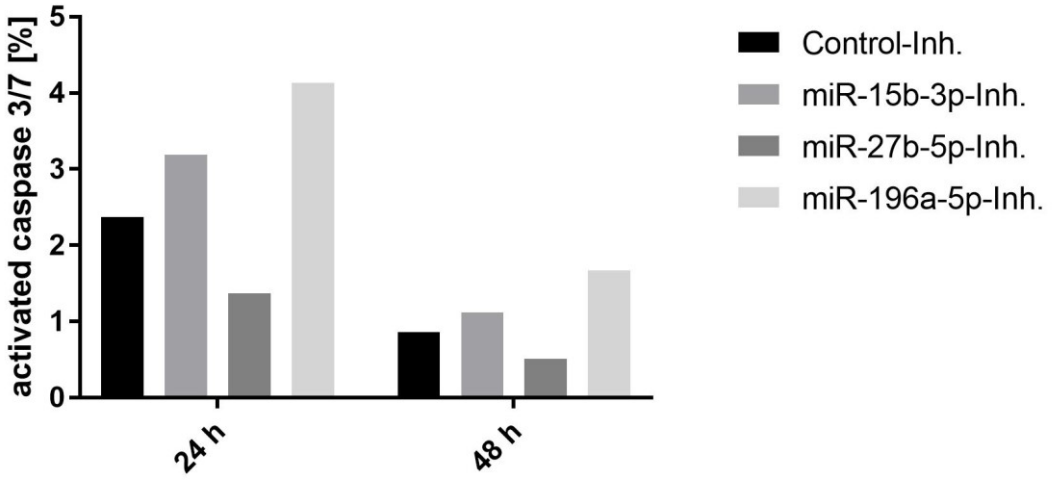

Figure 21: Caspase 3/7 activity at 24 h and 48 h after transfection with 30 nM miRNA-hairpin-inhibitors. A549 cells were transfected with 30 nM of inhibitors for 24 h and harvested at two different time points for analyzing their apoptotic status. Thus, the activities of caspase 3 and caspase 7 was measured by FACS. 10 000 events per construct were analyzed. n = 1 for all samples.

Discussion

Lung cancer is the most frequently diagnosed of all cancer types combined for both sexes. Therefore, fighting lung cancer is of particular interest for society. Especially in terms of cancer, methods of treatment rose to the next level over the last years. In this process personalized medicine bears big potential to elevate the chances of curing diseases. Modern genomic approaches open the door for further analyses individual tumors by sequencing their DNA, or detecting so called biomarkers, which define the tumors character in more detail. The, miRNAs discovered in 1980 not only act as such biomarkers but can, to certain extent, also be the cause of cancer cell malignancy. The use of miRNAs in diagnostic approaches opens up new opportunities for cancer treatment in general.

In the last two decades, the sonic hedgehog pathway (SHH) became prominent in cancer research as a driver pathway of cancer stem cells. Because relatively little is known about the SHH-pathway's regulation by miRNAs, we wanted to investigate if some miRNAs deregulated in the A549 cancer cell line can be connected to the most important sonic hedgehog pathway genes.

We used three different miRNA-mRNA *in silico* prediction tools to investigate, if a set of previously found deregulated miRNAs can be connected to the SHH pathway. Analysis of the top deregulated miRNAs with these web-based bioinformatic tools predicted that miR-141-3p regulates FOXA2 and PTCH1, miR-135a-5p regulates MTSS1, and miR-503-5p regulates βTRC.

A549 cells showed no significant phenotypic differences after complementing the expression of these downregulated miRNAs by transfecting cells with miRNA-mimics. That contradicts published results from other groups, who are working with the same miRNAs in A549 cells, though different miRNA-mimics concentrations were used.

In 2019, Li et al. showed that transfection of A549 cells with miR-141-3p-mimics could reduce cell proliferation, cell migration/invasion and the ability to form colonies. Due to the fact that miR-141-3p was also downregulated in their A549 cells and observing strong effects after mimic transfection, they concluded that miR-141-3p functions as a tumor suppressor in lung cancer cell lines (Li et al., 2019). The same effects showed Wei et al., after complementing the downregulated status of miR-503-5p in A549 (Wei

et al., 2019). It was also reported that transfection of A549 cells with miR-135a-5p-mimics led to reduced cancerous abilities (Zhou et al., 2017).

These results might suggest that we were not able to perform A549 cell transfection with mimics in an appropriate way. Although miRNA abundance after mimic transfection were verified by RT-qPCR and fluorescence microscopy, we cannot be sure that all of these detected miRNAs are located on the inside of the cell, nor that all are actually functional.

Since miRNA-mimics are affordable and fast solutions to investigate the role of particular miRNAs in different cell lines, they are frequently used in the last decade. Thereby, one problem can be observed throughout the field. Researchers use different amounts of mimics for their studies, commonly ranging from 25 nM to 100 nM. Considering our results in this study, transfecting A549 cells with 20 nM of specific miRNA- mimic led in average to a 1000-fold expression increase of particular miRNA. These amounts of transfected mimic are very high and probably cannot be set in a physiological context anymore. In 2015, Jin et al. investigated the effects of cell-transfection with different amounts of mimics commonly used and described throughout the literature, on cell survival and target specificity (Jin et al., 2015). They could show that cell growth is significantly retarded after transfecting cells upon 5 nM of cel-miR-67, a miRNA which can only be found in *C. elegans* and often used as a negative control in miRNA studies. They could also show that 100 nM of cel-miR-67 is able to repress the same targets on protein level as a mix of 100 nM of specific hsa-miR-15~92. This leads to the statement that high concentrations of miRNA-mimics can produce off-target effects, leading to false-positive results regarding phenotypical and molecular changes. This important work by Jin et al. questions all research on miRNAs, where mimics were used.

To overcome these concerns regarding transfection efficiency and unspecific effects, miRNAs should be expressed via plasmid-based transfection of the cells. Doubts about the proper cell transfection can be dismissed by detecting an increase of the expression level of specific miRNA via RT-qPCR, considering, that only inside the cell, miRNAs can be expressed from the plasmid. In addition, endogenous promotors decrease the chances for overloading the cell with miRNAs of one kind and therefore minimizes the possibility to observe unspecific effects.

Although transfecting A549 cells with 5 nM of miRNA-mimics did not show any phenotypical effects, it cannot be excluded that the predicted interactions are false. miR-503-5p-mimic could repress mRNA level of βTRC down to 50% after 24 h and 48 h. Immunoblots after cell transfection with 20 nM of miR-503-5p-mimic showed decreased expression of βTRC. These results indicate a true interaction of miR-503-5p with βTRC mRNA. A luciferase assay could not fully confirm this assumption, as 20 nM of miR-503-5p-mimics did not significantly decrease the expression of *Renilla*. Transfecting A549 cells with miR-135a-5p-mimics showed exactly the inverse results. miR-135a-5p-mimics could neither reduce mRNA level nor protein level of MTSS1, but on the other hand was able to inhibit the expression of *Renilla* in a much greater extent.

Despite the fact that the results of the luciferase assay for miR-503-5p/βTRC was not significant, miR-503-5p-mimics somehow affect βTRC expression. As mentioned before, 3'UTRs can often form secondary structures and therefore expose or mask potential miRNA-binding-sites. This is not considered into the experimental design of these luciferase assays, because not the whole 3'UTR of the target gene was cloned, but rather a sequence containing seed area. Therefore, this does not fully reflect the repressive extent of each miRNA *in situ* in this experimental approach. This could also explain our results concerning the interaction of miR-135a-5p with MTSS1. The predicted target sequence of MTSS1 might not be accessible for miR-135a-5p in the cell but is exposed for miRNA/mRNA interaction in our luciferase assay approach. Nevertheless, miR-503-5p-mimics show inhibition of βTRC on protein level, however, whether this inhibition is happening in a direct or indirect way needs to be further analyzed.

The beta-transducin repeat containing protein (βTRC) is a member of the F-box protein family which is involved in protein degradation by the proteasome. βTRC is a part of the E3 ubiquitin-ligase complex and forms together with the E1 ubiquitin-activating enzymes, the E2 ubiquitin-conjugating enzymes and the 26S proteasome the ubiquitin-proteasome-system. The E3 ubiquitin-ligase complex is responsible for substrate recognition. Several proteins are known to be regulated in a βTRC dependent manner, including different cell cycle proteins. It has been shown, that βTRC is overexpressed in certain cancer cell lines and tumor samples (Koch, 2005; Ougolkov et al., 2004). Additionally, the overexpression of βTRC in mice leads to tumor development in certain tissues (Belaïdouni et al., 2005).

Hence, the question arises, why we could not observe any phenotypical changes after cell transfection with miR-503-5p-mimic, which resulted in depletion of βTRC in A549 cells. This may be due to the fact, that mammals carry a paralog form of βTRC in their genome, called FBXW11 (βTRC2). FBXW11 is suggested to be mainly functional redundant to βTRC and can, therefore, compensate the loss of its related form. Additionally, while βTRC is only known in mammals, FBXW11 is highly conserved and can also be found in invertebrates, indicating a more fundamental role of FBXW11 than βTRC in general. Howsoever, a recent study questions the redundancy of the paralogs to each other, invalidating this explanations to a certain extant (Cui et al., 2019).

In contrast to investigation of downregulated miRNAs, lowering the expression status of selected upregulated miRNAs by transfecting A549 cells with specific miRNA-inhibitors, resulted in phenotypical effects for each miRNA. While transfecting cells with 30 nM of miR-15b-3p- and miR-196a-5p-inhibitors repressed cell growth, transfecting A549 cells with the same concentration of miR-27b-5p-inhibitors resulted in an increased cell growth.

Following our hypothesis that deregulated miRNAs lead to cancerous abilities (like enhanced growth rate), miR-15b-3p and miR-196a-5p are of great interest. Analyzing these miRNAs by searching for overlapping predictions in the top 100 hits of three target-prediction tools (DIANAmicroT CDS, MirWalkV3 and TargetScan 7.1) revealed interesting targets (data not shown). For example, it is predicted that miR-15b-3p targets TOPORS, a E3 ubiquitin ligase/E3 SUMO1-protein ligase, which is known to regulate cell growth by interacting with p53 (Lin et al., 2005), one of the most mutated proteins in all cancers combined. In addition, miR-15b-3p may regulate COMMD10, which is associated with the NF-kappaB pathway, acting as an inhibitor of the pathway and potentially as a tumor suppressor (Burstein et al., 2005).

For miR-196a-5p, among other hits, overlaps occurred for a possible interaction with RSPO2. RSPO2 acts as enhancer of the canonical Wnt-pathway by acting as a ligand for LGR4, LGR5 and LGR6 and inhibiting ZNRF3, another Wnt regulator (de Lau et al., 2011; Szenker-Ravi et al., 2018).

In a general perspective on this study, it has been observed that, in contrast to investigating downregulated miRNAs, changing the expression status of upregulated miRNAs has a much greater impact on the cells cancerous abilities. Whereas not one single downregulated miRNA showed any phenotypical effect when complemented,

individual inhibition of upregulated miRNAs resulted in severe alterations of cell growth. A precise explanation is still a matter of discussion and speculation. An idea would be, that complementing downregulated miRNAs have no effects, because their main targets also disappeared during cancer development. Therefore, changes in miRNA level would have no point of attack. Due to the small number of downregulated miRNAs investigated, this assumption remains speculative.

In fact, it has been observed that during cancer development, miRNA expression in general is downregulated, which will emerge as a common hallmark of cancer over the next years (Lin and Gregory, 2015). This was also indicated by our previous results, as 27 of 44 (~60%) miRNAs, deregulated in A549 cells compared to bronchial epithelial cells, are downregulated.

In summary, we managed to identify βTRC as a target of miR-503-5p, a significantly downregulated miRNA in the lung cancer cell line A549 compared to bronchial epithelial cells. This connection has never been shown before. Although, no differences in the cells cancerous abilities were identified on phenotypical level after transfection with 5 nM of miR-503-5p-mimics, on molecular levels these findings levels contribute to better a better understanding of the fine tuning of βTRCs expression network in tumor cells. Furthermore, we identified miR-15b-3p and miR-196a-5p as potential oncogenic miRNAs, as inhibiting their upregulated expression level led to severe growth defects of A549 cells in different experiments. Based on these promising results, future work will focus on identifying possible target genes of miR-15b-3p and miR-196a-5p, since these miRNAs or their target genes might play a role as possible drug targets in personalized medicine for lung cancer patients.

References

Agarwal, V., Bell, G.W., Nam, J.-W., and Bartel, D.P. (2015). Predicting effective microRNA target sites in mammalian mRNAs. ELife *4*, e05005.

Barr, M.P., Gray, S.G., Hoffmann, A.C., Hilger, R.A., Thomale, J., O'Flaherty, J.D., Fennell, D.A., Richard, D., O'Leary, J.J., and O'Byrne, K.J. (2013). Generation and Characterisation of Cisplatin-Resistant Non-Small Cell Lung Cancer Cell Lines Displaying a Stem-Like Signature. PLoS ONE *8*, e54193.

Beachy, P.A., Hymowitz, S.G., Lazarus, R.A., Leahy, D.J., and Siebold, C. (2010). Interactions between Hedgehog proteins and their binding partners come into view. Genes & Development *24*, 2001–2012.

Behm-Ansmant, I. (2006). mRNA degradation by miRNAs and GW182 requires both CCR4:NOT deadenylase and DCP1:DCP2 decapping complexes. Genes & Development *20*, 1885–1898.

Belaïdouni, N., Peuchmaur, M., Perret, C., Florentin, A., Benarous, R., and Besnard-Guérin, C. (2005). Overexpression of human βTrCP1 deleted of its F box induces tumorigenesis in transgenic mice. Oncogene *24*, 2271–2276.

Bhatia, N., Thiyagarajan, S., Elcheva, I., Saleem, M., Dlugosz, A., Mukhtar, H., and Spiegelman, V.S. (2006). Gli2 is targeted for ubiquitination and degradation by beta-TrCP ubiquitin ligase. J. Biol. Chem. *281*, 19320–19326.

Bjorge, J.D., Chan, T.O., Antczak, M., Kung, H.J., and Fujita, D.J. (1990). Activated type I phosphatidylinositol kinase is associated with the epidermal growth factor (EGF) receptor following EGF stimulation. Proceedings of the National Academy of Sciences *87*, 3816–3820.

Bowden, E.T., Stoica, G.E., and Wellstein, A. (2002). Anti-apoptotic Signaling of Pleiotrophin through Its Receptor, Anaplastic Lymphoma Kinase. J. Biol. Chem. *277*, 35862–35868.

Braun, J.E., Truffault, V., Boland, A., Huntzinger, E., Chang, C.-T., Haas, G., Weichenrieder, O., Coles, M., and Izaurralde, E. (2012). A direct interaction between DCP1 and XRN1 couples mRNA decapping to 5′ exonucleolytic degradation. Nat Struct Mol Biol *19*, 1324–1331.

Bray, F., Ferlay, J., Soerjomataram, I., Siegel, R.L., Torre, L.A., and Jemal, A. (2018). Global cancer statistics 2018: GLOBOCAN estimates of incidence and mortality worldwide for 36 cancers in 185 countries. CA: A Cancer Journal for Clinicians *68*, 394–424.

Buday, L., Downward, J., and Wc, L. Epidermal Growth Factor Regulates p21lils through the Formation of a Complex of Receptor, Grb2 Adapter Protein, and SOS Nucleotide Exchange Factor. 10.

Burden, S., and Yarden, Y. (1997). Neuregulins and Their Receptors: A Versatile Signaling Module in Organogenesis and Oncogenesis. Neuron *18*, 847–855.

Burstein, E., Hoberg, J.E., Wilkinson, A.S., Rumble, J.M., Csomos, R.A., Komarck, C.M., Maine, G.N., Wilkinson, J.C., Mayo, M.W., and Duckett, C.S. (2005). COMMD Proteins, a Novel Family of Structural and Functional Homologs of MURR1. J. Biol. Chem. *280*, 22222–22232.

Cantley, L.C. (2002). The Phosphoinositide 3-Kinase Pathway. Science *296*, 1655–1657.

Chamoun, Z. (2001). Skinny Hedgehog, an Acyltransferase Required for Palmitoylation and Activity of the Hedgehog Signal. Science *293*, 2080–2084.

Chen, L., Gibbons, D.L., Goswami, S., Cortez, M.A., Ahn, Y.-H., Byers, L.A., Zhang, X., Yi, X., Dwyer, D., Lin, W., et al. (2014). Metastasis is regulated via microRNA-200/ZEB1 axis control of tumour cell PD-L1 expression and intratumoral immunosuppression. Nat Commun *5*, 5241.

Chia, C.M., Winston, R.M.L., and Handyside, A.H. EGF, TGF-α and EGFR expression in human preimplantation embryos. 9.

Chiang, H.R., Schoenfeld, L.W., Ruby, J.G., Auyeung, V.C., Spies, N., Baek, D., Johnston, W.K., Russ, C., Luo, S., Babiarz, J.E., et al. (2010). Mammalian microRNAs: experimental evaluation of novel and previously annotated genes. Genes Dev. *24*, 992–1009.

Chu, C., and Rana, T.M. (2006). Translation Repression in Human Cells by MicroRNA-Induced Gene Silencing Requires RCK/p54. PLoS Biol *4*, e210.

Chuang, P.-T. (2003). Feedback control of mammalian Hedgehog signaling by the Hedgehog-binding protein, Hip1, modulates Fgf signaling during branching morphogenesis of the lung. Genes & Development *17*, 342–347.

Cui, D., Dai, X., Shu, J., Ma, Y., Wei, D., Xiong, X., and Zhao, Y. (2019). The cross talk of two family members of β-TrCP in the regulation of cell autophagy and growth. Cell Death Differ.

Duronio, V. (2008). The life of a cell: apoptosis regulation by the PI3K/PKB pathway. Biochem. J. *415*, 333–344.

Dweep, H., and Gretz, N. (2015). miRWalk2.0: a comprehensive atlas of microRNA-target interactions. Nat Methods *12*, 697–697.

Engelman, J.A., Luo, J., and Cantley, L.C. (2006). The evolution of phosphatidylinositol 3-kinases as regulators of growth and metabolism. Nat Rev Genet *7*, 606–619.

Fabbri, M., Garzon, R., Cimmino, A., Liu, Z., Zanesi, N., Callegari, E., Liu, S., Alder, H., Costinean, S., Fernandez-Cymering, C., et al. (2007). MicroRNA-29 family reverts aberrant methylation in lung cancer by targeting DNA methyltransferases 3A and 3B. Proceedings of the National Academy of Sciences *104*, 15805–15810.

Fang, D.D., Zhang, B., Gu, Q., Lira, M., Xu, Q., Sun, H., Qian, M., Sheng, W., Ozeck, M., Wang, Z., et al. (2014). HIP1–ALK, A Novel ALK Fusion Variant that Responds to Crizotinib. Journal of Thoracic Oncology *9*, 285–294.

Fujita, Y., Yagishita, S., Hagiwara, K., Yoshioka, Y., Kosaka, N., Takeshita, F., Fujiwara, T., Tsuta, K., Nokihara, H., Tamura, T., et al. (2015). The Clinical Relevance of the miR-197/CKS1B/STAT3-mediated PD-L1 Network in Chemoresistant Non-small-cell Lung Cancer. Molecular Therapy *23*, 717–727.

Fukaya, T., Iwakawa, H., and Tomari, Y. (2014). MicroRNAs Block Assembly of eIF4F Translation Initiation Complex in Drosophila. Molecular Cell *56*, 67–78.

Gentilella, A., Kozma, S.C., and Thomas, G. (2015). A liaison between mTOR signaling, ribosome biogenesis and cancer. Biochimica et Biophysica Acta (BBA) - Gene Regulatory Mechanisms *1849*, 812–820.

Grimson, A., Farh, K.K.-H., Johnston, W.K., Garrett-Engele, P., Lim, L.P., and Bartel, D.P. (2007). MicroRNA Targeting Specificity in Mammals: Determinants beyond Seed Pairing. Molecular Cell *27*, 91–105.

Grindley, J.C., Bellusci, S., Perkins, D., and Hogan, B.L. (1997). Evidence for the involvement of the Gli gene family in embryonic mouse lung development. Dev. Biol. *188*, 337–348.

Guzmán, C., Bagga, M., Kaur, A., Westermarck, J., and Abankwa, D. (2014). ColonyArea: An ImageJ Plugin to Automatically Quantify Colony Formation in Clonogenic Assays. PLoS ONE *9*, e92444.

Ha, M., and Kim, V.N. (2014). Regulation of microRNA biogenesis. Nat Rev Mol Cell Biol *15*, 509–524.

Hanahan, D., and Weinberg, R.A. (2000). The Hallmarks of Cancer. Cell *100*, 57–70.

Hanahan, D., and Weinberg, R.A. (2011). Hallmarks of Cancer: The Next Generation. Cell *144*, 646–674.

Ingham, P.W., Nakano, Y., and Seger, C. (2011). Mechanisms and functions of Hedgehog signalling across the metazoa. Nat Rev Genet *12*, 393–406.

Iqbal, M.A., Arora, S., Prakasam, G., Calin, G.A., and Syed, M.A. (2019). MicroRNA in lung cancer: role, mechanisms, pathways and therapeutic relevance. Molecular Aspects of Medicine *70*, 3–20.

Iwahara, T., Fujimoto, J., Wen, D., Cupples, R., Bucay, N., Arakawa, T., Mori, S., Ratzkin, B., and Yamamoto, T. Molecular characterization of ALK, a receptor tyrosine kinase expressed speci®cally in the nervous system. 11.

Ji, M., Guan, H., Gao, C., Shi, B., and Hou, P. (2011). Highly frequent promoter methylation and PIK3CA amplification in non-small cell lung cancer (NSCLC). BMC Cancer *11*, 147.

Ji, Z., Mei, F.C., Xie, J., and Cheng, X. (2007). Oncogenic KRAS Activates Hedgehog Signaling Pathway in Pancreatic Cancer Cells. J. Biol. Chem. *282*, 14048–14055.

Jia, J., Tong, C., Wang, B., Luo, L., and Jiang, J. (2004). Hedgehog signalling activity of Smoothened requires phosphorylation by protein kinase A and casein kinase I. Nature *432*, 1045–1050.

Jin, H.Y., Gonzalez-Martin, A., Miletic, A.V., Lai, M., Knight, S., Sabouri-Ghomi, M., Head, S.R., Macauley, M.S., Rickert, R.C., and Xiao, C. (2015). Transfection of microRNA Mimics Should Be Used with Caution. Front. Genet. *6*.

Johnson, R.L., Rothman, A.L., Xie, J., Goodrich, L.V., Bare, J.W., Bonifas, J.M., Quinn, A.G., Myers, R.M., Cox, D.R., Epstein, E.H., et al. (1996). Human homolog of patched, a candidate gene for the basal cell nevus syndrome. Science *272*, 1668–1671.

Jones-Rhoades, M.W., Bartel, D.P., and Bartel, B. (2006). MicroRNAs AND THEIR REGULATORY ROLES IN PLANTS. Annu. Rev. Plant Biol. *57*, 19–53.

Kasiri, S., Shao, C., Chen, B., Wilson, A.N., Yenerall, P., Timmons, B.C., Girard, L., Tian, H., Behrens, C., Wistuba, I.I., et al. (2017). GLI1 Blockade Potentiates the Antitumor Activity of PI3K Antagonists in Lung Squamous Cell Carcinoma. Cancer Res *77*, 4448–4459.

Kasper, M., Schnidar, H., Neill, G.W., Hanneder, M., Klingler, S., Blaas, L., Schmid, C., Hauser-Kronberger, C., Regl, G., Philpott, M.P., et al. (2006). Selective Modulation of Hedgehog/GLI Target Gene Expression by Epidermal Growth Factor Signaling in Human Keratinocytes. Molecular and Cellular Biology *26*, 6283–6298.

Khvorova, A., Reynolds, A., and Jayasena, S.D. Functional siRNAs and miRNAs Exhibit Strand Bias. 8.

Kim, D., Sung, Y.M., Park, J., Kim, S., Kim, J., Park, J., Ha, H., Bae, J.Y., Kim, S., and Baek, D. (2016). General rules for functional microRNA targeting. Nat Genet *48*, 1517–1526.

Koch, A. (2005). Elevated Expression of Wnt Antagonists Is a Common Event in Hepatoblastomas. Clinical Cancer Research *11*, 4295–4304.

Kozomara, A., Birgaoanu, M., and Griffiths-Jones, S. (2019). miRBase: from microRNA sequences to function. Nucleic Acids Research *47*, D155–D162.

Lapidot, T., Sirard, C., Vormoor, J., Murdoch, B., Hoang, T., Caceres-Cortes, J., Minden, M., Paterson, B., Caligiuri, M.A., and Dick, J.E. (1994). A cell initiating human acute myeloid leukaemia after transplantation into SCID mice. Nature *367*, 645–648.

de Lau, W., Barker, N., Low, T.Y., Koo, B.-K., Li, V.S.W., Teunissen, H., Kujala, P., Haegebarth, A., Peters, P.J., van de Wetering, M., et al. (2011). Lgr5 homologues associate with Wnt receptors and mediate R-spondin signalling. Nature *476*, 293–297.

Lewis, B.P., Shih, I., Jones-Rhoades, M.W., Bartel, D.P., and Burge, C.B. (2003). Prediction of Mammalian MicroRNA Targets. Cell *115*, 787–798.

Li, W., Cui, Y., Wang, D., Wang, Y., and Wang, L. (2019). MiR-141-3p functions as a tumor suppressor through directly targeting ZFR in non-small cell lung cancer. Biochemical and Biophysical Research Communications *509*, 647–656.

Lin, S., and Gregory, R.I. (2015). MicroRNA biogenesis pathways in cancer. Nat Rev Cancer *15*, 321–333.

Lin, L., Ozaki, T., Takada, Y., Kageyama, H., Nakamura, Y., Hata, A., Zhang, J.-H., Simonds, W.F., Nakagawara, A., and Koseki, H. (2005). topors, a p53 and topoisomerase I-binding RING finger protein, is a coactivator of p53 in growth suppression induced by DNA damage. Oncogene *24*, 3385–3396.

Mao, G., Liu, Y., Fang, X., Liu, Y., Fang, L., Lin, L., Liu, X., and Wang, N. (2015). Tumor-derived microRNA-494 promotes angiogenesis in non-small cell lung cancer. Angiogenesis *18*, 373–382.

Marcotullio, L.D., Greco, A., Mazzà, D., Canettieri, G., Pietrosanti, L., Infante, P., Coni, S., Moretti, M., Smaele, E.D., Ferretti, E., et al. (2011). Numb activates the E3 ligase Itch to control Gli1 function through a novel degradation signal. Oncogene *30*, 65–76.

McCormick, F. (2015). The potential of targeting Ras proteins in lung cancer. Expert Opinion on Therapeutic Targets *19*, 451–454.

McMahon, A.P., Ingham, P.W., and Tabin, C.J. (2003). Developmental roles and clinical significance of hedgehog signaling. Curr. Top. Dev. Biol. *53*, 1–114.

Milla, L.A., González-Ramírez, C.N., and Palma, V. (2012). Sonic Hedgehog in cancer stem cells: a novel link with autophagy. Biol. Res. *45*, 223–230.

Mizuarai, S., Kawagishi, A., and Kotani, H. (2009). Inhibition of p70S6K2 down-regulates Hedgehog/GLI pathway in non-small cell lung cancer cell lines. Mol. Cancer *8*, 44.

Motoyama, J., Liu, J., Mo, R., Ding, Q., Post, M., and Hui, C.C. (1998). Essential function of Gli2 and Gli3 in the formation of lung, trachea and oesophagus. Nat. Genet. *20*, 54–57.

Murray, P.B., Lax, I., Reshetnyak, A., Ligon, G.F., Lillquist, J.S., Natoli, E.J., Shi, X., Folta-Stogniew, E., Gunel, M., Alvarado, D., et al. (2015). Heparin is an activating ligand of the orphan receptor tyrosine kinase ALK. Sci. Signal. *8*, ra6–ra6.

Nüsslein-Volhard, C., and Wieschaus, E. (1980). Mutations affecting segment number and polarity in Drosophila. Nature *287*, 795–801.

Ott, C.E., Grünhagen, J., Jäger, M., Horbelt, D., Schwill, S., Kallenbach, K., Guo, G., Manke, T., Knaus, P., Mundlos, S., et al. (2011). MicroRNAs Differentially Expressed in Postnatal Aortic Development Downregulate Elastin via 3′ UTR and Coding-Sequence Binding Sites. PLoS ONE *6*, e16250.

Ougolkov, A., Zhang, B., Yamashita, K., Bilim, V., Mai, M., Fuchs, S.Y., and Minamoto, T. (2004). Associations Among -TrCP, an E3 Ubiquitin Ligase Receptor, -Catenin, and NF- B in Colorectal Cancer. JNCI Journal of the National Cancer Institute *96*, 1161–1170.

Palazzo, I.E.G. de, Adams, G.P., Sundareshan, P., Wong, A.J., Testa, J.R., Bigner, D.D., and Weiner, L.M. (1993). Expression of Mutated Epidermal Growth Factor Receptor by Non-Small Cell Lung Carcinomas. Cancer Res *53*, 3217–3220.

Pan, Y., Bai, C.B., Joyner, A.L., and Wang, B. (2006). Sonic hedgehog Signaling Regulates Gli2 Transcriptional Activity by Suppressing Its Processing and Degradation. Molecular and Cellular Biology *26*, 3365–3377.

Paraskevopoulou, M.D., Georgakilas, G., Kostoulas, N., Vlachos, I.S., Vergoulis, T., Reczko, M., Filippidis, C., Dalamagas, T., and Hatzigeorgiou, A.G. (2013). DIANA-microT web server v5.0: service integration into miRNA functional analysis workflows. Nucleic Acids Research *41*, W169–W173.

Perner, S., Wagner, P.L., Demichelis, F., Mehra, R., LaFargue, C.J., Moss, B.J., Arbogast, S., Soltermann, A., Weder, W., Giordano, T.J., et al. (2008). EML4-ALK Fusion Lung Cancer: A Rare Acquired Event. Neoplasia *10*, 298–302.

Petrova, R., and Joyner, A.L. (2014). Roles for Hedgehog signaling in adult organ homeostasis and repair. Development *141*, 3445–3457.

Po, A., Silvano, M., Miele, E., Capalbo, C., Eramo, A., Salvati, V., Todaro, M., Besharat, Z.M., Catanzaro, G., Cucchi, D., et al. (2017). Noncanonical GLI1 signaling promotes stemness features and in vivo growth in lung adenocarcinoma. Oncogene *36*, 4641–4652.

Porter, J.A., Young, K.E., and Beachy, P.A. (1996). Cholesterol Modification of Hedgehog Signaling Proteins in Animal Development. Science *274*, 255–259.

Powers, C., Aigner, A., Stoica, G.E., McDonnell, K., and Wellstein, A. (2002). Pleiotrophin Signaling through Anaplastic Lymphoma Kinase Is Rate-limiting for Glioblastoma Growth. J. Biol. Chem. *277*, 14153–14158.

Qin, Q., Wei, F., Zhang, J., Wang, X., and Li, B. (2016). miR-134 inhibits non-small cell lung cancer growth by targeting the epidermal growth factor receptor. J. Cell. Mol. Med. *20*, 1974–1983.

Quinlan, M.P., and Settleman, J. (2009). Isoform-specific ras functions in development and cancer. Future Oncology *5*, 105–116.

Rekhtman, N., Paik, P.K., Arcila, M.E., Tafe, L.J., Oxnard, G.R., Moreira, A.L., Travis, W.D., Zakowski, M.F., Kris, M.G., and Ladanyi, M. (2012). Clarifying the Spectrum of Driver Oncogene Mutations in Biomarker-Verified Squamous Carcinoma of Lung: Lack of EGFR/KRAS and Presence of PIK3CA/AKT1 Mutations. Clinical Cancer Research *18*, 1167–1176.

Ren, X.-S., Yin, M.-H., Zhang, X., Wang, Z., Feng, S.-P., Wang, G.-X., Luo, Y.-J., Liang, P.-Z., Yang, X.-Q., He, J.-X., et al. (2014). Tumor-suppressive microRNA-449a induces growth arrest and senescence by targeting E2F3 in human lung cancer cells. Cancer Letters *344*, 195–203.

Riobó, N.A., Lu, K., Ai, X., Haines, G.M., and Emerson, C.P. (2006). Phosphoinositide 3-kinase and Akt are essential for Sonic Hedgehog signaling. PNAS *103*, 4505–4510.

Rohatgi, R., Milenkovic, L., and Scott, M.P. (2007). Patched1 regulates hedgehog signaling at the primary cilium. Science *317*, 372–376.

Salim, H., Akbar, N.S., Zong, D., Vaculova, A.H., Lewensohn, R., Moshfegh, A., Viktorsson, K., and Zhivotovsky, B. (2012). miRNA-214 modulates radiotherapy response of non-small cell lung cancer cells through regulation of p38MAPK, apoptosis and senescence. Br J Cancer *107*, 1361–1373.

Samatar, A.A., and Poulikakos, P.I. (2014). Targeting RAS–ERK signalling in cancer: promises and challenges. Nat Rev Drug Discov *13*, 928–942.

Schneider, C.A., Rasband, W.S., and Eliceiri, K.W. (2012). NIH Image to ImageJ: 25 years of image analysis. Nat Methods *9*, 671–675.

Schneider, P., Miguel Bayo-Fina, J., Singh, R., Kumar Dhanyamraju, P., Holz, P., Baier, A., Fendrich, V., Ramaswamy, A., Baumeister, S., Martinez, E.D., et al. (2015). Identification of a novel actin-dependent signal transducing module allows for the targeted degradation of GLI1. Nat Commun *6*, 8023.

Scrima, M., De Marco, C., Fabiani, F., Franco, R., Pirozzi, G., Rocco, G., Ravo, M., Weisz, A., Zoppoli, P., Ceccarelli, M., et al. (2012). Signaling Networks Associated with AKT Activation in Non-Small Cell Lung Cancer (NSCLC): New Insights on the Role of Phosphatydil-Inositol-3 kinase. PLoS ONE *7*, e30427.

Shaw, R.J., and Cantley, L.C. (2006). Ras, PI(3)K and mTOR signalling controls tumour cell growth. Nature *441*, 424–430.

Silvennoinen, O., Schindler, C., Schlessinger, J., and Levy, D. (1993). Ras-independent growth factor signaling by transcription factor tyrosine phosphorylation. Science *261*, 1736–1739.

Soda, M., Choi, Y.L., Enomoto, M., Takada, S., Yamashita, Y., Ishikawa, S., Fujiwara, S., Watanabe, H., Kurashina, K., Hatanaka, H., et al. (2007). Identification of the transforming EML4–ALK fusion gene in non-small-cell lung cancer. Nature *448*, 561–566.

Stecca, B., and Ruiz i Altaba, A. (2009). A GLI1-p53 inhibitory loop controls neural stem cell and tumour cell numbers. The EMBO Journal *28*, 663–676.

Stecca, B., Mas, C., Clement, V., Zbinden, M., Correa, R., Piguet, V., Beermann, F., and Altaba, A.R. i (2007). Melanomas require HEDGEHOG-GLI signaling regulated by interactions between GLI1 and the RAS-MEK/AKT pathways. PNAS *104*, 5895–5900.

Stjernström, A., Karlsson, C., Fernandez, O.J., Söderkvist, P., Karlsson, M.G., and Thunell, L.K. (2014). Alterations of INPP4B, PIK3CA and pAkt of the PI3K pathway are associated with squamous cell carcinoma of the lung. Cancer Med *3*, 337–348.

Stoica, G.E., Kuo, A., Aigner, A., Sunitha, I., Souttou, B., Malerczyk, C., Caughey, D.J., Wen, D., Karavanov, A., Riegel, A.T., et al. (2001). Identification of Anaplastic Lymphoma Kinase as a Receptor for the Growth Factor Pleiotrophin. J. Biol. Chem. *276*, 16772–16779.

Stoica, G.E., Kuo, A., Powers, C., Bowden, E.T., Sale, E.B., Riegel, A.T., and Wellstein, A. (2002). Midkine Binds to Anaplastic Lymphoma Kinase (ALK) and Acts as a Growth Factor for Different Cell Types. J. Biol. Chem. *277*, 35990–35998.

Szenker-Ravi, E., Altunoglu, U., Leushacke, M., Bosso-Lefèvre, C., Khatoo, M., Thi Tran, H., Naert, T., Noelanders, R., Hajamohideen, A., Beneteau, C., et al. (2018). RSPO2 inhibition of RNF43 and ZNRF3 governs limb development independently of LGR4/5/6. Nature *557*, 564–569.

Takeuchi, K., Choi, Y.L., Togashi, Y., Soda, M., Hatano, S., Inamura, K., Takada, S., Ueno, T., Yamashita, Y., Satoh, Y., et al. (2009). KIF5B-ALK, a Novel Fusion Oncokinase Identified by an Immunohistochemistry-based Diagnostic System for ALK-positive Lung Cancer. Clinical Cancer Research *15*, 3143–3149.

The Cancer Genome Atlas Research Network (2012). Comprehensive genomic characterization of squamous cell lung cancers. Nature *489*, 519–525.

The Cancer Genome Atlas Research Network (2014). Comprehensive molecular profiling of lung adenocarcinoma. Nature *511*, 543–550.

Tian, J., Hu, L., Li, X., Geng, J., Dai, M., and Bai, X. (2016). MicroRNA-130b promotes lung cancer progression via PPARγ/VEGF-A/BCL-2-mediated suppression of apoptosis. J Exp Clin Cancer Res *35*, 105.

Togashi, Y., Soda, M., Sakata, S., Sugawara, E., Hatano, S., Asaka, R., Nakajima, T., Mano, H., and Takeuchi, K. (2012). KLC1-ALK: A Novel Fusion in Lung Cancer Identified Using a Formalin-Fixed Paraffin-Embedded Tissue Only. PLoS ONE *7*, e31323.

Travis, W.D., Brambilla, E., Noguchi, M., Nicholson, A.G., Geisinger, K.R., Yatabe, Y., Beer, D.G., Powell, C.A., Riely, G.J., Van Schil, P.E., et al. (2011). International Association for the Study of Lung Cancer/American Thoracic Society/European Respiratory Society International Multidisciplinary Classification of Lung Adenocarcinoma. Journal of Thoracic Oncology *6*, 244–285.

Travis, W.D., Brambilla, E., Nicholson, A.G., Yatabe, Y., Austin, J.H.M., Beasley, M.B., Chirieac, Lucian.R., Dacic, S., Duhig, E., Flieder, D.B., et al. (2015). The 2015 World Health Organization Classification of Lung Tumors. Journal of Thoracic Oncology *10*, 1243–1260.

Vescovo, V.D., and Denti, M.A. (2015). microRNA and Lung Cancer. In MicroRNA: Cancer, G. Santulli, ed. (Cham: Springer International Publishing), pp. 153–177.

Vogelstein, B., Papadopoulos, N., Velculescu, V.E., Zhou, S., Diaz, L.A., and Kinzler, K.W. (2013). Cancer Genome Landscapes. Science *339*, 1546–1558.

Wan, P.T.C., Garnett, M.J., Roe, S.M., Lee, S., Niculescu-Duvaz, D., Good, V.M., Project, C.G., Jones, C.M., Marshall, C.J., Springer, C.J., et al. (2004). Mechanism of Activation of the RAF-ERK Signaling Pathway by Oncogenic Mutations of B-RAF. Cell *116*, 855–867.

Wang, B., and Li, Y. (2006). Evidence for the direct involvement of {beta}TrCP in Gli3 protein processing. Proc. Natl. Acad. Sci. U.S.A. *103*, 33–38.

Wang, H., Zhan, Y., Jin, J., Zhang, C., and Li, W. (2017). MicroRNA-15b promotes proliferation and invasion of non-small cell lung carcinoma cells by directly targeting TIMP2. Oncology Reports *37*, 3305–3312.

Wang, Y., Ding, Q., Yen, C.-J., Xia, W., Izzo, J.G., Lang, J.-Y., Li, C.-W., Hsu, J.L., Miller, S.A., Wang, X., et al. (2012). The Crosstalk of mTOR/S6K1 and Hedgehog Pathways. Cancer Cell *21*, 374–387.

Wang, Y.-W., Tu, P.-H., Lin, K.-T., Lin, S.-C., Ko, J.-Y., and Jou, Y.-S. (2011). Identification of Oncogenic Point Mutations and Hyperphosphorylation of Anaplastic Lymphoma Kinase in Lung Cancer. Neoplasia *13*, 704-IN24.

Wei, X., Shen, X., Ren, Y., and Hu, W. (2018). The Roles of microRNAs in Regulating Chemotherapy Resistance of Non-Small Cell Lung Cancer. CPD *23*, 5983–5988.

Wei, Y., Liao, Y., Deng, Y., Zu, Y., Zhao, B., and Li, F. (2019). MicroRNA-503 Inhibits Non-Small Cell Lung Cancer Progression By Targeting PDK1/PI3K/AKT Pathway. OTT *Volume 12*, 9005–9016.

Wellbrock, C., Karasarides, M., and Marais, R. (2004). The RAF proteins take centre stage. Nat Rev Mol Cell Biol *5*, 875–885.

Wightman, B., Ha, I., and Ruvkun, G. (1993). Posttranscriptional regulation of the heterochronic gene lin-14 by lin-4 mediates temporal pattern formation in C. elegans. Cell *75*, 855–862.

Wong, D.W.-S., Leung, E.L.-H., So, K.K.-T., Tam, I.Y.-S., Sihoe, A.D.-L., Cheng, L.-C., Ho, K.-K., Au, J.S.-K., Chung, L.-P., Pik Wong, M., et al. (2009). The *EML4-ALK* fusion gene is involved in various histologic types of lung cancers from nonsmokers with wild-type *EGFR* and *KRAS*. Cancer *115*, 1723–1733.

Wu, H., Ye, C., Ramirez, D., and Manjunath, N. (2009). Alternative processing of primary microRNA transcripts by Drosha generates 5’ end variation of mature microRNA. PLoS ONE *4*, e7566.

Wulf, M.-A., Bode, B., Zimmermann, D., Rufibach, K., Weder, W., Moch, H., Soltermann, A., and Tischler, V. (2012). Silver-enhanced In Situ Hybridization for Determination of EGFR Copy Number Alterations in Non–Small Cell Lung Cancer: The American Journal of Surgical Pathology *36*, 1801–1808.

Yanagawa, N., Leduc, C., Kohler, D., Saieg, M.A., John, T., Sykes, J., Yoshimoto, M., Pintilie, M., Squire, J., Shepherd, F.A., et al. (2012). Loss of Phosphatase and Tensin Homolog Protein Expression Is an Independent Poor Prognostic Marker in Lung Adenocarcinoma. Journal of Thoracic Oncology *7*, 1513–1521.

Yarden, Y., and Sliwkowski, M.X. (2001). Untangling the ErbB signalling network. Nat Rev Mol Cell Biol *2*, 127–137.

Zaporozhchenko, I.A., Morozkin, E.S., Ponomaryova, A.A., Rykova, E.Y., Cherdyntseva, N.V., Zheravin, A.A., Pashkovskaya, O.A., Pokushalov, E.A., Vlassov, V.V., and Laktionov, P.P. (2018). Profiling of 179 miRNA Expression in Blood Plasma of Lung Cancer Patients and Cancer-Free Individuals. Sci Rep *8*, 6348.

Zekri, L., Kuzuoğlu-Öztürk, D., and Izaurralde, E. (2013). GW182 proteins cause PABP dissociation from silenced miRNA targets in the absence of deadenylation. EMBO J *32*, 1052–1065.

Zhen, Q., Liu, J., Gao, L., Liu, J., Wang, R., Chu, W., Zhang, Y., Tan, G., Zhao, X., and Lv, B. (2015). MicroRNA-200a Targets EGFR and c-Met to Inhibit Migration, Invasion, and Gefitinib Resistance in Non-Small Cell Lung Cancer. Cytogenet Genome Res *146*, 1–8.

Zheng, M. (2016). Classification and Pathology of Lung Cancer. Surgical Oncology Clinics of North America *25*, 447–468.

Zhou, Y., Li, S., Li, J., Wang, D., and Li, Q. (2017). Effect of microRNA-135a on Cell Proliferation, Migration, Invasion, Apoptosis and Tumor Angiogenesis Through the IGF-1/PI3K/Akt Signaling Pathway in Non-Small Cell Lung Cancer. Cell Physiol Biochem *42*, 1431–1446.

Zhu, B., Cao, X., Zhang, W., Pan, G., Yi, Q., Zhong, W., and Yan, D. (2019). MicroRNA-31-5p enhances the Warburg effect *via* targeting FIH. The FASEB Journal *33*, 545–556.

(2018). International Agency for Research on Cancer PRESS RELEASE N° 263, September 2018. 3.

ΔΔCt A549 vs BEC	miRNA	Gene	TargetScan SiteType	TargetScan context++	TargetScan context++ percentile	TargetScan Pct	DIANAmicroT CDS Ranking	DIANAmicroT CDS miTG-Score	DIANAmicroT CDS in organisms conserved	MirWalk 2v pValue	SUM
-8,22	hsa-miR-141-3p	PTCH1	8mer	-0,18	92	0,7	43	0,9969	10	0,13	**14**
-8,22	hsa-miR-141-3p	FOXA2	7mer-A1	-0,22	95	0,46	391	0,9248	12	0,05	**11**
-8,22	hsa-miR-141-3p	IGF2	8mer	-0,14	87	0,73	946	0,799	4	0,0575	**3**
-3,85	hsa-miR-155-5p	SUFU	7mer-A1	-0,19	88	0,72	270	0,9101	12	0,1824	**8**
-3,14	hsa-miR-135a-5p	MTSS1	8mer	-0,25	93	0,87	308	0,9128	11	0,0311	**15**
-2,87	hsa-miR-429	PTCH1	7mer-m8	-0,13	89	0,56	1242	0,7819	13	0,0509	**4**
-2,05	hsa-miR-664a-3p	PTCH1	7mer-A1	-0,03	33	N/A	679	0,9006	13	0,1886	**4**
-2,05	hsa-miR-664a-3p	GLI2	8mer	-0,03	70	N/A	147	0,9822	2	0,0274	**10**
-1,80	hsa-miR-503-5p	BTRC	7mer-A1	-0,32	98	0,84	118	0,8863	10	0,2268	**18**
-1,53	hsa-miR-944	PTCH1	8mer	-0,03	81	N/A	277	0,9664	16	0,1886	**8**
-1,53	hsa-miR-944	GAS1	7mer-m8	-0,04	89	N/A	1649	0,8236	11	0,0211	**5**
1,77	hsa-miR-769-5p	PTCH1	7mer-A1	-0,06	67	N/A	226	0,7708	8	0,1886	**2**
1,82	hsa-miR-589-3p	MTSS1	7mer-m8	-0,09	77	N/A	646	0,8287	9	0,1261	**0**
1,82	hsa-miR-589-3p	MKI67	7mer-m8	-0,03	53	N/A	709	0,8142	2	0,038	**1**
1,82	hsa-miR-589-3p	CTNNB1	7mer-m8	-0,07	71	N/A	593	0,8395	10	0,0042	**5**

Points	TOP-Hits
1st Place	**5**
2nd Place	**4**
3rd Place	**3**
4th Place	**2**
5th Place	**1**

Supplementary Figure 1: Detailed evaluation of all miRNAs, which possibly interact with one or more Hedgehog pathway genes, predicted in TargetsScan 7.1, DIANAmicroT CDS and MirWalk 2v. Hits in all three target-prediction tools were further analyzed by ranking their individual scores, originally assigned by the algorithm of the target-prediction tool. Five predicted miRNA-mRNA pairs with the top scores within a category were rewarded with points, indicated at the bottom right. Each miRNA-mRNA pairs' points were summed up and the top five predicted interactions were picked for further characterization.

Abbreviations

ALK	Anaplastic lymphoma kinase
AKT	Protein kinase B
APS	Ammonium persulfate
BAD	Bcl2 associated agonist of cell death
BAX	Bcl-2-associated X protein
BCA	Bicinchoninc acid
BCL-2	B-cell lymphoma 2
BOC	Brother of CDO
BSA	Bovine serum albumin
CCR4-NOT	Multisubunit complex, that regulates gene expression
CDKNA2	Cyclin-dependent kinase Inhibitor 2A
CDO	Cell adhesion molecule-related
CKS1B	Cyclin-dependent kinases regulatory subunit 1
CLIP-seq	cross-linked immune precipitation – sequencing
COMMD10	COMM domain-containing protein 10
DPBS	Dulbecco's phosphate-buffered saline
DCP2	m7GpppN-mRNA hydrolase
DDX6	Probable ATP-dependent RNA helicase DDX6
DHH	Desert hedgehog ligand
DMSO	Dimethylsulfoxid
DNA	Deoxyribonucleic acid
DNMT3A	DNA (cytosine-5)-methyltransferase 3A
DNMT3B	DNA (cytosine-5)-methyltransferase 3B
DYRK	Dual specificity tyrosine-phosphorylation-regulated kinase
EIF4A	Eukaryotic initiation factor 4A
EGF	Epidermal growth factor
EGFR	Epidermal growth factor receptor
EML4	Echinoderm microtubule-associated protein like-4

E2F3	Transcription factor E2F3
FBXW11	beta-transducin repeat containing protein 2
FCS	Fetal calf serum
FIH	Hypoxia-inducible factor 1-alpha inhibitor
FOXA2	Hepatocyte nuclear factor 3-beta
GAS1	Growth arrest-specific protein 1
GDP	Guanosine diphosphate
GLI1	Zinc finger protein GLI1
GLI2	Zinc finger protein GLI2
GLI3	Zinc finger protein GLI3
GTP	Guanosine triphosphate
GSK3β	Glycogen synthase kinase-3 beta
HER2-4	Human epidermal growth factor receptor 2-4
HH	Hedgehog ligand
HHIP	Hedgehog-interaction protein
IHH	Indian hedgehog ligand
IKK	I-kappaB Kinase komplex
I-kappaB	Nuclear factor of kappa light polypeptide gene enhancer in B-cells inhibitor
ITCH	E3 ubiquitin-protein ligase Itchy homolog
JNK	c-Jun N-terminal kinase
LRP	Prolow-density lipoprotein receptor-related protein
LGR4	Leucine-rich repeat-containing G-protein coupled receptor 4
LGR5	Leucine-rich repeat-containing G-protein coupled receptor 5
LGR6	Leucine-rich repeat-containing G-protein coupled receptor 6
MAPK	Mitogen-activated protein kinase
MDK	Midkine
MEK	Mitogen-activated protein kinase kinase
miR/miRNA	micro RNA
mTOR	Mechanistic target of rapamycin
mTORC1	mTOR Complex 1

MTSS1	Missing in metastasis 1
NF-kappaB	Nuclear factor kappa-light-chain-enhancer of activated B cells
NRG4	Pro-neuregulin-4
NSCLC	Non-small cell lung cancer
NUMB	Protein numb homolog
PABP	Polyadenylate-binding protein 1
PAN2	PAN2-PAN3 deadenylation complex catalytic subunit PAN2
PAN3	PAN2-PAN3 deadenylation complex subunit PAN3
PI3K	Phosphoinositol-3-Kinase-AKT
PLCγ	Phospholipase Cγ
PPARγ	Peroxisome proliferator-activated receptor γ
PIP2	Phosphatidylinositol 4,5-bisphosphate
PIP3	Phosphatidylinositol 3,4,5-trisphosphate
PTCH	Protein patched homolog
PTEN	Phosphatase and tensin homolog
PTN	Pleiotrophin
p120-GAP	GTPase activating protein p120
p190-B	GTPase activating protein p190-B
RAC	RAS-related C3 botulinum toxin substrate 1
RAF	Rapidly accelerated fibrosarcoma
RAS	Rat sarcoma
RNA	Ribonucleic acid
RSPO2	R-spondin-2
RTK	Receptor tyrosine kinase
SCLC	Small cell lung carcinoma
SDS-PAGE	Sodium dodecyl sulfate polyacrylamide gel electrophoresis
SHH	Sonic hedgehog ligand
SMO	Smoothened homolog
STAT	Signal transducer and activators of transcription
SUFU	Suppressor of fused homolog
TEMED	Tetramethylethylenediamine

TP53	Tumor protein p53
TOPORS	E3 ubiquitin-protein ligase Topors
UTR	Untranslated region
VEGFA	Vascular endothelial growth factor A
WHO	World health organization
XRN1	5'-3' exoribonuclease 1
ZEB1	Zinc finger E-box-binding homeobox 1
ZNRF3	E3 ubiquitin-protein ligase ZNRF3
βTRC	β-transducing repeat-containing protein
4E-T	Eukaryotic translation initiation factor 4E transporter